AFML-TR-75-216

20

DEVELOPMENT OF IMPACT RESISTANT METAL MATRIX COMPOSITES

AD A030800

UNITED TECHNOLOGIES RESEARCH CENTER
400 MAIN STREET
EAST HARTFORD, CONNECTICUT 06108

MARCH 1976

TECHNICAL REPOI T AFML-TR-75-216
FINAL REPORT FO1 PERIOD MARCH 1974 - SEPTEMBER 1975

AIR FORCE MATERIALS LABORATORY
AIR FORCE WRIGHT AERONAUTICAL LABORATORIES
AIR FORCE SYSTEMS COMMAND
WRIGHT-PATTERSON AIR FORCE BASE, OHIO 45433

NOTICE

When Government drawings, specifications, or other data are used for any purpose other than in connection with a definitely related Government procurement operation, the United States Government thereby incurs no responsibility nor any obligation whatsoever; and the fact that the government may have formulated, furnished, or in any way supplied the said drawings, specifications, or other data, is not to be regarded by implication or otherwise as in any manner licensing the holder or any other person or corporation, or conveying any rights or permission to manufacture, use, or sell any patented invention that may in any way be related thereto.

This report has been reviewed and cleared for open publication and/or public release by the appropriate Office of Information (OI) in accordance with AFR 190-170 and DODD 5230.9. There is no objection to unlimited distribution of this report to the public at large or by DDC to the National Technical Information Service (NTIS).

This technical report has been reviewed and is approved for publication.

James S. Wilbeck

J. S. Wilbeck, Capt. USAF
Project Engineer

FOR THE COMMANDER

Wesley B. Crow

W. B. Crow, Major USAF
Structural Metals Branch
Metals & Ceramics Division
Air Force Materials Laboratory

Copies of the report should not be returned unless return is required by security considerations, contractual obligations, or notice on a specific document.

AFML - WPAFB - OH SEPTEMBER 76 - 300

UNCLASSIFIED

SECURITY CLASSIFICATION OF THIS PAGE (When Data Entered)

REPORT DOCUMENTATION PAGE	READ INSTRUCTIONS BEFORE COMPLETING FORM
1. REPORT NUMBER: AFML-TR-75-216	2. GOVT ACCESSION NO. / 3. RECIPIENT'S CATALOG NUMBER
4. TITLE (and Subtitle): DEVELOPMENT OF IMPACT RESISTANT METAL MATRIX COMPOSITES	5. TYPE OF REPORT & PERIOD COVERED: Final Report, March 1974 - September 1975 / 6. PERFORMING ORG. REPORT NUMBER
7. AUTHOR(s): Karl M. Prewo	8. CONTRACT OR GRANT NUMBER(s): F33615-74-C-5062
9. PERFORMING ORGANIZATION NAME AND ADDRESS: United Technologies Corporation, Research Center, East Hartford, Connecticut 06108	10. PROGRAM ELEMENT, PROJECT, TASK AREA & WORK UNIT NUMBERS
11. CONTROLLING OFFICE NAME AND ADDRESS: Air Force Materials Laboratory, Air Force Systems Command, Wright-Patterson Air Force Base, Ohio 45433	12. REPORT DATE: September 30, 1975 / 13. NUMBER OF PAGES: 124
14. MONITORING AGENCY NAME & ADDRESS (if different from Controlling Office)	15. SECURITY CLASS. (of this report): Unclassified / 15a. DECLASSIFICATION/DOWNGRADING SCHEDULE

16. DISTRIBUTION STATEMENT (of this Report)

Approved for public release; distribution unlimited

17. DISTRIBUTION STATEMENT (of the abstract entered in Block 20, if different from Report)

18. SUPPLEMENTARY NOTES

19. KEY WORDS (Continue on reverse side if necessary and identify by block number)

Impact Tolerance	Boron Aluminum	Ballistic Impact
Composites	Boron Titanium	Pendulum Impact
Boron Fiber	Metal Matrix Composites	Charpy Impact

20. ABSTRACT (Continue on reverse side if necessary and identify by block number)

Metal matrix composites consisting of boron reinforced aluminum, boron-aluminum-titanium, and Borsic reinforced titanium were fabricated to achieve improved impact tolerance. Test procedures included both static, instrumented pendulum impact, and ballistic impact. It was demonstrated that composite specimens can be fabricated and tested to achieve a wide range of impact resistance. Energy dissipation can exceed that of monolithic engineering alloys, however, this superiority is very geometry dependent.

DD FORM 1 JAN 73 1473 EDITION OF 1 NOV 65 IS OBSOLETE
S/N 0102-014-6601

UNCLASSIFIED

SECURITY CLASSIFICATION OF THIS PAGE (When Data Entered)

PREFACE

This report describes research conducted by the United Technologies Research Center, Division of United Technologies Corporation, East Hartford, Connecticut, under USAF Contract No. F33615-74-C-5062. The author is Dr. Karl M. Prewo.

The effort described was conducted in support of Project No. 7351 and Task 735107 for the Structural Metals Branch of the Metals and Ceramics Division during the period March 1974 - September 1975. The contract monitor was Capt. James S. Wilbeck. This program was partially funded with Air Force Materials Laboratory DIRECTOR'S FUNDS.

This report was submitted by the author in January 1976 for publication as a Materials Laboratory Technical Report.

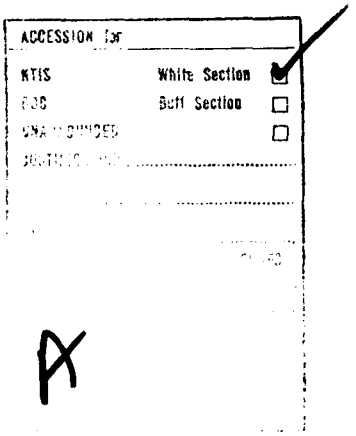

TABLE OF CONTENTS

LIST OF TABLES

LIST OF ILLUSTRATIONS

List Of Illustrations (Cont'd)

List Of Illustrations (Cont'd)

I. INTRODUCTION

At the inception of this program the major inhibitor to the use of metal matrix composites for jet engine fan blades was the low impact resistance of this class of materials. This observation has, in the past, been demonstrated through both actual component and laboratory specimen tests in which, when compared to current monolithic titanium, composite specimens appeared less resistant to impact by objects. The herein described program was begun, however, because of several findings which indicated that metal matrix composite impact tolerance could be significantly improved.

The first of these findings was a demonstration that the impact resistance of boron aluminum composites, as measured by the total energy to failure of a standard notched Charpy specimen, could be significantly altered by control of fiber effective strength, filament volume percent, filament diameter and matrix shear strength (Ref. 1). As shown in Fig. 1, this dependence was found to exist over a wide range of filament and matrix combinations and indicated that significant improvements in energy dissipation capability could be achieved if a high strength 8.0 mil diameter filament could be developed and used in conjunction with a low shear strength matrix.

Shortly thereafter, guided by the data developed in Ref. 1, it was demonstrated that boron reinforced aluminum composites could be fabricated and tested to achieve notched Charpy impact energy levels significantly greater than those characteristic of titanium alloys (Refs. 2, 3). This demonstration illustrated, for the first time, the point that aluminum matrix composites were not necessarily brittle and, in fact by a selected test procedure, they were superior in impact tolerance to state-of-the-art engineering alloys. The specimen shown in Fig. 2 dissipated over 22 ft lbs of impact energy and remained substantially unbroken while similar geometry specimens of Ti-6Al-4V failed after dissipating approximately 15-20 ft lbs of energy. In this work, Ref. 2, it was also shown that a hybridization concept, which included the use of both low shear strength matrix areas (for high impact energy) and high strength matrix areas (for high shear and transverse strength), could be utilized to combine high impact tolerance with high off-axis composite strength in one composite system.

Indications that the measured impact resistance of composites is strongly affected by composite specimen geometry were also reported (Refs. 1, 2, 3). The rationale for this was postulated to depend on the relative contributions of matrix plasticity and filament fracture to ultimate composite failure. Very large amounts of energy can be dissipated by matrix deformation, however, the applied stress state must be such as to permit this to be a controlling mode

of failure. The comparison of tensile stress-strain curves for boron aluminum shown in Fig. 3 is illustrative of this point. The matrix shear controlled failure of a 45° specimen dissipated a much larger quantity of energy than the filament controlled failure of a 0° specimen or the constrained matrix controlled failure of the 90° specimen. The recognition of this importance of stress state-composite interaction clearly pointed out the need for testing and descriptive procedures going beyond the simple overall notched Charpy impact energy.

Finally, another concern which contributed to the formulation of this program was the recognition that impact energy dissipation capability was not the only criterion important in achieving a highly impact resistant composite. The load-time history and maximum load sustained during impact are also of great importance. This was clearly illustrated for the case of silica filament reinforced epoxy, (Ref. 4), where the exposure to a steam environment of these composites caused only a small (14 percent) decrease in specimen impact energy; however, the maximum impact load carrying capacity decreased by 45 percent. The description of material impact resistance solely on the basis of energy dissipation can be misleading and hence, the herein described program emphasized the use of an instrumented test procedure which permitted the evaluation of both the load-time impact history of a specimen as well as the overall impact energy. It should also be noted that this additional loading information is absolutely essential if composite specimen performance is to be used to design actual engine components. Charpy impact energy is not a design tool, it is only a qualitative indicator of material performance. The use of more sophisticated treatments such as those based on fracture mechanics, (Refs. 5, 6 and 7) are needed for structural design in the presence of flaws and, as will be demonstrated in this report, analyses relating performance to test geometry and stress state are necessary to effectively select materials for the fabrication of structures resistant to impact.

II. EXPERIMENTAL PROCEDURE

A. MATERIALS

The following materials were purchased from the indicated sources.

5.6 mil diameter boron filament - Composite Materials Corporation
5.7 mil diameter Borsic filament - Composite Materials Corporation
Al alloy foils - Composite Materials Corporation
Al alloy powder - Composite Materials Corporation
8 mil diameter boron filament - Avco Corporation
Ti - 6Al -4V foil - Teledyne Rodney Metals
5.7 Borsic Reinforced - Ti-6Al-4V - TRW Corporation

B. COMPOSITE FABRICATION

1. Boron Reinforced Aluminum

All of the boron filament reinforced aluminum composites evaluated during this program were fabricated at UTRC using plasma sprayed precursor tapes and diffusion bonding procedures. The fabrication of the precursor tapes has been described in detail in several previous reports (Refs. 1, 8), and will not be repeated here. All diffusion bonding was performed in a vacuum of 10^{-5} Torr, at applied pressures in excess of 2,000 psi and with the composite layers confined in close walled dies.

The temperature of bonding depended on the composition of the matrix, however, it was always below the alloy solidus temperature.

The properties of the aluminum alloys used during this investigation are tabulated in Table I.

2. Boron-Aluminum-Titanium

Composite specimens were fabricated containing added layers of Ti-6Al-4V. Bonding conditions used were substantially similar to those used for all aluminum matrix composites, however, in this case temperatures were also limited to prevent the formation of an intermetallic layer between the added titanium foils and the aluminum.

3. Borsic-Titanium

Two sources of Borsic reinforced titanium were evaluated under this program. Several panels, fabricated by TRW, were purchased and additional panels

were fabricated at UTRC. The composite panels fabricated at UTRC were diffusion bonded using polystyrene bonded precursor tapes. Each tape consisted of Ti-6Al-4V foil with an overlayer of evenly spaced Borsic fibers bonded to the foil by the polystyrene fugitive. Hot pressing was performed by heating in vacuum to 450-490°C to first remove the polystyrene and then raising to the ultimate bonding temperature followed by final high pressure application.

C. INSTRUMENTED PENDULUM IMPACT TESTING

All pendulum impact tests were performed using an instrumented tup which permits the generation of load-time traces describing the impact event. Continuous load measurement is achieved through the use of strain gages mounted on the tup and a calibration to translate strain readings into load. The strain gage output is monitored on an oscilloscope producing a load-time trace which is then photographically recorded.

Two instrumented impact testers were constructed at UTRC for this purpose using standard 23 ft lb and 260 ft lb capacity pendulum impact machines. The 23 ft lb tester is shown in Fig. 4.

Specimens of both standard and thin nonstandard sizes were tested during this program. To insure uniform impact loading of the thin specimens, shims have been fabricated to position the specimen impact face properly with respect to the bottom of the pendulum swing.

D. TENSILE TESTING

Composite tensile specimens were parallel sided with fiberglass doubler pads bonded onto each end. The overall specimen dimensions were five inches long and 0.4 inch wide with a final effective gage length of 1.0 inch.

Measurements of modulus and failure strain were obtained using strain gages mounted on opposite specimen sides.

The pendulum impact specimen geometries tested are shown in Fig. 4. The specimen orientations tested are indicated in Fig. 5. They consist of two basic types, LT and TT. This notation was first introduced during another UTRC program, (Ref. 1). The letters refer to the directions which are longitudinal (L) or transverse (T) with respect to the specimen principal fiber axis. The first letter of each pair refers to the normal to the crack growth plane while the second letter refers to the direction of crack growth. The LT type specimens were also tested in two orientations, edgewise or chordwise. These designations refer to impact orientations based on jet engine fan blade terminology. A chordwise impact on a fan blade consisting of layers

of boron aluminum tape is simulated by the uppermost specimen in Fig. 5, in that the direction of impact is normal to the tape plies. An edgewise fan blade impact configuration is simulated by the impact direction being in the plane of the tape plies.

E. BALLISTIC IMPACT TESTING

All ballistic impact tests were performed at the Air Force Materials Laboratory, Wright Patterson Air Force Base. Two geometries of impact were utilized (Fig. 7) to demonstrate, as in the case of pendulum impact, the dependence of material performance or imposed stress state. Strain gages were located on some of the ballistic specimens and their locations are indicated in Fig. 7. All ballistic tests were performed using RTV cylinders having a weight of approximately 0.36 gm. The cylinders were 0.295" diameter, 0.295" long, and were fired with the use of a sabot which was caught prior to specimen impact.

All ballistic tests were monitored using a slit camera which recorded specimen and projectile motions at the point of impact. In addition strain gage data and framing camera records were taken on selected specimens. The use of these data to interpret and correlate specimen performance was not within the scope of this program. However, these data will prove extremely useful to other investigators who may wish to investigate material impact resistance.

III. RESULTS AND DISCUSSION

A. INSTRUMENTED PENDULUM IMPACT

The instrumented pendulum impact test was the test used most extensively during the performance of this program. As stated in the introduction, it was clear to the investigator that a simple measure of the total energy to fail a standard Charpy specimen was not a sufficient criterion by which to rank potential fan blade materials. The use of the instrumented tup was a major step forward in achieving truly meaningful data. Many previous publications have described the details of the procedure and precautions necessary to achieve accurate instrumented impact data, Refs. 8, 9, 10. The major problem lies in recording a signal which accurately describes the loading history of the tup during impact. Extensive precautions were taken at UTRC to insure that this was the case and impact specimens were shared with two other independent laboratories, Refs. 11, 12, to insure that the equipment and procedures developed at UTRC were capable of providing accurate and precise data. It was concluded that this was the case.

The interpretation of load and energy data obtained from the instrumented pendulum impact test is only meaningful if one considers the dependance of the composite response on specimen geometry and hence imposed stress state. Multiple composite failure modes are possible, depending on the dimensions of the specimens tested.

Figure 8 illustrates the problem at hand. Specimen dimensions of L and h are shown in this figure. For Charpy impact or three point bend, the L refers to the specimen span and h to the width over which crack propagation must occur. The standard Charpy test with an L/h ratio of 5 (notched) or 4 (unnotched) is not at all similar to the intended blade application where effective L/h values can exceed 100. On a local damage scale, the similarity may be closer; however, it is clear that the geometry dependence of composite performance must be understood prior to any extension of pendulum impact data to blade design. The inclusion of this geometry dependence can be accomplished with existing understanding of composite beam testing, Refs. 13, 14. Through the use of these concepts, and simple beam equations, it is possible to plot interaction diagrams which illustrate the dependence of unnotched composite beam strength on specimen geometry. Although these equations were developed for the standard bend tests which are performed at slow rates of load application, usually 0.01 to 0.1 inches per minute, they apply equally well to specimens impacted at 7,000 to 10,000 inches per minute, which is the

usual range of velocity for Charpy impact testing. The dependence of material strength on impact velocity is another matter independent of the method of analysis.

For an unnotched bend test of a simply supported composite beam of rectangular cross section, simple equations predict nominal levels of maximum shear and flexural stresses. The maximum shear stress occurs at the neutral surface and is given by

$$\tau_{max} = 3/4 \frac{P}{bh}$$

The maximum flexural stress occurring at the same time is

$$\sigma_{max} = 3/2 \frac{PL}{bh^2}$$

and occurs at midspan at the top fibers (side away from the loading nose). The use of these equations presupposes a series of assumptions which are satisfied quite well by composites of the types tested in this program and for which the principal axes of orthotropy coincide with the axes of symmetry of the test specimen. The use of these equations is recognized by the investigator to be overly simplistic in light of effects of stress concentrations in the areas of the loading points, Ref. 15, and the need for more sophisticated stress analyses to completely characterize the existant stresses, particularly for multiaxially reinforced specimens Refs. 16, 17, 18. However, as will be demonstrated in this report these simple equations are useful in rationalizing and predicting composite beam response.

Figure 9 is a theoretical construction of a series of shear interaction diagrams for various boron fiber reinforced metal matrix composite systems in the LT orientation based on assumed values of composite and matrix strengths. The horizontal lines in the low L/h region indicate the expected levels of composite shear strength obtainable for composites either yielding or fracturing due to matrix yield or failure. These true levels of material shear strength τ_{max} are independent of specimen geometry (L/h), however, the measured (observed) values of τ_{max} will not be independent at higher levels of (L/h) due to a transition of failure mode from shear to flexural. In the higher L/h regions a calculation of shear strength would be incorrect. The calculated curves of decreasing observed shear strength are based on assumed values of composite flexural strength, σ_o. Similarly, in Fig. 10, a flexural interaction diagram, the transition into a shear failure region is noted by the drop in calculated composite flexural strength at small values of L/h.

In both figures the L/h values for notched and unnotched standard sized Charpy specimens are denoted by the shaded regions indicating that, for 1100 and 6061 aluminum matrix composites, the specimen behavior is controlled by shear strength.

To experimentally demonstrate the validity of the above approach, a series of unnotched 5.6 mil diameter boron reinforced 6061 specimens of the LT-chordwise orientation were tested in three point bend. These specimens were tested over a range of span to width (L/h) ratios by varying both L and h. The resultant load-deflection traces were analyzed utilizing the flexural interaction diagram approach. Calculation of the flexural strength of each specimen based on the maximum load to failure, and plotting the resultant values as a function of L/h resulted in Fig. 11. As has been discussed above, the apparent flexural strength is a function of L/h, and only for large values of L/h does the flexural strength reach a constant level. The sloping line for low values of L/h was calculated using the known shear strength of 6061 aluminum and agrees well with the observed decrease in apparent flexural strength. The actual matrix shear strength was multiplied by a factor of 1.15 which is introduced to include the effects of constraint due to the fibers present.

It is interesting to compare the behavior of specimens tested in different regions of the interaction diagram. Figure 12 presents the load-deflection traces for three specimens. Specimen 2317-1 exhibited a large degree of plasticity and a very round curve. Specimen 2320-1, however, with a larger value of L/h, failed more abruptly and with less energy dissipated by plasticity. Finally, specimen 2320-4 exhibited no signs of plasticity at all. These modes of fracture agree well with the behavior expected, i.e., shear controlled or flexural strength controlled, as shown in Fig. 11 depending on L/h value.

Another method used to examine the effect of specimen L/h ratio was to determine the energy required to raise each of the specimens in Fig. 11 to the maximum load prior to failure. This value is less than the total required to fracture each specimen by that amount required to propagate a crack through the system (i.e., we observed stable crack growth). When the initial energy is divided by the total volume of each specimen, a very strong dependence on L/h is evident, Fig. 13. In the flexural strength controlled region (high L/h), this value reaches the theoretical limit calculated for fully elastic behavior as shown in the figure.

The same type of dependence on L/h is true for the testing of notched metal matrix specimens. The data in Figs. 14 and 15 were obtained previous to this study at UTRC, Ref. 19; however, now they are plotted as a function of L/h. Once again the interaction diagram concept provides agreement between calculation (based on 1100 matrix shear strength) and experimental data.

Because of the above noted very strong dependences of composite performance on test specimen geometry, it is unrealistic to try and rank composite systems simply on the basis of a standard Charpy energy value. At least this is true if one wishes to achieve more than just a qualitative understanding of composite behavior.

B. PENDULUM IMPACT OF BORON ALUMINUM

The following sub-sections will describe the most important points derived from the instrumented pendulum impact testing of boron fiber reinforced specimens. The data will be presented primarily in graphical form, however, tabulations of the basic data are also included.

The major observation to be made is that the pendulum impact performance of boron reinforced aluminum composites can be varied over a very wide range through choice of matrix, fiber and orientation. Extremes of impact energies, for standard Charpy specimens, of from 1 ft lb to specimens that could not be fractured by a 260 ft lb pendulum strike, were recorded. The controlling factors are discussed below.

(1) Matrix Composition

The impact data obtained by testing unidirectionally reinforced 5.6 mil diameter boron reinforced aluminum matrix composites are listed in Table II. The comparison of LT-type specimen data, Fig. 16, indicates the role of matrix composition and strength in both the shear controlled (low L/h) and tensile strength controlled (high L/h) regions. The lines drawn in the low L/h regions were calculated on the basis of matrix alloy shear strengths and found to agree in each case quite well with the experimentally observed specimen strength. The maximum load (hence specimen strength) withstood during impact, increased with increasing matrix strength. It is interesting to note that the matrix control of observed flexural strength is similarly significant in the high L/h region. The increase of strength with increasing matrix strength was unexpected, at least to the degree to which it is evident. Tensile specimen data, Table III, for axially reinforced specimens did not indicate the same dependence of 0° tensile strength on matrix strength, although previous investigations have demonstrated the axial composite strength can increase with increasing matrix strength.

The observed ability of LT type specimens to dissipate energy during impact and fracture was also strongly dependent on composite matrix strength. In this case, however, increasing matrix strength caused a decrease in performance. This is best demonstrated by discussion of the oscilloscope traces obtained during impact and the resultant specimen deformations observed.

(a) LT Type 5.6 Boron Reinforced 1100

1100 matrix specimens have demonstrated the ability to dissipate a large amount of energy in the LT orientation, however, at the expense of fracture strength. Figure 17 demonstrates the importance of impact orientation with regard to the tape ply planes. Examination of Figs. 17 and 18 demonstrates that interlaminar shear between tape plies effectively diverts the fracture path and dissipates large quantities of energy. Little change in maximum load is observed.

Figures 19 and 20 demonstrate the differences between notched and unnotched specimens with large h dimensions. Both specimens sheared off at one end during passage through the impact machine. (The sheared off end was lost for the notched specimen). Thus, in both cases the observed energy levels are less than could have been dissipated. This explains the anomaly of a lower energy value for the unnotched specimen than the notched.

The load-time traces for additional specimens of decreasing thickness (h) in both notched and unnotched condition are shown in Figs. 21, 22, and 23. In Fig. 21 the unnotched specimen required two impacts to cause fracture and both traces are shown in the same photo.

(b) LT Type 5.6 Boron Reinforced 6061

The 6061 matrix specimens failed at considerably higher maximum load (and stress) levels than the previously described 1100 matrix specimens. This was, however, accompanied by lower values of energy dissipation, and as shown in Fig. 24, by less extended load-time traces. One interesting anomaly occurred, however, in Fig. 25. The unnotched specimen 2287-3 exceeded by 139 lbs the maximum load of similar specimens 2287-2,4. This was accompanied by a very large amount of interlaminar shear and delamination which was not typical of the other 6061 specimens, Fig. 26. Specimen 3 indicates crack diversion and link up with the cracks emanating from the zone of damage in the contact region. Specimen 4 also exhibited small amounts of interlaminar failure, however, these were not as extensive as those of specimen 3. The slightly higher maximum load apparently succeeded in causing the extension of interlaminar cracks and the more gradual decrease in load with time, Fig. 25, due to effective crack blunting.

(c) LT Type 5.6 Boron Reinforced 2024 and 5052/56

Both 2024 and 5052/56 matrix type specimens exhibited only small indications of plasticity even for the specimens with low values of (L/h). The instrumented traces indicate only a small degree of nonlinearity, Figs. 27 and 28, with the specimens of smallest h exhibiting a completely linear

behavior, Fig. 29. The fractured specimens, Fig. 30, clearly indicate this lack of extensive plasticity for both notched and unnotched configurations. Absence of damage in the region of contact with the tup is also noted.

(2) Fiber Orientation

The dependence of composite impact performance on fiber orientation is even greater than that noted above for matrix strength.

(a) 5.6 B - Uniaxially Reinforced Specimens

As indicated by the data in Table II there is a very large decrease in impact load and impact energy by changing from the LT to the TT orientation. The reasons for this are that; firstly the matrix is so highly constrained by the fibers that it can not exhibit much plasticity during failure in the 90° mode; and secondly composite transverse strength is so much lower than axial strength.

(b) $\pm 15^{\circ}$ -5.6 Boron Reinforced 1100

Figure 31 presents the instrumented impact traces for $\pm 15^{\circ}$ reinforced specimens with an 1100 matrix. Both in maximum load carrying capability and impact energy dissipation, these specimens performed in a manner similar to LT type specimens. Figure 32 illustrates that a considerable amount of delamination took place as well as the shearing off of one end of the specimen.

(c) $\pm 22^{\circ}$ -5.6 Boron Reinforced 1100, 6061 and 2024

The load-time traces for 5.6 boron-1100 specimens of edgewise and chordwise orientations are compared in Fig. 33. It is interesting to note the higher level of energy dissipated for the notched specimen which delaminated more severely than the unnotched specimen, Fig. 34. This observation is unexplained, particularly in view of the expected higher load carrying capacity of the unnotched specimen. On the basis of maximum stress, however, the notched specimen reached a flexural tensile stress of 102,000 psi while the unnotched specimen only reached a level of 84,000 psi. The edgewise impact of similar specimens, Figs. 34 and 36, resulted in much higher maximum loads to failure but also lower energy dissipation. The photos in Fig. 36 show the areas of contact of specimen and tup illustrating the very large amounts of local damage.

Figures 37 and 38 demonstrate the impact behavior of thin specimens with varying matrix composition. The 2024 and 6061 matrix composite specimens exhibited very high failure strengths while the 1100 matrix specimen failed

at a much lower strength level. The level of energy dissipated was not decreased, however, due to the post maximum load energy dissipation exhibited by the 1100 specimen.

The $\pm 68^{\circ}$ orientation was also tested, Figs. 39 and 40, and found to be very poor in impact tolerance. Both maximum loads and energy dissipation capacity were very low. It is interesting to note that specimen 2277-1 did not fracture; ductility was sufficient to permit a large amount of deformation.

The data for these specimens are tabulated in Table IV.

(d) $\pm 45^{\circ}$ -5.6 Boron Reinforced 1100, 6061 and 2024

Figures 41 and 42 illustrate the large deformation and hence energy dissipation capacity of the 1100 matrix with $\pm 45^{\circ}$ fibers. Both chordwise and edgewise impacts deform, but do not fracture, the specimens. The narrow, C-2231, as well as wide, C-2226-1, specimens exhibit this capacity. The 6061 matrix specimens of similar orientation also exhibit high energy dissipation capacity, however, this is accomplished with a very significant increase in load carrying capacity, Figs. 43, 44. Similar observations can be made for the 2024 matrix composite system, Figs. 45, 46. It can be noted that for both the 6061 and 2024 composite specimen types, crack propagation was more extensive than for the 1100 matrix system.

The data for these specimens are tabulated in Table V.

(e) Shell-Core and Distributed Ply Lay Up

A comparison was made between two different methods of achieving multiaxially reinforced blade structures. The first scheme was to have the outer shell of each specimen consist of 45° plys and the inner core consist of 0° plys. The second arrangement consisted of intermixing these plys in the shell with fewer 0° plys in the core.

The comparison of the shell/core and distributed ply layup schemes is given in Table IV on the basis of pendulum impact testing. As might be expected, the maximum loads exhibited during failure were highest for the distributed ply specimens with 0° plys near the outer specimen surfaces. The $\pm 45^{\circ}/90^{\circ}$ specimens of the distributed ply type were also significantly stronger than the $\pm 45^{\circ}/90^{\circ}$ shell/core specimens and at present this is not explainable. In contrast to this, the shell/core specimens consistently dissipated larger levels of energy than the distributed specimens. The load-time traces in Fig. 47 illustrate the difference in performance. The shell core specimen failed at a fairly high initial load and then continued to

support a lower impact load as the $\pm 45^{\circ}$ plys deformed to the point of fracture. In contrast for the other lay up the distributed 45° plys were constrained by their 0° neighbors and fracture was much more abrupt after the initial load drop. This caused the specimen to dissipate far less energy.

(f) Angle Ply Comparison

Flexural strengths obtained by calculation based on 1100 matrix pendulum impact data are presented in Fig. 48 as a function of L/h. The data reported in 1973 (Ref. 19) are also included for comparison. The drawn line in the low L/h region is calculated on the basis of 1100 matrix shear strength and fits well the data for all orientations. In the higher L/h regions the data separate into groups depending on the true flexural strengths of each composite type.

(3) Fiber Diameter

As was discussed in the introduction, previous work at UTRC, Ref. 1, had demonstrated that the use of larger diameter boron fiber can cause significant increases in composite impact energy dissipation. This was investigated further in this study through the reinforcement of 1100 aluminum with 8 mil diameter boron fiber. Impact data are presented in Table VII. Figures 49 and 50 demonstrate the very large capacity of 8.0 mil boron reinforced 1100 matrix specimens to dissipate energy. The initiation and propagation of the crack is effectively blunted by interlaminar shear so that, as shown in Fig. 50, shear, delamination and bending prevent fracture of the specimens. The unnotched specimen dissipated a lower level of energy than the notched specimen due to the shearing off of one end.

Composites with a 6061 matrix behaved very differently. The maximum loads are much higher than those for 1100 matrix specimens, however, the energy levels dissipated are lower and actually less than those typical of 5.6 mil boron reinforced specimens, Fig. 51. The specimens shown in Fig. 52 demonstrate this low energy dissipation capacity by exhibiting little or no distortion.

The superiority of the 1100 matrix in energy dissipation can also be demonstrated in thin specimens, Fig. 53. The ability to sustain load after the initial peak in the load-time curve is the reason for the 1100 composite superiority.

The results of tensile testing 8 mil boron-reinforced composites were quite disappointing, Table VIII-A. The fiber was observed to split in transverse tensile specimens Fig. 54, and low axial strengths were generally

obtained. As a point of interest, data obtained independently at UTRC using 8 mil boron from another source (Table VIII-B) gave much higher axial and transverse composite strength values and did not show any signs of splitting. Impact specimens fabricated and tested using this fiber, however, did not demonstrate the same high levels of impact energy dissipation. The differences in tensile and impact performance noted indicate an as yet unexplained fundamental difference between these two fibers.

(4) Comparison With Unreinforced Materials

Because unreinforced titanium alloys have exhibited sufficient FOD tolerance, impact specimens of Ti-6Al-4V were also tested and subjected to analysis similar to that described previously herein for boron aluminum. Specimens of 6061-T6 metal were also tested for additional comparison. The interaction diagram concept was used to analyze the data obtained for these two monolithic unreinforced metals. Instrumented impact tests were performed on specimens having a variety of notch depths. The data are presented in Fig. 55. It is interesting to note the constant level of flexural strength obtained. No data were obtained in the very low L/h region (where a drop off in strength might be expected) due to specimen size restrictions. Therefore, the extensions of the drawn curves into this region are conjecture and were calculated for the sake of completeness. The value of observed flexural strength for these materials was found to be quite high and correspond to between 2.5 and 2.9 times the tensile yield strength of the alloys. This is not unreasonable in the presence of the notch constraint, however, a more usual method to represent metal resistance to crack growth is by use of fracture mechanics. Therefore, values of K_{ID} were also calculated for several of these specimens using standard fracture mechanics formulations. These values are given in Table IX along with data available from a standard handbook for comparison. The herein obtained values in both cases exceed the literature data. This is probably due to the fact that full constraint is not obtained in the Charpy specimen thickness as well as the fact that the Charpy notch is fairly blunt.

The load-time traces for full sized notched and unnotched Ti-6Al-4V specimens are given in Fig. 56. Cumulative energy dissipated as a function of time is also given for both. As illustrated by the tested specimens in Fig. 57, it is clear that the notched specimen failed in a fairly brittle manner while the unnotched specimen deformed to a very large extent, and could not be fractured using the 260 ft-lb impact machine. Narrow shear lips on the notched specimen outer edges indicate the low level of local plasticity. The load-time traces of notched specimen performance with decreasing specimen width (h) are shown in Figs. 58 and 59, indicating small amounts of plastic deformation at the maximum loads prior to failure. All specimens failed at the notch with signs of extensive plasticity.

Figure 60 compares the data obtained for the unreinforced metals with composite data. As has been shown in the past in several fracture mechanics programs, the energy dissipated in fracturing a notched unreinforced metal 3-point bend specimen varies linearly with net specimen width (h). Both the Ti-6Al-4V and 6061-T6 demonstrate this. When compared with 5.6 boron reinforced 1100 material, which also displays a linear dependence, it is observed that large differences which exist for large values of h disappear in the small h regime. The fact that the order of superiority may reverse in the small h region may be of particular importance for thin blade-like structures.

C. PENDULUM IMPACT OF BORON - ALUMINUM - TITANIUM

Boron fiber (5.6 mil diameter) reinforced 1100 aluminum matrix composites were fabricated with the added reinforcement of Ti-6Al-4V foils. These foils were 0.003 in. thick and improved both the off axis tensile strength and impact resistance of the base composites. The Ti-6Al-4V foils were interspersed with the layers of B/Al tape. Two sets of composites were fabricated. Specimens 2384, 2385, and 2386 were assembled with one layer of Ti foil for each two layers of tape, as well as on both composite surfaces, while composites 2387 and 2388 consisted of one layer of Ti for every three layers of tape and again foil on both outer composite surfaces.

The data obtained from the Ti-6Al-4V foil enhanced B/Al specimens are presented in Table X and Fig. 61. The major improvement in impact performance for these specimens occurred when testing in the off-axis (TT) orientation. Both energy and maximum load values were considerably higher than those of uniaxially reinforced B/Al alone. It is interesting to note that most of the specimens tested did not fracture completely due to the added titanium foils.

A major difference was found to exist between the chord and edge orientations of these specimens, Fig. 62. The lower interlaminar shear strength of the former, due to the continuous layers of aluminum available for shear, cause both a low maximum impact load and a high impact energy. Chordwise failure is strongly related to 1100 aluminum matrix shear and, as can be seen in Fig. 61 the strength of specimens in the low L/h region agrees well with calculations based on 1100 aluminum shear strength. The edgewise specimen tested failed at a much higher stress level due to the importance of the Ti foils in preventing interlaminar shear in this orientation. Figures 63 and 64 are additional load-time traces for specimens of higher L/h values in both the LT (chordwise) and TT orientations. The addition of the titanium foils has improved considerably the TT specimen performance over that of uniaxial B/Al both from energy and maximum sustained load points of view.

D. PENDULUM IMPACT OF BORSIC REINFORCED TITANIUM

The pendulum impact testing of 5.7 mil Borsic uniaxially reinforced Ti-6Al-4V specimens revealed that, in all orientations and geometries, the overall ability to dissipate energy was considerably less than that of both boron reinforced aluminum and boron aluminum titanium. Table XI, contains the data for the impact specimens tested and includes materials supplied by TRW and also specimens fabricated at UTRC. The data obtained for unnotched and notched (with a sharp Charpy notch) specimens were used to calculate a flexural interaction diagram, Fig. 65. The maximum load data reported in Table XI for standard sized Charpy specimens indicated a very high load carrying capability for Borsic-titanium as compared with B/Al. As can be seen from Fig. 65, however, this was simply due to the fact that specimens were well away from the L/h region in which shear failure would be expected to occur. In actuality, a level of flexural strength of 240,000-280,000 psi is slightly lower than that for 5.6 boron/6061 of the same orientation. The tensile data for both UTRC and TRW fabricated materials are presented in Tables XII and XIII. As would be expected, the levels of axial strength measured were also somewhat less than those of 5.6B/6061, Table III, in agreement with the flexural diagram analysis.

A comparison with 5.6B/1100 on the basis of energy dissipated as a function of specimen geometry, Fig. 66, reveals that for large values of h (e.g., low values of L/h) the aluminum matrix composite is far superior. At the lower values of h, however, where the deformation of aluminum contributes little to overall specimen failure, the values of energy become comparable. In this region the primary contribution to energy dissipation is through elastic deformation and fracture, and since both systems exhibited nearly the same flex strength (Figs. 16 and 65), this convergence of performance is to be expected.

Instrumented impact traces for several composite specimens are presented in Figs. 67 and 68. The 5.7 Borsic reinforced titanium specimens of the chordwise orientation exhibited a marked duplex load trace with a sharp drop from maximum load followed by a plateau prior to final failure, Fig. 67. This was not true of the edgewise specimens Fig. 68, which failed abruptly after the maximum load had been achieved. Examination of the specimen fracture surfaces indicated that interlaminar failure occurred, on a small scale, in the chordwise specimens and not in the edgewise. It is not clear as to whether this interply failure occurred prior to or during gross crack propagation. In all cases chordwise specimens failed at flexural stress levels slightly below those of edgewise specimens which may indicate some interply failure prior to final fracture. The net effect of this lower interply strength was to increase the total energy required to fail a specimen by making crack propagation more difficult. Edgewise specimens dissipated only approximately 75 percent of the energy typical of chordwise specimens.

E. BALLISTIC TESTING

On the basis of the data obtained by pendulum impact testing, a series of composites was selected for ballistic impact testing. Matrices of 6061, 1100, Ti-6Al-4V, and hybrid aluminum-titanium were selected to make comparisons on the basis of matrix plasticity and shear strength. In addition, both 5.6 mil and 8.0 mil diameter fibers were utilized as well as orientation of $\pm 45/0$, ± 22, and 0. Because of the very important effect of specimen geometry noted during pendulum impact, comparisons were made between cantilevered and simply supported specimens whenever possible.

The ballistic test data are presented in Tables XIV, XV, and XVI. In each case the specimen numbers and descriptions are given, along with a series of projectile impact velocities. Resultant specimen condition is indicated, in each case, by a notation beneath each of the impact velocities.

The data in Table XIV are for multiple impacts of specimens, which were performed to attain an indication of the relative damage tolerances of each material. The remaining tests, Tables XV and XVI, were then performed using only one impact per specimen.

(1) Matrix Composition

As in the case of pendulum impact, matrix composition (matrix shear strength) was an important determinant of composite performance. As an example one can compare the performance of $\pm 22^{\circ}$ oriented specimens reinforced with 5.6 mil boron, Fig. 69. In this series of cantilevered tests the B/6061 specimens deformed much less than B/1100 specimens. The B/6061 specimens also failed at the root after an impact at 936 fps while the B/1100 specimens did not fail until a velocity of 1297 fps was reached and then failure occurred at the point of impact. The very large capacity of the B/1100 specimens to deform relieved the buildup of high tensile stresses in the root area while the higher shear strength 6061 matrix specimens could not achieve the same relief. So, on the basis of survivability in this cantilever test, it could be stated that 1100 matrix specimens appear to be more FOD tolerant than 6061 matrix specimens. Of course, one should also consider the excessive amount of deformation which took place in the case of the B/1100 specimens which could be undesirable for fan blade performance.

It is also interesting to note for the cantilevered tests that both the 6061 and 1100 matrix specimens exhibited approximately the same tolerance for local damage. The B/6061 specimens failed completely at the point of impact (FI) at 1233 fps while the B/1100 specimens failed at this location at 1297 fps.

A similar survivability ranking in the case of the simply supported beam test geometry (Fig. 70) would reverse the order of preference. In this case the B/6061 specimens failed at approximately 1160 fps while the B/1100 specimens failed at a lower velocity of 941 fps. The B/1100 specimens are delaminated and heavily deformed at the region of failure (which corresponds to the region of impact) and it appears that the deformation capacity of the system had been locally exceeded. The higher shear strength 6061 matrix specimens, however, did not delaminate and, because high tensile stresses were not generated near a retention in this test geometry, they deformed under the point of impact until final failure.

Thus, from the above it is clear that material ranking cannot be stated without regard for the test geometry used. It is also anticipated that if the cantilevered specimens had been impacted at several different positions, to alter the ratio of root tensile stresses to local tensile and shear stresses, a variation of material ranking could occur for just cantilevered specimens. The relationship of these test results to fan blade considerations is also very difficult to clearly define. Depending on blade design and location of impact, a wide variety of stress states can be generated by FOD events which could resemble either of the herein described, or other, ballistic tests.

(2) Borsic Reinforced Titanium

Both types of Borsic-reinforced titanium specimens (heavily clad and unclad) behaved like the B/6061 specimens described above. They failed at the root location for the cantilevered tests and showed minimal deformation in this configuration (Fig. 72). In the simply supported test, however, they exhibited a very high resistance to failure and deformed a great deal. Again, this is due to the ability to generate higher ratios of shear to tensile stress in the simply supported configuration. The BORSIC-Ti specimens with 0.012 in. of Ti on each face were among the most impact resistant of all the specimens tested. The large amount of Ti on the surface is clearly the reason for this performance advantage.

(3) Boron-Aluminum-Titanium

Specimens 2473-74 and 2475-76 were constructed with outer layers of Ti over a uniaxial core of B/1100. These specimens, in the cantilever tests, behaved in a manner remarkably similar to the BORSIC-titanium specimens having equivalent thickness Ti surface layers (Fig. 72). They failed at the root at velocities in the same range. The simply supported specimens, however, failed at much lower velocities than the similar BORSIC-Ti specimens. This relates, again, to the poor performance of the 1100 matrix material in the simply supported test. The local shear stresses and extensive interlaminar deformation exceed the capacity of the 1100 aluminum. This is most

pronounced in the simply supported (S.S.) configuration because the ratio of maximum shear stress to maximum tensile stress for a S.S. beam is twice that of a cantilevered beam of the same dimensions. It would appear that for the construction of future hybrids of this type, a higher strength 6061, 2024, or 5052/5056 matrix should be used.

(4) Fiber Diameter

Three sets of ballistic specimens were fabricated, and tested in the cantilevered configuration using 8.0 mil diameter boron in the 1100 matrix. As would be expected from the pendulum impact data, these specimens all exhibited high levels of deformation, Figs. 73, 74. By cladding a uniaxially reinforced composite with 0.015" thick surface layers of Ti-6Al-4V it was possible to achieve the most impact resistant composite of the entire program. The comparison between 8 mil and 5.6 mil boron reinforced 1100, in the $\pm$22 orientation, indicates that little if any advantage is achieved with the larger diameter fiber. Comparison of Figs. 69 and 73 indicates that both composite types exhibit large amounts of deformation prior to failure at both impact site and root. The magnitude of the differences between the above specimens is, however, somewhat clouded by the variation in thickness. It is likely that this effect is at least linear and, in fact, may go as the square of the thickness, in which case ranking may change. Again, geometry effects become every bit as important as material effects.

IV. SUMMARY AND CONCLUSIONS

The initial purpose of this program was to achieve a metal matrix composite with optimum impact resistance. It has been demonstrated, however, that a material fabrication and test program cannot achieve this goal in a simple "build and bust" manner. Metal matrix composites, because of their multiplicity of failure modes, can exhibit a wide range of impact tolerance depending on not only material, but also imposed stress state.

The major test technique utilized during this program was a three point bend instrumented pendulum impact procedure, based on the standard Charpy impact test. This test technique provides not only the total energy dissipated by a specimen during impact, but also a continuous record of the load applied to the specimen throughout the impact event. It was this ability to characterize the loading history of an impacted specimen which led to the use of the interaction diagram concept to describe the impact load tolerance of composite and also monolithic material specimens. Based on a simple beam analysis, used in the past to reconcile specimen geometry and material variables in the short beam shear test, it was possible to demonstrate that measured material impact resistance is significantly influenced by applied stress state. It is the interaction of this imposed stress state with the multiple failure modes of the composite specimens which then determined composite behavior. Composite specimens which were fabricated to have a small (L/h) ratio of span length (L) to width (h) were subjected to a large ratio of maximum applied shear stress to flexural stress. These specimens would tend to deform in shear prior to extensive crack growth and the maximum load sustained during impact would be controlled by the shear strength of the matrix. Such specimens would frequently appear highly deformed after impact and very large levels of impact energy were usually dissipated. In contrast, specimens of the same composite material could be made to behave in a fully elastic manner during impact by testing with a much larger (L/h) ratio. The uppermost specimen in Fig. 8 illustrates the test specimen geometry while the load-deflection traces in Fig. 12 demonstrate the very significant variation possible. A single composite material, in this case 5.6 mil boron reinforced 6061 can exhibit a significant variation in load-deflection history. With an L/h ratio of 3.8 the material is capable of large scale deformation prior to crack growth and, when crack growth does occur, it occurs in a controlled manner, i.e., additional increments of energy must be supplied to continue crack growth. In contrast, the very same material tested with an L/h ratio of 21.4, exhibited no evidence of plasticity and complete specimen fracture occurred utilizing the elastic energy stored in the specimen and test system prior to instability. Figures 11 and 12 further demonstrate the point.

For Fig. 11, the maximum load sustained by each specimen was converted to the maximum applied flexural stress, and plotted as a function of (L/h). Only for values of (L/h) greater than approximately 11 was there the expected constancy of composite tensile strength. Below this value matrix shear determined specimen strength. Similarly, it is shown in Fig. 13 that for (L/h) values less than 11 the energy per unit volume required to raise specimens to their maximum load prior to fracture is well above that required elastically.

Thus it was demonstrated that the interaction between applied stress state (which is controlled by test configuration) and composite failure modes (which are controlled by composite failure criteria) both determine overall composite response. No one single test can be used to determine a fundamental quantity which characterizes material impact tolerance. It was shown that the combined use of interaction diagrams Figs. 10, 11, 14, 15, 16, 48, 61, 65 and energy dissipation vs (h) diagrams, Figs. 60, 66 provides a much more complete picture of the impact tolerance of composite specimens. In addition, comparisons can be made with existing engineering materials.

The second test technique used to evaluate impact resistance was a ballistic test. Small RTV cylinders were fired over a range of velocities at composite specimens. Once again, to point out the importance of test geometry, specimens were held in both simply supported and cantilevered configurations. Impact tolerance was then judged on the basis of the projectile velocities required to cause visible damage and fracture of the specimens. As in the case of the pendulum impact test, specimen behavior was related to both the material and the test geometry. It was shown that relative material rankings could be altered by changing the test procedure and again, higher levels of plasticity and specimen deformation were obtained for test configurations which maximized applied shear stresses and minimized beam surface flexural stresses.

One of the most important points to be noted from this study is that very substantial changes in composite performance can be achieved by changing material composition and layup. Levels of energy dissipation can exceed those of monolithic aluminum and titanium alloys, if these materials are constrained to fail locally, i.e., in the presence of stress raisers such as a notch. Composites containing low shear strength matrices such as 1100 aluminum, with high strength fibers, cause extensive shear deformation to take place over large volumes of matrix material. The use of larger diameter fibers, of high strength, provides both longer transfer lengths and more massive inter-fiber matrix areas for shear deformation to take place. For this reason, of the uniaxially reinforced composites, 8 mil boron reinforced 1100 dissipated the highest levels of energy. This ability to deform also extends over

a large range of (L/h) values. It is, however, obtained at the expense of composite maximum load carrying capability. Thus 1100 matrix specimens will deform under a lower threshold impact event than comparable 6061, 2024 or even Ti-6Al-4V matrix specimens. Further, it is only by deformation that 1100 matrix composites can indicate a superiority over higher shear strength matrix composites. Thus, increased resistance to catastrophic failure and material separation can be achieved by paying the penalty of structural deformation. Clearly, in the case of close tolerance aerodynamic structures such as fan blades, a careful balance must be achieved between threshold level and deformability.

A highly deformable matrix can also provide a benefit in reducing the stresses transmitted to other areas of a fan blade removed from the point of impact. Thus, the choice of air foil deformation threshold must be chosen in light of the blade root retention construction. Blade designs incorporating high strength retention schemes will likely permit the use of higher shear strength matrices in the air foil.

The use of Ti-6Al-4V foils to hybridize aluminum matrix specimens was shown to be an effective way to increase ballistic impact tolerance. It was also shown, however, that since the titanium foils are essentially bonded together with interlayers of aluminum alloy, in the presence of high interlaminar shear stresses (effectively low L/n region) composite performance is once again controlled by the aluminum matrix.

The all titanium matrix composite system was shown to behave in a less ductile manner due to the very high shear strength of the matrix. Thus, of all the systems, this one dissipated the lowest levels of energy over the largest range of L/h values. It, however, has one significant advantage. It can be bonded to a surface layer of titanium by a very high shear strength bond. During impact this lowers the effective flexural stresses on the composite and, most significantly, provides a very effective FOD tolerant cladding.

From the above it can be concluded that the achievement of the maximum FOD tolerance in a structure will require knowledge about both overall material performance and the stress state during operation and impact. Ultimate success without both of these will not be impossible, however, it will be fortuitous.

V. FUTURE DIRECTIONS

The following are areas in which future research should be conducted to improve the FOD tolerance of metal matrix composite materials and fan blades fabricated out of these composites.

- Additional laboratory scale testing should be performed to provide a technique which will provide meaningful quantitative data characterizing the impact resistance of composites. The results of this program are a first step along this line.

- Ballistic testing of specimens closely resembling the intended fan blade application should be pursued. The choices of specimen and test geometries are critical and should be based on probable real blade design concepts. The data obtained from this type of test are necessary to assess the validity of any laboratory test procedures.

- Because of recent advances made in the low cost fabrication of metal matrix composites, emphasis should be placed on evaluating the impact tolerance of materials made by these new procedures. Future fan blades will have to combine low cost and FOD tolerance.

Table I

Experimentally Determined Properties of Plasma Sprayed Material with Foil

Alloy	Elastic Modulus 10^6 psi	Yield Stress at 0.2% Offset 10^3 psi	Ultimate Tensile Strength 10^3 psi	Strain to Fracture (1 in. gage length)
6061	10.2	11.2	19.6	16%
2024	10.4	18.6	35.0	13%
1100-1145	9.1	6.2	12.5	20%
5052/56	9.8	19.5	38.6	13%

Typical Properties of Wrought Material in the Annealed Condition*

Alloy	Yield Stress 10^3 psi	Ultimate Tensile Strength 10^3 psi	Strain to Fracture (2 in. gage length)
6061	8.0	18.0	25%
2024	11.0	27.0	20%
1100	5.0	13.0	35%
5052	13.0	28.0	25%
5056	22.0	42.0	35%

* "Aluminum, Vol. 1 Properties, Physical Metallurgy and Phase Diagrams" Ed. by Kent R. Van Horn, 1967

Table II

5.6 mil Boron-Uniaxially Reinforced Pendulum Impact Specimens

Composite	Orientation	Matrix	v/o Fiber	Notch	Net Width* (in.)	Impact Energy (ft-lbs)	Maximum Load (lbs)	Post Impact Condition
2223-1	LT-edge	1100	52	Yes	0.318	31	1,860	2 pcs
-2	LT-chord	1100		Yes	0.318	52	1,670	2 pcs
2257-1	LT-chord	1100	54	Yes	0.274	29	1,623	2 pcs
-2	LT-chord	1100		Yes	0.318	48	1,461	Bent - delam.
-3	LT-chord	1100		No	0.394	39	1,692	Bent - shear end
2260-1	LT-chord	1100	54	Yes	0.215	11.5	1,210	2 pcs
-2	LT-chord	1100		Yes	0.215	13.3	1,392	2 pcs
-3	LT-chord	1100		No	0.294	23	1,624	Bent - shear end
-4	LT-chord	1100		No	0.294	-		
2259-1	LT-chord	1100	53	Yes	0.121	3.9	450	2 pcs
-2	LT-chord	1100		Yes	0.121	4.2	492	2 pcs
-3	LT-chord	1100		No	0.200	12.0	853	Bent - shear end
-4	LT-chord	1100		No	0.200	14.4	881	Bent - shear end
2258-1	LT-chord	1100	51	No	0.076	1.6	264	2 pcs
-2	LT-chord	1100		No	0.076	1.6	241	2 pcs
2274-1**	LT-chord	1100	54	No	0.396	-	990	Bent - shear end
-2**	LT-chord	1100		Yes	0.315	-	960	Bent - delam.
-3	LT-chord	1100		Yes	0.315	60	1,300	Bent - delam.
-4	LT-chord	1100		No	0.394	29	1,375	Bent - shear end
2275-1	TT	1100	54	Yes	0.301	0.33	223	2 pcs
-2	TT	1100		Yes	0.301	0.34	172	2 pcs
-3	TT	1100		No	0.392	0.52	311	2 pcs
-4	TL	1100		No	0.395	0.46	338	2 pcs

* This dimension corresponds to the overall width minus the notch depth for notched specimens.
**Slow bend test.

Table II (Cont'd)

Composite	Orientation	Matrix	v/o Fiber	Notch	Net Width (in)	Impact Energy (ft-lbs)	Maximum Load (lbs)	Post Impact Condition
2302-1	LT-chord	1100	55	Yes	0.311	28	1,950	2 pcs
-2	LT-chord	1100		No	0.390	54	2,600	2 pcs
2303-1	LT-chord	1100	54	Yes	0.317	20	1,485	2 pcs
-2	LT-chord	1100		No	0.396	41	1,810	4 pcs - delam.
2286-1	LT-chord	6061	53	Yes	0.323	16	2,412	2 pcs
-2	LT-chord	6061		Yes	0.323	16	2,365	2 pcs
-3	LT-edge	6061		Yes	0.317	19	2,226	2 pcs
-4	LT-edge	6061		Yes	0.317	20	2,319	2 pcs
2287-1	LT-chord	6061	53	Yes	0.329	26	2,783	2 pcs
-2	LT-chord	6061		No	0.411	34	3,200	2 pcs
-3	LT-chord	6061		Yes	0.408	54	3,334	2 pcs
-4	LT-chord	6061		Yes	0.406	36	3,200	2 pcs
2288-1	LT-chord	6061	50	No	0.071	1.1	250	2 pcs
-2	LT-chord	6061		No	0.071	1.1	278	2 pcs
-3	LT-chord	6061		No	0.071	-	306	2 pcs
2289-1	TT	6061	54	Yes	0.321	0.78	482	2 pcs
-2	TT	6061		Yes	0.329	0.79	427	2 pcs
-3	TT	6061		No	0.408	1.20	-	2 pcs
-4	TT	6061		No	0.400	-	436	2 pcs
2310-1	LT-chord	5052/56	56	Yes	0.304	10	3,240	2 pcs
-2	LT-chord	5052/56		Yes	0.304	10	3,110	2 pcs
-3	LT-chord	5052/56		No	0.383	21	4,910	2 pcs
-4	LT-chord	5052/56		No	0.383	20	4,910	2 pcs

Table II (Cont'd)

Composite	Orientation	Matrix	v/o Fiber	Notch	Net Width (in.)	Impact Energy (ft-lbs)	Maximum Load (lbs)	Post Impact Condition
2309-1	LT-chord	5052/56	54	No	0.066	0.97	306	2 pcs
-2	LT-chord	5052/56		No	0.066	0.97	297	2 pcs
2304-1	LT-chord	2024	56	Yes	0.300	10	-	2 pcs
-2	LT-chord	2024		Yes	0.300	10	3,340	2 pcs
-3	LT-chord	2024		No	0.379	20	4,920	2 pcs
-4	LT-chord	2024		No	0.379	20	4,720	2 pcs
2305-1	LT-chord	2024	52	No	0.068	0.94	278	2 pcs
-2	LT-chord	2024		No		0.96	297	2 pcs
-3	LT-chord	2024		No		-	288	2 pcs

Table III

Tensile Test Data
5.6 mil Boron-Reinforced Aluminum

Comp. No.	Matrix	Vol % Fiber	Layup	UTS 10^3 psi	E 10^6 psi	ε_f %
2273	1100	53	[0]	242.5	34.4	0.87
				231.5	33.7	0.70
				234.0		
				220.0		
2278	1100	52	[±22]	51.1	-	-
				80.5	-	-
				60.0	-	-
				81.6	-	-
2279	1100	52	[±45]	8.2		
				8.1		
				7.0		
				6.7		
2280	1100	54	$[\pm 45/0_3]_s$	147.2	-	-
				152.9	-	-
				148.9	-	-
				160.5	-	-
2281	1100	54	$[0/-45/0/+45/0]_s$	144.5	-	-
				150.0	-	-
				148.8	-	-
				152.2	-	-
2282	1100	52	$[0/-22/0/+22/0]_s$	161.0	-	-
				142.5	-	-
				145.0	-	-
				143.0	-	-
2283	6061	50.6	[0]	181.0	35.3	0.606
				226.0	34.2	0.76
				232.5		
				222.0		

Table III (Cont'd)

Comp. No.	Matrix	Vol % Fiber	Layup	UTS 10^3 psi	E 10^6 psi	ε_f %
2284	6061	49	[±22]	146.0	29.4	1.24
				157.5	31.3	1.42
				138.0		
				153.0		
2285	6061	51	[±45]	52.5	-	
				63.5	-	43.5
				45.5	-	38.5
				52.7	-	43.0
2306	2024	52	[0]	229.0	36.8	0.70
				224.0	37.0	0.66
				227.0		
				194.0		
2307	5052/56	53	[0]	268.2	39.5	0.85
				215.5	35.8	0.66
				241.0		
				254.0		
2419	6061	50	$[\pm 45/0_3]_s$	172.6	28/18	0.90
				166.8	30/19	0.86
2422	1100	53	$[\pm 45/0_3]_s$	145.5	27/19	0.81
				140.4	25/19	0.76
2428	6061	52	$[\pm 45/0_3]_s$	169.7	33/19	0.86
				176.8	31/20	0.88

Table IV

5.6 mil Boron - ±22° Reinforced Pendulum Impact Specimens

Composite Number	Orientation	Matrix	v/o Fiber	Notch	Net Width (in.)	Impact Energy (ft-lbs)	Maximum Load (lbs)	Post Impact Condition
2262-1	Chord	1100	54	Yes	.315	30	1670	2 pcs
-2	Chord	1100		Yes	.315	54	1693	Bent + Delam.
-3	Chord	1100		No	.393	52	2180	2 pcs
2262-1	Chord	1100	54	Yes	.121	2.8	371	2 pcs
-2	Chord	1100		Yes	.119	3.1	380	2 pcs
-3	Chord	1100		No	.198	8.4	909	2 pcs
-4	Chord	1100		No	.196	9.4	928	2 pcs
2261-1	Chord	1100	53	No	.073	1.71	167	2 pcs
-2	Chord	1100		No	.073	1.76	172	2 pcs
2276-1	Edge	1100	54	Yes	.307	19	2782	2 pcs
-2	Edge	1100		Yes	.313	24	2782	2 pcs
-3	Edge	1100		No	.394	48	3617	2 pcs
2326-1	Chord	6061	53	No	.088	1.71	361	2 pcs
-2	Chord	6061		No	.088	1.76	371	2 pcs
2327-1	Chord	2024	54	No	.079	1.36	371	2 pcs
-2	Chord	2024		No	.079	1.48	371	2 pcs

5.6 mil Boron - ±68 Reinforced Pendulum Impact Specimens

2277-1	Chord	1100	54	No	.397	18	464	Bent
-2	Chord	1100		No	.397	16	417	Bent
-3	Edge	1100		No	.392	8	417-456	2 pcs
-4	Edge	1100		No	.393	9	315-408	2 pcs

Table V

5.6 Mil Boron - ±45° Reinforced Pendulum Impact Specimens

Composite Number	Orientation	Matrix	v/o Fiber	Notch	Net Width (in)	Impact Energy (ft-lbs)	Maximum Load (lbs)	Post Impact Condition
2226-1	Chord	1100	53	No	0.407	92	1625	Bent
-2	Edge	1100		No	0.395	95	-	Bent
2230-1	Chord	1100	53	No	0.201	13.25	-	Bent
-2	Chord	1100		No	0.201	12.67	260	Bent
2231-1	Chord	1100	53	No	0.066	1.23	33	Bent
-2	Chord	1100		No	0.067	1.18	26	Bent
2232-1	Chord	1100	51	No	0.028	0.23	7.4	Bent
-2	Chord	1100		No	0.028	0.22	5.6	Bent
2322-1	Chord	6061	49	No	0.435	155	3080	Bent
-2	Edge	6061		No	0.396	105	2410	2 pieces
2323-1	Chord	6061	47	No	0.090	2.92	70	
-2	Chord	6061		No	0.090	3.03	72	
2324-1	Chord	2024	56	No	0.380	88	2790	Bent
-2	Chord	2024		No	0.380	75	2500	Bent
2325-1	Chord	2024	54	No	0.077	3.53	-	Bent
-2	Chord	2024		No	0.077	3.62	98	Bent

Table VI

5.6 mil Boron - Comparison of Shell-Core and Distributed Ply Concepts

Panel Identification	Lamination Information	Matrix	v/o Fiber	Notch	Net Width (in.)	Impact Energy ft-lbs	Maximum Load lbs	Post Impact Condition
[illegible]-1	$[\pm 45_2/0_4]_s$	1100	50%	No	0.370	1.9	3[illegible]	Bent
-2	"		52%		0.370	1.4	3[illegible]	2 pieces
-3	$[\pm 45_2/0_4]_s$		52%		0.370	1.[illegible]	1[illegible]	
-4	"		52%		0.37[illegible]	1.[illegible]	3[illegible]	
[illegible]-1	$[\pm 45_2/0_4]_s$		54.7		0.196	11.7	[illegible]6	
-2	"		54.3		0.196	11.6	9[illegible]	
-3	$[\pm 45_2/90_2/0_2]_s$		54.[illegible]		0.19[illegible]	10.[illegible]	39[illegible]	Bent and partial
-4	"		54.7		0.19[illegible]	11.7	41[illegible]	fracture
3370-1	$[90/\pm 45\ 90_2/\pm 45/90_2]_s$		50%		0.370	1.9	[illegible]0	2 pieces
-2	"		50%		0.370	1.[illegible]	7[illegible]	
-3	$[90/\pm 45\ 90_2/\pm 45/90_2]_s$		50%		0.370	1.9	1[illegible]6	
-4	"		50%		0.370	1.[illegible]	1[illegible]4	
[illegible]-1-1	$[90/\pm 45\ 90^{\circ}\pm 45/90_3]_s$		53%		0.[illegible]0	1.[illegible]	5[illegible]0	
[illegible]-2	"		53%		0.3[illegible]	1.[illegible]	5[illegible]0	
[illegible]-1	$[90/\pm 45/0\ \pm 45/0_3]_s$		53%		0.[illegible]0	2.[illegible]	1[illegible]2	
[illegible]-2	"		53%		0.[illegible]0	1.[illegible]	1[illegible]2	

Table VII

8.0 Mil Boron-Uniaxially Reinforced Pendulum Impact Specimens

Composite	Orientation	Matrix	v/o Fiber	Notch	Net Width (in)	Impact Energy (ft-lbs)	Maximum Load (lbs)	Post Impact Condition
2242-1	LT-Chord	1100	57	Yes	0.315	78	-	
-2	LT-Edge	1100		Yes	0.315	66	-	
2293-1	LT-Chord	1100	55	Yes	0.337	59	1,580	2 pcs + Delam.
-2	LT-Chord	1100		Yes	0.337	77	1,625-1,715	No Brk + Delam.
-3	LT-Chord	1100		No	0.416	49	1,760-1,810	Delam + Shear-Off End
2294-1	LT-Chord	6061	55	Yes	0.339	14	3,430	2 pcs
-2	LT-Chord	6061		Yes	0.339	14	3,430	2 pcs
-3	LT-Chord	6061		No	0.418	25	4,460	2 pcs
2297-1	LT-Chord	1100	53	No	0.073	3.4	167	2 pcs
-2	LT-Chord	1100		No		3.0	185	2 pcs
-3	LT-Chord	1100		No		-	-	-
-4	LT-Chord	1100		No		-	232	2 pcs
2298-1	LT-Chord	6061	53	No	0.073	1.1	218	2 pcs
-2	LT-Chord	6061		No		1.1	218	2 pcs
-3	LT-Chord	6061		No		-	232	2 pcs
-4	LT-Chord	6061		No		-	260	2 pcs
2311-1	LT-Chord	1100	51	No	0.075	2.1	315	2 pcs
-2	LT-Chord	1100		No	0.075	1.6	297	2 pcs
-3	LT-Chord	1100		No	0.075	1.8	278	2 pcs
2312-1	LT-Chord	1100	51	No	0.075	1.4	315	2 pcs
-2	LT-Chord	1100		No	0.075	1.7	334	2 pcs

Table VII (Cont'd)

Composite	Orientation	Matrix	v/o Fiber	Notch	Net Width (in)	Impact Energy (ft-lbs)	Maximum Load (lbs)	Post Impact Condition
2313-1	LT-Chord	1100	51	No	0.075	1.3	297	2 pcs
-2	LT-Chord	1100		No	0.075	1.3	315	2 pcs
2314-1	LT-Chord	1100	51	No	0.075	1.2	297	2 pcs
-2	LT-Chord	1100		No	0.075	1.3	315	2 pcs
2315-1	LT-Chord	1100	52	No	0.072	1.3	278	2 pcs
-2	LT-Chord	1100		No	0.072	1.1	278	2 pcs
2316-1	LT-Chord	1100	55	No	0.069	1.2	297	2 pcs
-2	LT-Chord	1100		No	0.069	1.3	294	2 pcs
-3	LT-Chord	1100		No	0.069	1.3	297	2 pcs

Table VIII

A. 8.0 mil Boron-Reinforced Aluminum (Avco Fiber)

Composite Number	Matrix	Vol % Fiber	Layup	0° UTS 10^3 psi	0° E 10^6 psi	0° ϵ_f %	90° UTS 10^3 psi	90° E 10^6 psi	90° ϵ_f %
[illegible]	1100	49	[0]	131.0 110.0 117.5 119.0	32.1 31.[illegible]	0.47 0.[illegible]			
[illegible]	6061	49	[0]	142.5 136.[illegible]	33.6 32.1				
2[illegible]E	6061	49		189.0 210.0					
2303	6061	52	[0]				11.6 9.0 9.6 8.57		0.15 0.21
2243	1100	60	[0]	250.0 208.0	-	-	5.2 4.4	-	-

B. 8.0 mil Boron-Reinforced Aluminum (CMC Fiber)

Composite	Matrix	v/o Fiber %	0° UTS 10^3 psi	0° E 10^6 psi	0° ϵ_f %	90° UTS 10^3 psi	90° E 10^6 psi	90° ϵ_f %
2244	6061	60	287.0 273.0 272.[illegible] 242.[illegible]	37.4 35.3	0.86 0.80	24.[illegible] 20.1 16.4 18.6	18.1 18.2	0.16 0.20

Table IX

Calculated K_{ID} Values for Charpy V-Notch Specimens

Material	Total Crack Length (in)	Total Specimen Width (in)	Maximum Failure Load lbs	K_{ID} ksi$\sqrt{in.}$
6061-T6	0.079	0.394	1670	31.6
	0.174	0.394	835	30.0
			Handbook Value*	26.5
Ti-6Al-4V	0.079	0.394	6500	123.0
	0.174	0.394	3430	123.0
			Handbook Value*	96.0

*Damage Tolerant Design Handbook MCIC-HD-01

Table X

5.6 mil Boron - Uniaxially Reinforced Pendulum
Impact Specimens with 1100 Matrix and Ti-6Al-4V Foil* Additions

Composite	Orientation	v/o Fiber	v/o Ti-6Al-4V	Notch	Net Width (in.)	Impact Energy ft-lbs	Maximum Load lbs	Post Impact Condition
2354-1	LT-Chord	45%	20%	No	0.381	>23	3060	Bent
-2	LT-Edge	45%	20%	No	0.396	16.6	5150	2 pieces
2355-1	LT-Chord	45%	20%	No	0.192	6.6	1040	2 pieces
-2	LT-Chord	45%	20%	No	0.192	6.2	1020	
-3	TT	45%	20%	No	0.196	3.9	370	
-4	TT	45%	20%	No	0.193	4.0	370	
2356 -1	LT-Chord	43%	22%	No	0.067	1.1	255	
-2	LT-Chord	43%	22%	No	0.067	1.1	250	All have one or
-3	TT	43%	22%	No	0.067	1.1	69	more foils untriken
-4	TT	43%	22%	No	0.067	1.0	84	with remainder frac-
2357-1	TT	48%	15%	No	0.200	3.3	510	tured into at least
-2	LT-Chord	48%	15%	No	0.200	8.7	1390	2 pieces
-3	TT	48%	15%	No	0.200	2.-	510	
-4	LT-Chord	48%	15%	No	0.200	7.1	1300	
2358-1	LT-Chord	46%	17%	No	0.070	1.6	232	
-2	LT-Chord	46%	17%	No	0.070	1.3	255	

*Ti-6Al-4V foils are 0.003 in. thick

Table XI

5.7 BORSIC-Uniaxially Reinforced Ti-6Al-4V**

Composite	Orientation	v/o Fiber	Notch	Net Width (in.)	Impact Energy ft-lbs	Maximum Load lbs	Post Impact Condition
SN-139-1	LT-Chord		Yes*	0.327	5.8	-	2 pieces
-2	LT-Chord		Yes*	0.333	7.1	4000	
-3	LT-Edge		Yes*	0.317	3.8	4000	
-4	LT-Edge		Yes*	0.317	4.0	4000	
-5	LT-Chord		No	0.412	11.4	5180	
-6	LT-Chord		No	0.412	9.6	6120	
-7	LT-Edge		No	0.396	7.4	6490	
-8	LT-Edge		No	0.396	7.6	6490	
-9	TT		Yes*	0.332	2.2	1760	
-10	TT		No	0.412	3.3	-	
-11	LT-Chord		Yes*	0.332	6.8	4080	
-12	LT-Chord		Yes	0.313	7.8	3556	
SN-129-3-8	LT-Chord		No	0.052	1.1	144	
-9	LT-Chord		No	0.052	1.0	140	
-11	TT		No	0.052	0.3	74	
-12	TT		No	0.052	0.3	84	
***SN-141-3-8	LT-Chord		No	0.063	2.2	186	
-9	LT-Chord		No	0.063	2.5	167	
-11	TT		No	0.063	0.7	102	
-12	TT		No	0.063	1.1	133	
SN-148-1	LT-Chord		Yes	0.317	7.6	3627	
-2	LT-Chord		Yes	0.317	7.8	3627	
-3	LT-Edge		Yes	0.321	4.7	3840	
-4			Yes	0.321	4.9	3840	
-5			No	0.396	7.9	6542	
-6			No	0.395	7.3	6115	
-7			No	0.202	3.0	1849	
-8			No	0.203	3.3	1849	
-9			No	0.100	1.9	469	
-10			No	0.100	1.8	469	
-12			Yes	0.318	-	3690	
-13			Yes	0.324	-	3840	

Table XI (Cont'd)

Composite	Orientation	v/o Fiber	Notch	Net Width (in.)	Impact Energy ft-lbs	Maximum Load lbs	Post Impact Condition
2472-1	LT-Chord	49	No	0.133	1.9	825	2 pieces
-2	LT-Chord		No	0.132	1.7	711	
2470a-1	LT-Chord	45	No	0.064	1.3	178	
b-1	LT-Chord		No	0.062	1.1	164	
c-1	LT-Chord		No	0.062	1.0	164	

* The notches machined into these specimens were 0.079 in. deep, however, due to the use of the wrong cutting wheel they were flat bottomed - not V-shaped.

** Spec. 129, 139, 141 and 148 were obtained from TRW.

*** Specimens of set 141 all had extra 0.012 in. thick layers of Ti-3Al-2 1/2 V on each surface.

Table XII

Tensile Properties of 5.7 mil BORSIC Uniaxially Reinforced Ti-6Al-4V (UTRC)

Composite Number	v/o Fiber	Orientation	UTS 10^3 psi	E 10^6 psi	ε_f %
2465	51	0°	167.1		
			155.7		
			127.6		
2466	44	0°	150.0		
			134.2		
2467	48	0°	151.8	35.6	0.44
		30 extracted fibers average UTS = (362 ± 83) 10^3 psi			
2468	48	0°	123.6		
			152.1	35.0	0.45
2470a	40	0°	177.3		
			182.7		
2470b	46	0°	163.8		
2469	39	90°	42.3		
			42.8	24.0	0.30
			38.5	28.5	0.21
2471a	38	90°	39.2		
			40.6	29.1	0.22
2471b	38	90°	41.6		
			41.9	31.2	0.25

Table XIII

Tensile Properties of 5.7 BORSIC Uniaxially Reinforced Ti-6Al-4V (TRW)

Specimen Number	Orientation	E 10^6 psi	UTS 10^3 psi	ε_f %
SM-139-3				
-1	0°	38.0	145.8	0.40
-2	0°	39.0	148.0	0.40
-3	0°	-	135.0	-
-4	90°	31.5	53.8	0.46
-5	90°	33.2	62.7	0.55
-6	90°	-	64.0	-
-7	90°	-	64.9	-
SM-141-3*				
-1	0°	34.2	132.0	0.41
-2	0°	33.0	128.0	0.40
-3	30 extracted fibers - avg. UTS = (334 ± 125) x 10^3 psi			
-4	90°	27.4	67.3	0.58
-5	90°	22.8	69.3	0.73
-6	90°	-	65.2	-
-7	90°	-	62.1	-

*Total specimen thickness was 0.063 in. with 0.013 in. of Ti-3-2 1/2 on

Table XIV

Cantilevered Ballistic Impact Specimens
(Multiple Impact per Specimen)

Specimen	Material	Velocity (ft/sec) and Damage						
		V_1	V_2	V_3	V_4	V_5	V_6	V_7
2419-2420	5.6B/6061 $[\pm 45/0_3]_2$ t = 0.070 in.	126 NV	186 NV	331 D	483 D	698 D	884 D	1746 F-I-R
2422-2424	5.6B/1100 $[\pm 45/0_3]_2$ t = 0.067 in.	129 NV	282 NV	467 NV	718 D	910 F-R (Incomplete Fracture)		
2427-2428	5.6B/6061 $[\pm 45/0_3]_2$ t = 0.067 in.	158 NV	339 NV	721 D	858 D	1238 F-R		
SN-129-2	5.7 BORSIC Ti-6Al-4V t = 0.052 in.	133 NV	173 NV	326 D	714 F-R			
2479	5.6B/6061 $[\pm 22]_5$ t = 0.069 in.	188 NV	438 NV	692 NV	841 DI	1122 FR		
2480	5.6B/1100 $[\pm 22]_5$ t = 0.066 in.	196 NV	440 D	694 D-DI	870 D-DI	903 D-DI		
2473-74	5.6B/1100 0° 0.003 in.- Ti-6Al-4V on each face t = 0.053 in.	532 DI	604 DI	688 DI				

Table XIV (Cont'd)

Specimen	Material	Velocity (ft/sec) and Damage						
		V_1	V_2	V_3	V_4	V_5	V_6	V_7
SN-129-1	5.7 BORSIC/ Ti-6Al-4V 0° 0.003 in. - Ti-3-2 1/2 on each face t = 0.052	697 D	872 FR					

NV = no visible damage
D = deformation
F = fracture
I = at impact site
R = at root

Table XV

Cantilevered Ballistic Impact Specimens
(Single Impact per Specimen)

Specimen	Material	Velocity (ft/sec) and Damage					
		V_1	V_2	V_3	V_4	V_5	V_6
2419-2420	5.6B/6061 $[\pm 45/0_3]_s$ t = 0.070 in.	187 NV	383 NV	715 D	1437 F-I-R		
2422-2424	5.6B/1100 $[\pm 45/0_3]_s$ t = 0.067 in.	186 NV	381 D	627 D	1132 F-I		
2427-2428	5.6B/6061 $[\pm 45/0_3]_s$ t = 0.067 in.	202 NV	390 D	607 D	718 D		
SN-129-2	5.7 BORSIC Ti-6Al-4V t = 0.052 in.	172 NV	237 NV	360 NV	647 F-R		
2479	5.6B/6061 $[\pm 22]_5$ t = 0.069	707 D-DI	713 D-DI	936 D-FR	1076 D-FR	1233 FI-FR	
2480	5.6B/1100 $[\pm 22]_5$ t = 0.066	898 D-DI	950 I-DI	1116 CR-DI	1297 CR-FI	1334 FR-FI	1362 FR-FI
2473-74	5.6B/1100 0° 0.003 in. - Ti-6Al-4V on each face t = 0.053 in.	813 DI-FR	844 DI-FR				
2475-76	5.6B/1100 0° 0.009 in. - Ti-6Al-4V on each face t = 0.066 in.	705 D-DI	799 D-DI	845 D-DI	999 D-DI	1050 D-DI	1270 DI-FR

Table XV (Cont'd)

Specimen	Material	Velocity (ft/sec) and Damage V_1	V_2	V_3	V_4	V_5	V_6
SN-129-1	5.7 B0R5IC/ Ti-6Al-4V 0° 0.052 in.	705 D	786 D-FI	816 D-FI	865 D-FI		
SN-141-4,5	5.7 B0R5IC/ Ti-6Al-4V 0° 0.012 in. - Ti-3-2 1/2 on each face t = 0.063	902 D	1011 D-DI	1218 D-DI	1424 D-DI	1510 D-DI-FR	
2578	8.0B/1100 $[\pm 22°]_4$ t = 0.075 in.	446 D	553 D-DI	656 D-DI	1096 D-FI	1116 D-DI-CF	1359 FI-FI
2779	8.0B/1100 $[\pm 45/0_2]_2$ t = 0.075 in.	718 D-DI	792 D-DI	896 I-FI	880 D-DI	1120 FR-FI	1170 FI-FI
2580	8.0B/1100 three layers of 0.005 in. Ti-6Al-4V on each face t = 0.085	880 D-DI	1052 D-DI	1408 D-FI	1562 D-DI	1645 D-DI	1868 D-DI

NV = no visible damage
D = deformation
F = fracture
C = cracking visible
I = at impact area
R = at root area

Table XVI

Simply Supported Ballistic Impact Specimens
(Single Impact per Specimen)

Specimen	Material	Velocity (ft/sec) and Damage				
		V_1	V_2	V_3	V_4	V_5
2419-2420	5.6B/6061 $[\pm 45/0_3]_2$ t = 0.070 in.	199 D	442 D	872 D	1043 D	
2422-2424	5.6B/1100 $[\pm 45/0_3]_2$ t = 0.067 in.	199 D	447 D	907 D	1283 F-I	
2427-2428	5.6B/6061 $[\pm 45/0_3]_2$ t = 0.067 in.	190 D	439 D	897 D	1392 F-I	
SN-129-2	5.7 BORSIC-0° Ti-6Al-4V t = 0.052 in.	190 NV	439 D	903 D	1330 D	
2479	5.6B/6061 $[\pm 22]_5$	846 D	933 D	1155 D	1160 FI	1245 FI
2480	5.6B/1100 $[\pm 22]_5$	352 D	761 D	941 FI	1193 FI	
2473-74	5.6B/1100 0° 0.003 in. - Ti-6Al-4V on each face t = 0.053 in.	549 DI	872 FI	952 FI	1157 FI	1197 FI
2475-76	5.6B/1100 0° 0.009 in. - Ti-6Al-4V on each face t = 0.066 in.	967 DI	1040 DI	1291 FI		

Table XVI (Cont'd)

Specimen	Material	Velocity (Ft/sec) and Damage				
		V_1	V_2	V_3	V_4	V_5
SN-129-4,5	5.7 BORSIC/ Ti-6Al-4V 0° t = 0.052	801 D	803 D	853 D	970 D	
SN-141-2,4	5.7 BORSIC/ Ti-6Al-4V 0° 0.012 in. - Ti-3-2 1/2 on each face t = 0.063 in.	1020 D	1089 D	1124 I	1389 D	

NV = no visible damage
D = deformation
F = fracture
I = at impact site

Table XVII

Unnotched Instrumented Impact Testing of Specimens
Also Tested by Ballistic Impact

Specimen	Material	Total Impact Energy ft-lbs	Maximum Load lbs	Flexural Strength (10^3 psi)
2420	5.6B/6061	1.1	142	170
	$[\pm 45/0_3]_2$	1.0	142	170
	t = 0.070 in.			
2424	5.6B/1100	1.3	121	145
	$[\pm 45/0_3]_2$	1.3	121	142
	t = 0.070 in.			
2428	5.6B/6061	1.0	142	180
	$[\pm 45/0_3]_2$	0.8	142	179
	t = 0.070 in.			
SN-129	5.7 BORSIC/Ti-6Al-4V	1.1	144	320
	0°	1.0	140	310
	0.003" - Ti-3-2 1/2 on each face			
	t = 0.052 in.			
SN-141	5.7 BORSIC/Ti-6Al-4V	2.2	186	280
	0°	2.5	167	252
	0.012" - Ti-3-2 1/2 on each face			
	t = 0.063 in.			
2473-74	5.6B/1100	1.1	139	297
	0°	1.2	139	295
	0.003" - Ti-6Al-4V on each face			
	t = 0.053 in.			
2475-76	5.6B/1100	1.3	174	321
	0°	1.5	174	329
	0.009" - Ti-6Al-4V on each face			
	t = 0.066 in.			

Table XVII (Cont'd)

Specimen	Material	Total Impact Energy ft-lbs	Maximum Load lbs	Flexural Strength (10^3 psi)
2479	5.6B/6061	1.5	191	229
	$[\pm 22°]_5$	1.5	198	223
	t = 0.069 in.			
2480	5.6B/1100	2.5	111	150
	$[\pm 22°]_5$	3.4	125	168
	t = 0.066 in.			
2578	8.0B/1100	1.8	146	146
	$[\pm 22°]_4$	2.0	153	149
	t = 0.075 in.			
2579	8.0B/1100	1.2	97	97
	$[\pm 45/0_2]_2$	1.6	97	100
	t = 0.075 in.			
2580	8.0B/1100	2.5	264	218
	$0°$	2.9	264	216
	three layers of 0.005 in. Ti-6Al-4V on each face			
	t = 0.085			

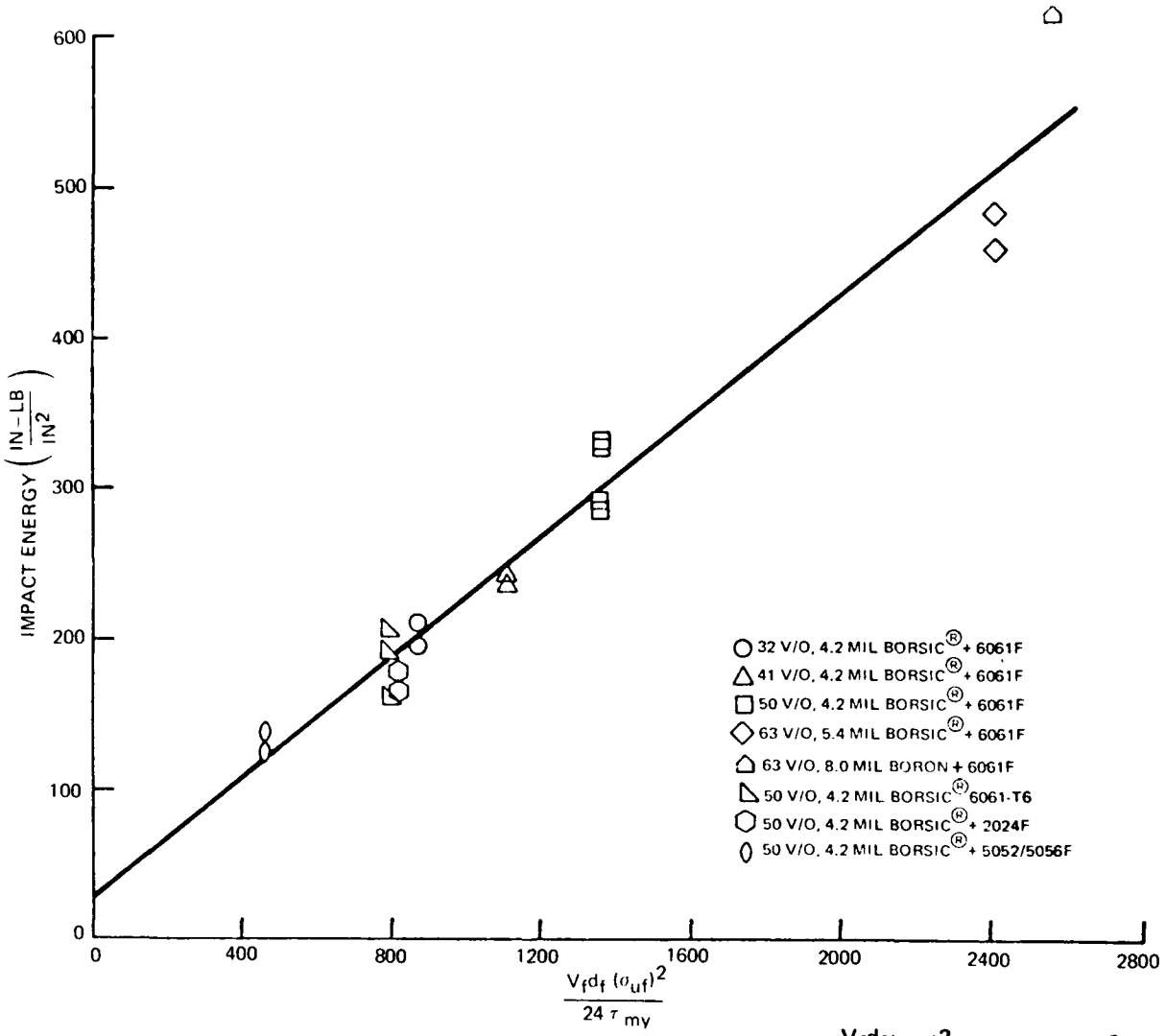

FIG. 1 VARIATION OF IMPACT ENERGY PER UNIT AREA WITH THE PARAMETER $\frac{V_f d_f (\sigma_{uf})^2}{24 \tau_{my}}$ FOR BORSIC ® + ALUMINUM AND BORON + ALUMINUM COMPOSITES OF THE LT TYPE

TOP--NOTCHED ENERGY GREATER THAN 23 FT LBS
BOTTOM UNNOTCHED ENERGY 48 FT LBS
(REF. 2–1972)

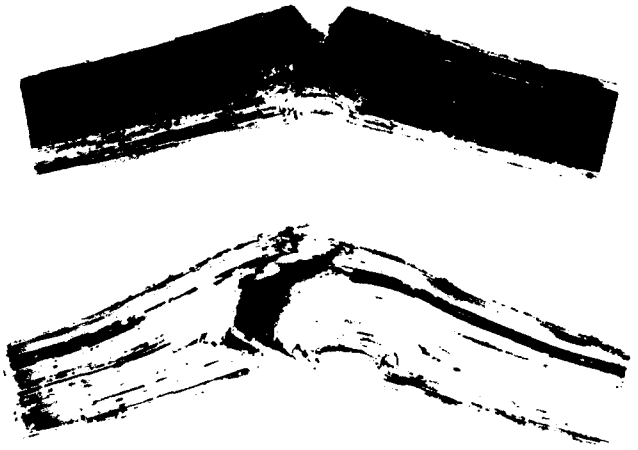

FIG. 2 5.6 mil BORON–1100 ALUMINUM CHARPY IMPACT SPECIMENS

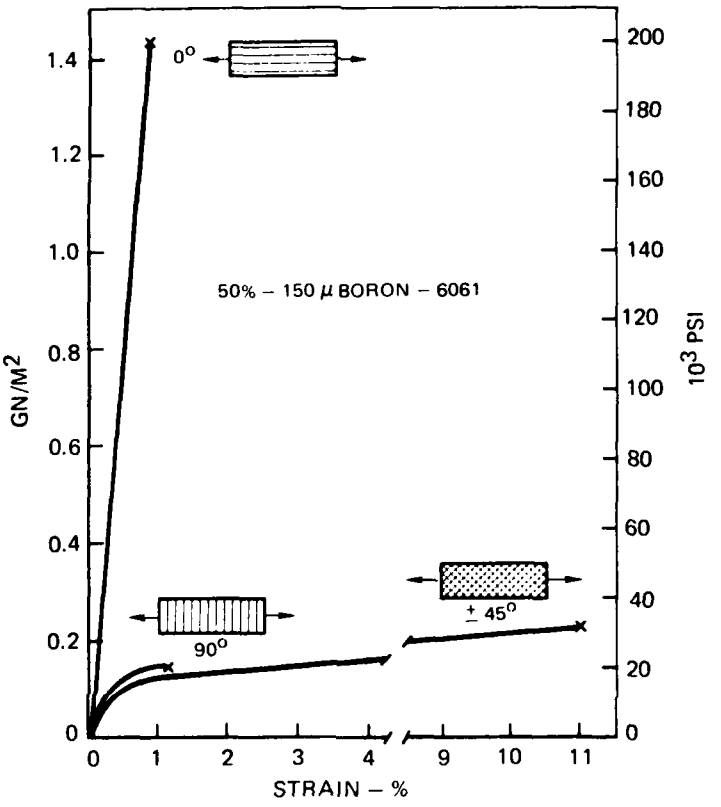

FIG. 3 STRESS STRAIN BEHAVIOR OF 5.6 MIL BORON–6061

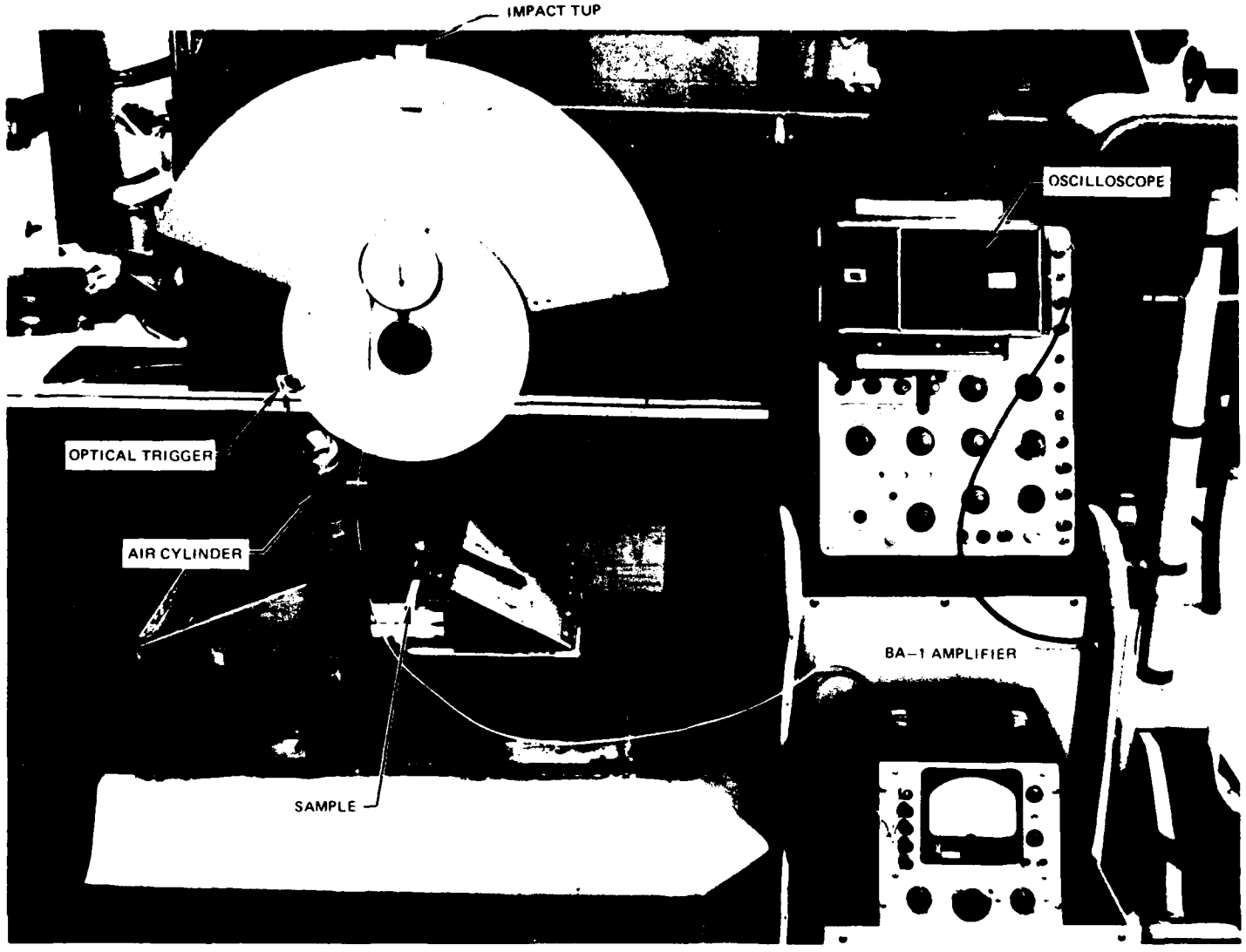

FIG. 4 INSTRUMENTED CHARPY IMPACT MACHINE

STANDARD V NOTCHED SPECIMEN

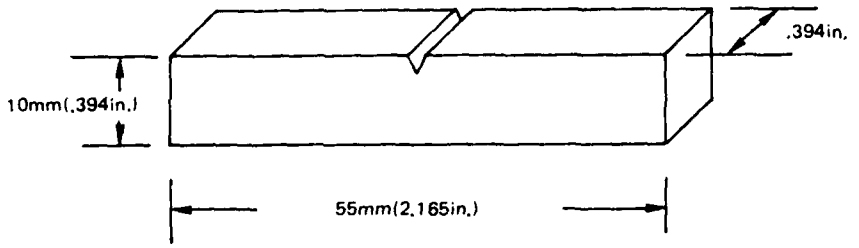

UN–NOTCHED FULL SIZE SPECIMEN

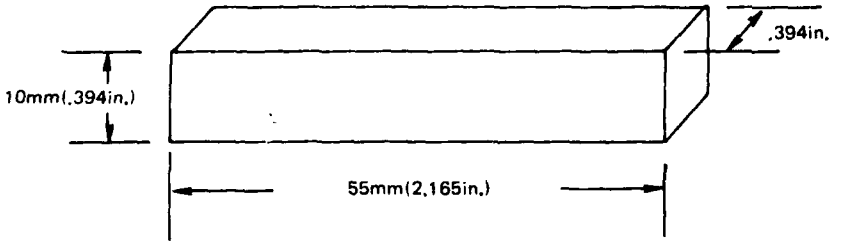

THIN UN–NOTCHED SPECIMEN

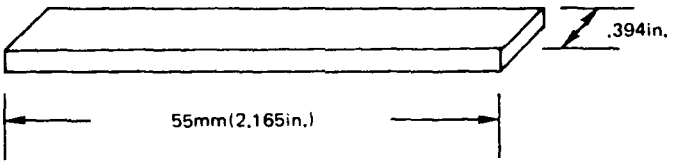

FIG. 5 PENDULUM IMPACT SPECIMEN GEOMETRY

LT–CHORDWISE IMPACT SPECIMEN

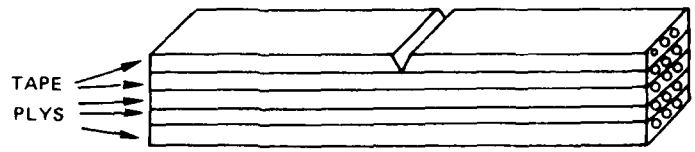

LT–EDGEWISE IMPACT SPECIMEN

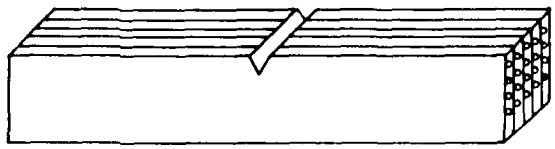

TT–IMPACT SPECIMEN

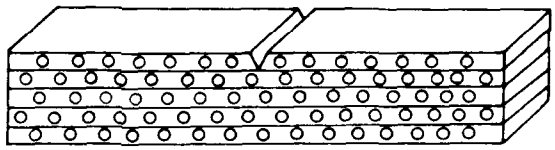

FIG. 6 PENDULUM IMPACT SPECIMEN ORIENTATIONS

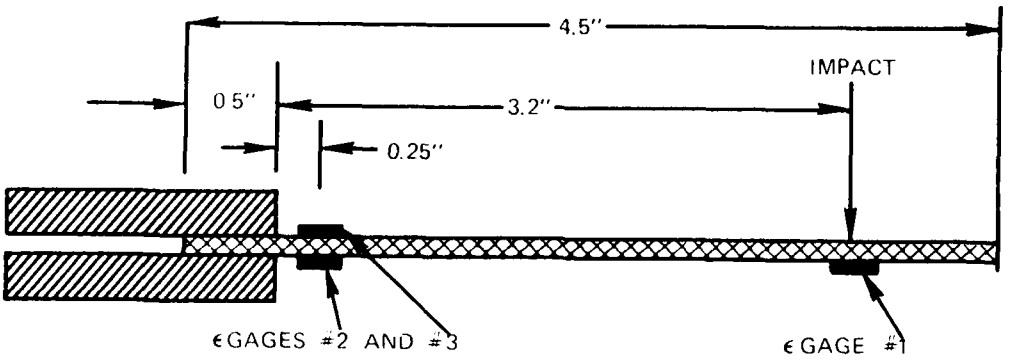

CATILEVERED SPECIMENS

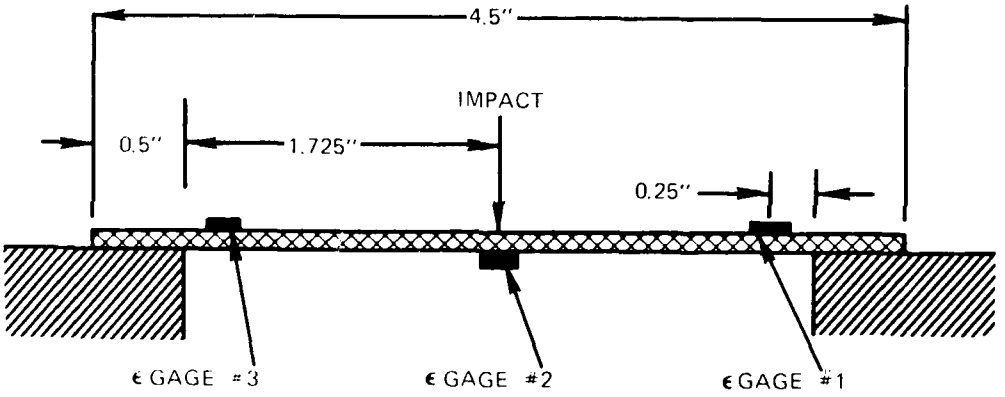

SIMPLY SUPPORTED SPECIMENS

FIG. 7 BALLISTIC IMPACT SPECIMEN CONFIGURATIONS

CHARPY IMPACT

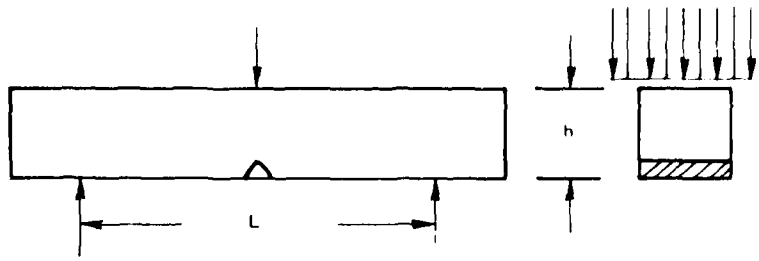

BLADE–OVERALL RESPONSE

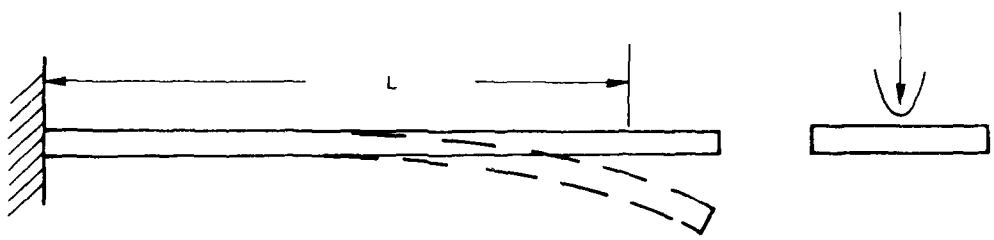

BLADE–LOCAL RESPONSE

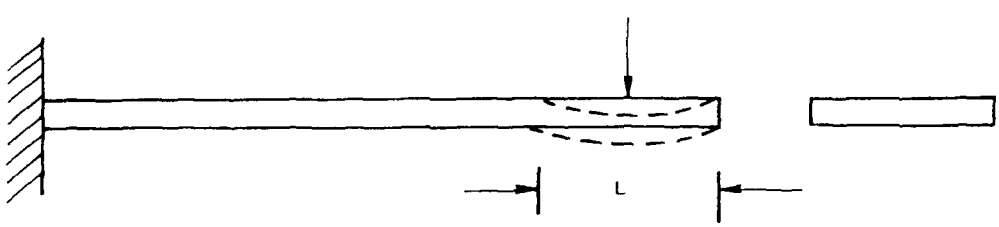

FIG. 8 IMPACT SPECIMEN GEOMETRY

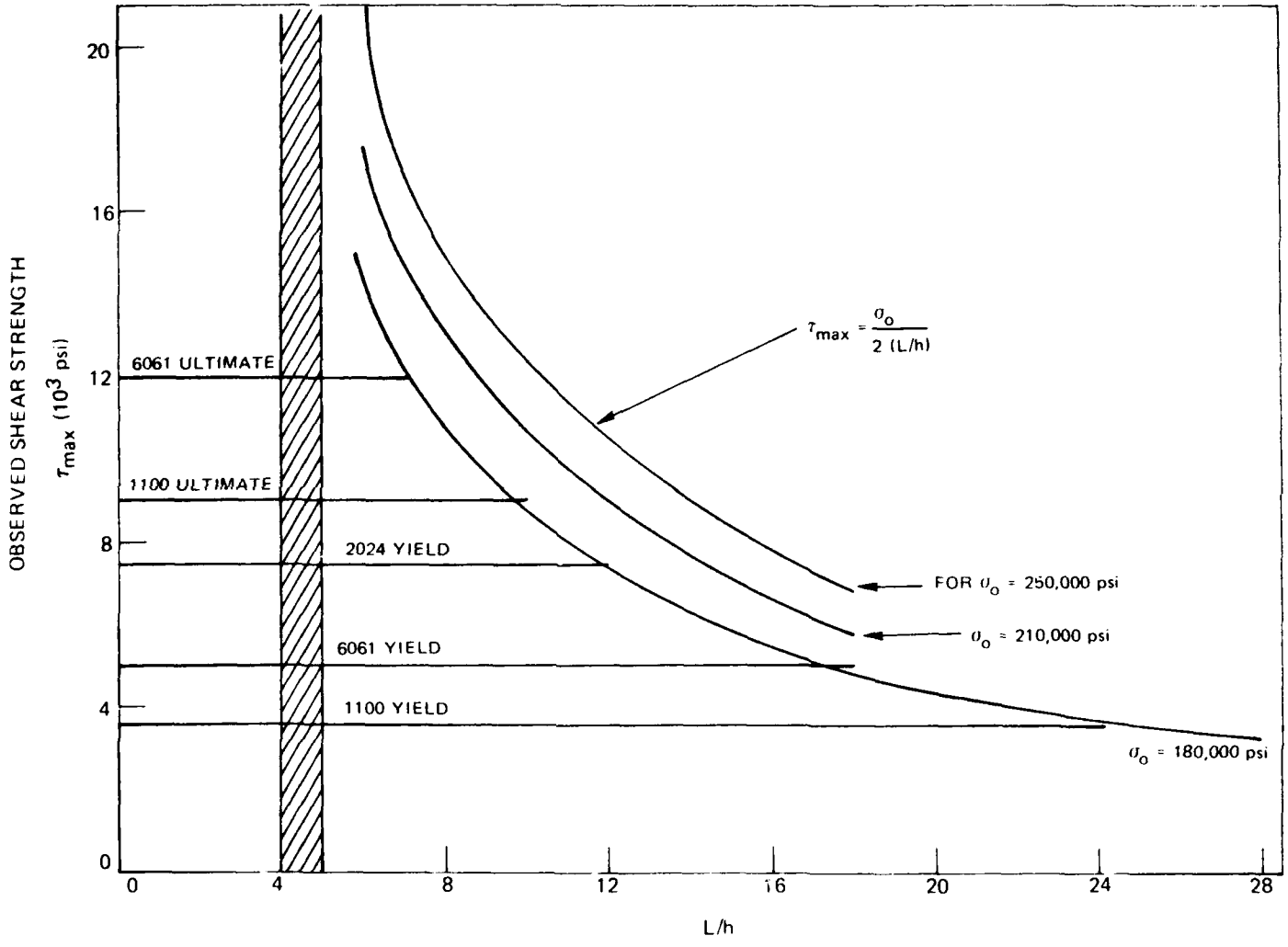

FIG. 9 THEORETICAL SHEAR INTERACTION DIAGRAM FOR ALUMINUM MATRIX COMPOSITES (LT ORIENTATION)

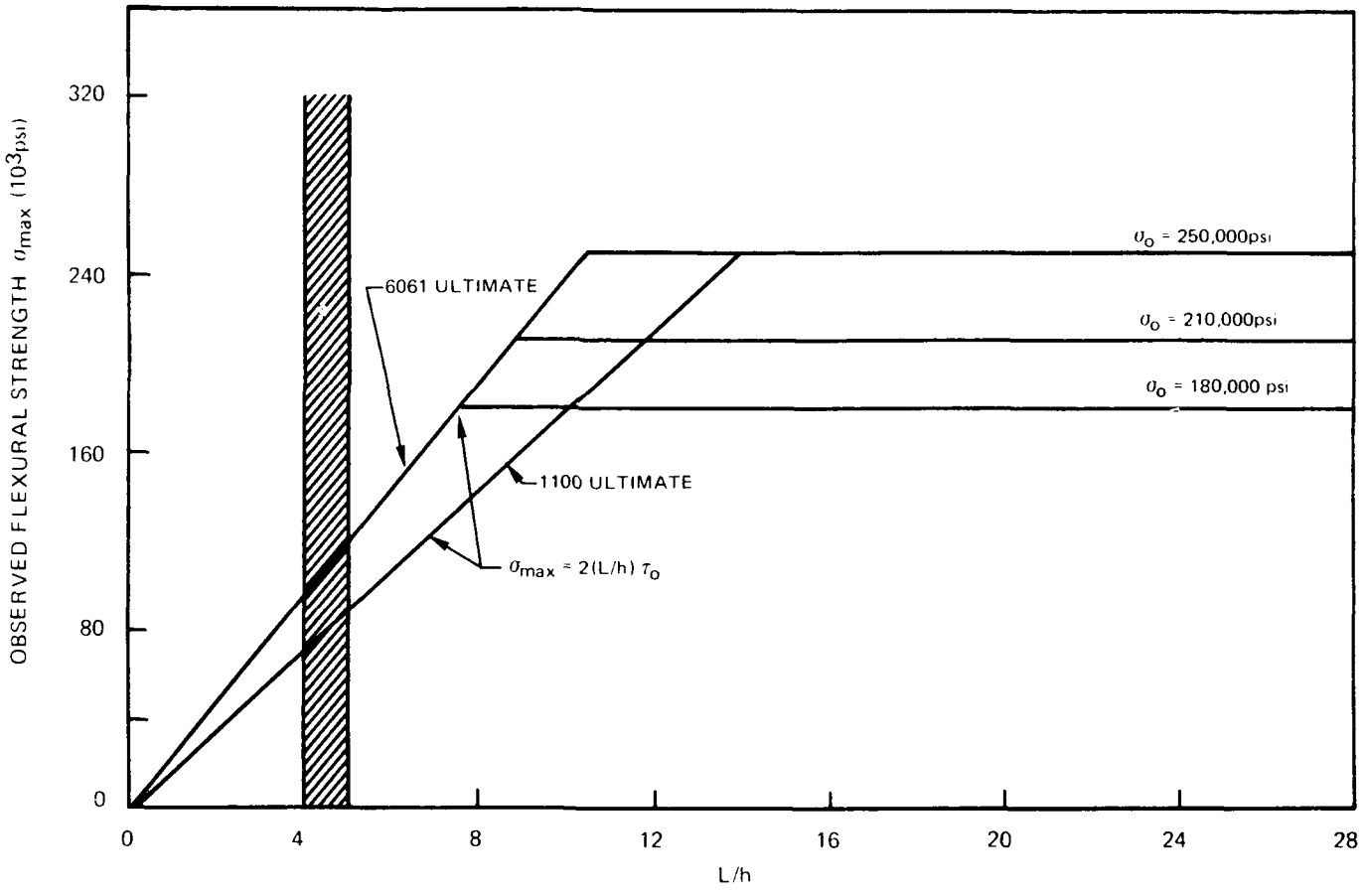

FIG. 10 THEORETICAL FLEXURAL INTERACTION DIAGRAM FOR ALUMINUM MATRIX COMPOSITES (LT ORIENTATION)

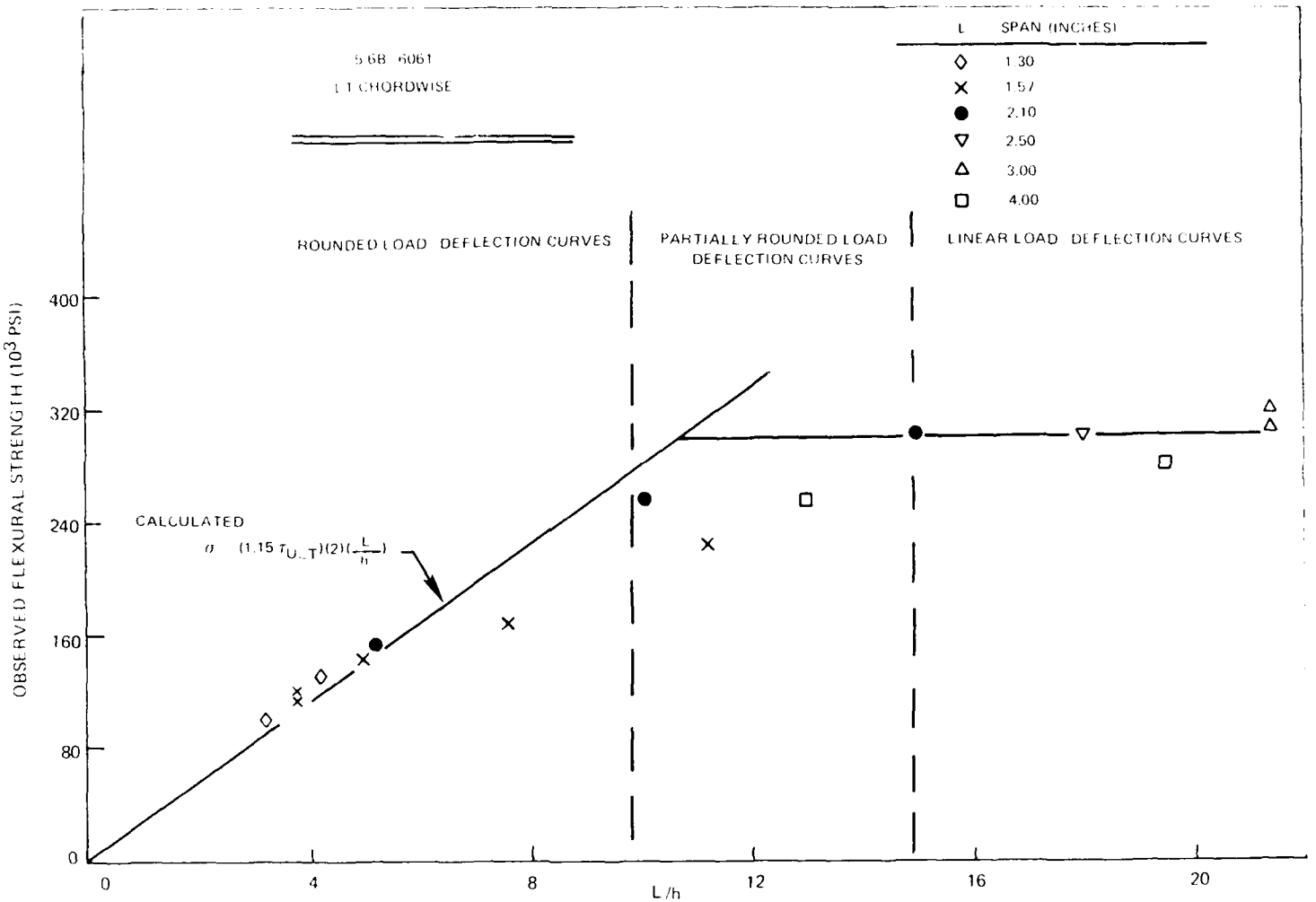

FIG. 11 FLEXURAL INTERACTION DIAGRAM

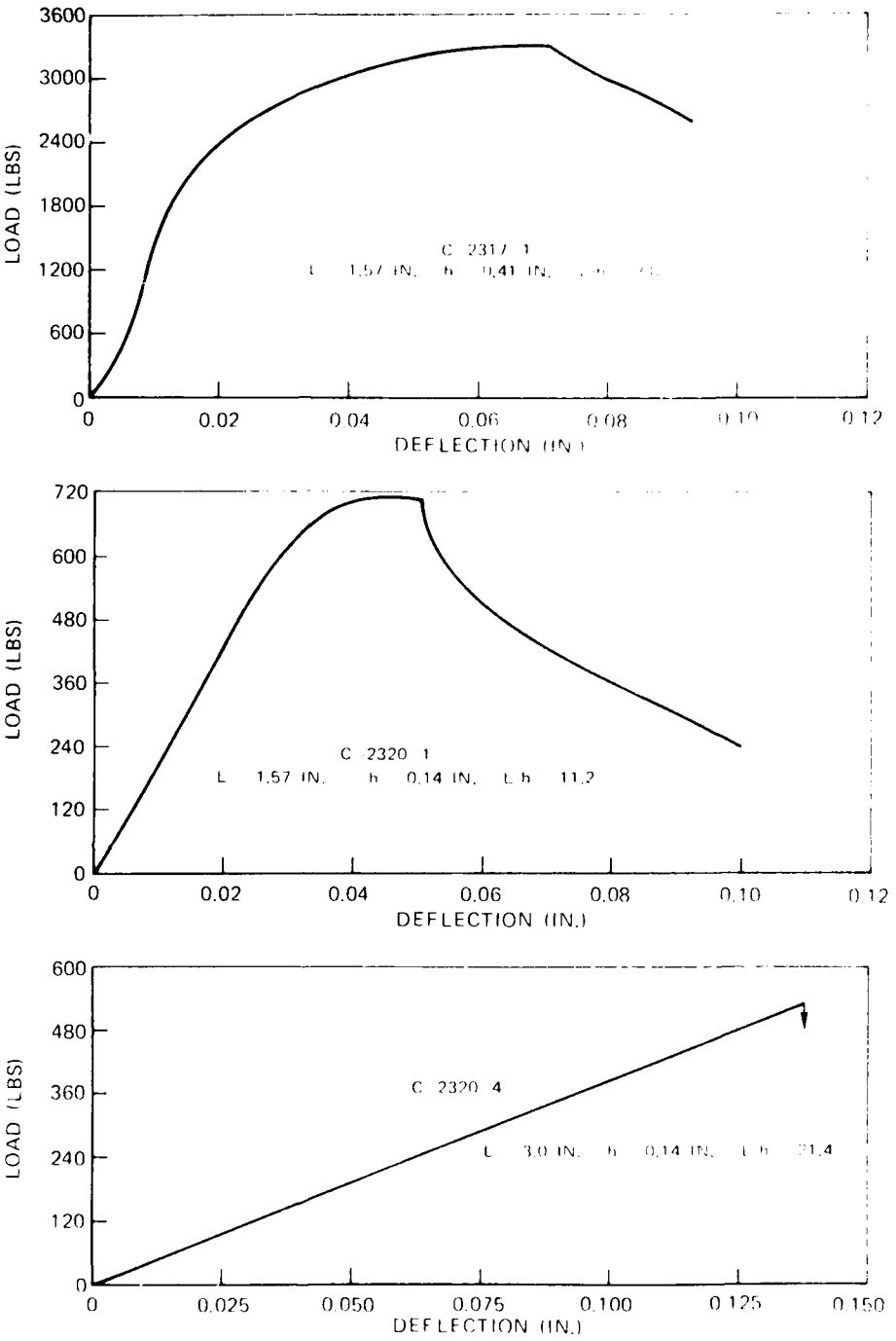

FIG. 12 LOAD DEFLECTION CURVES FOR LT-5.6 B-6061 UNNOTCHED THREE POINT BEND SPECIMENS

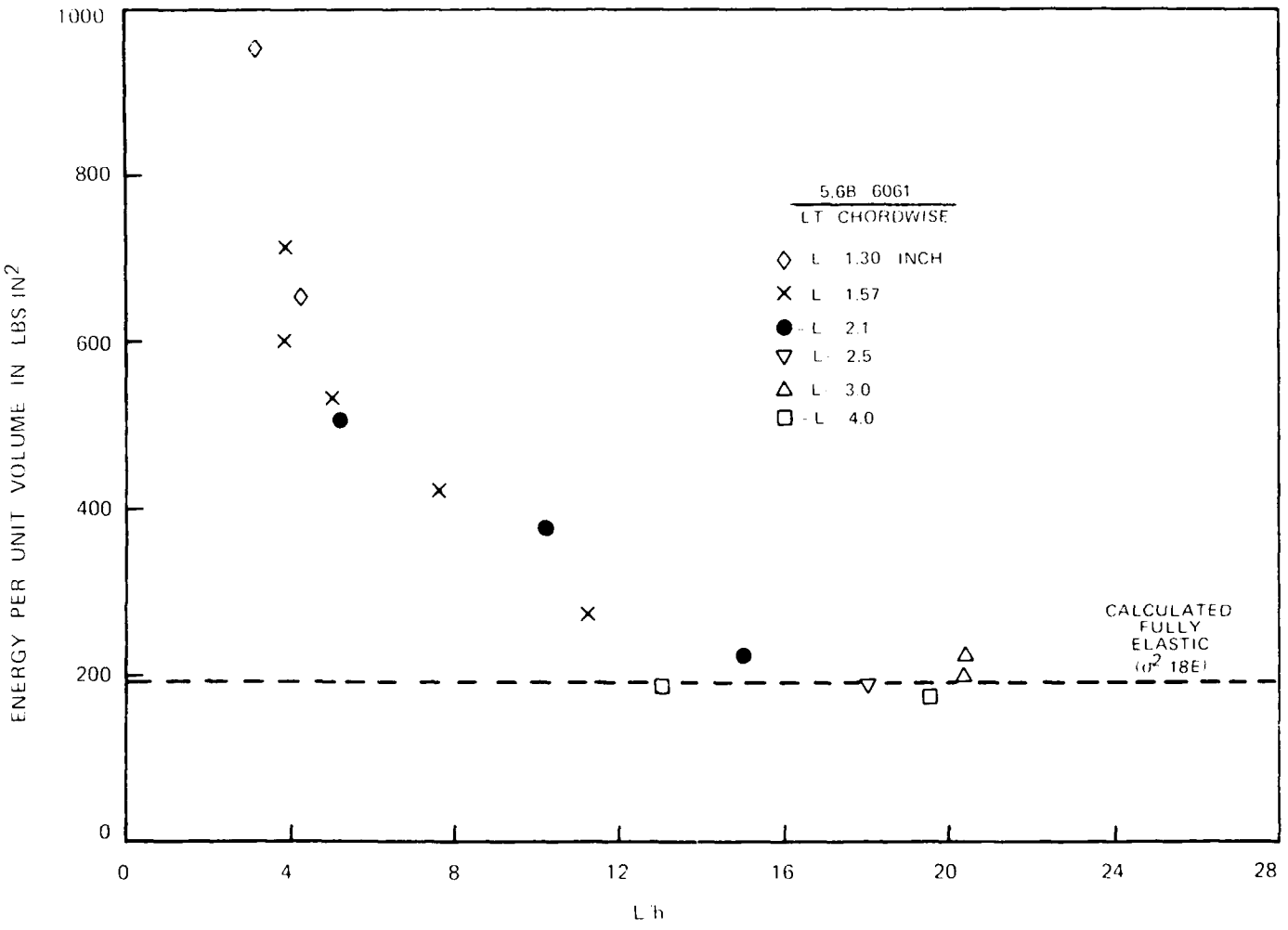

FIG. 13 ENERGY PER UNIT VOLUME TO MAXIMUM LOAD

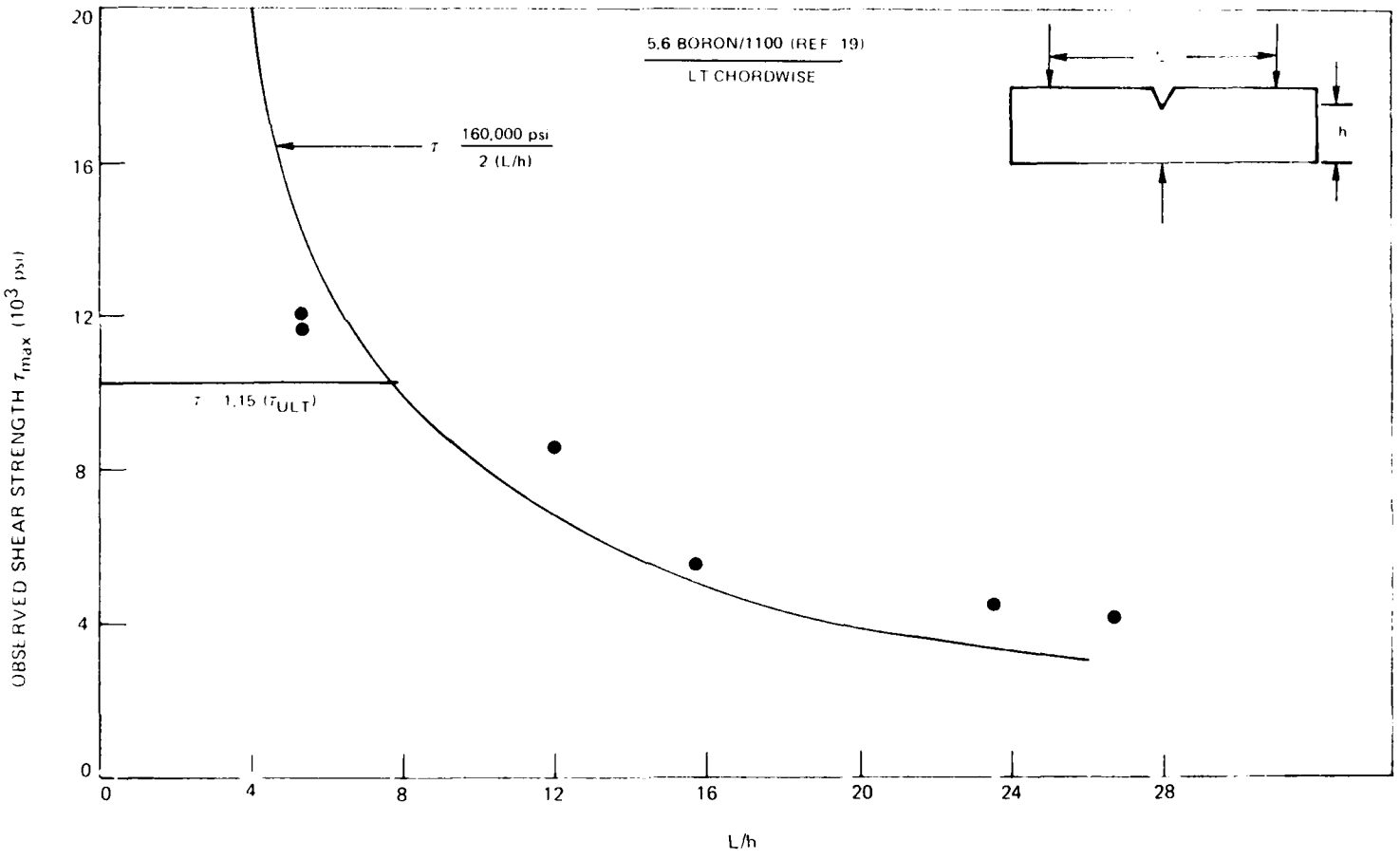

FIG. 14 SHEAR INTERACTION DIAGRAM

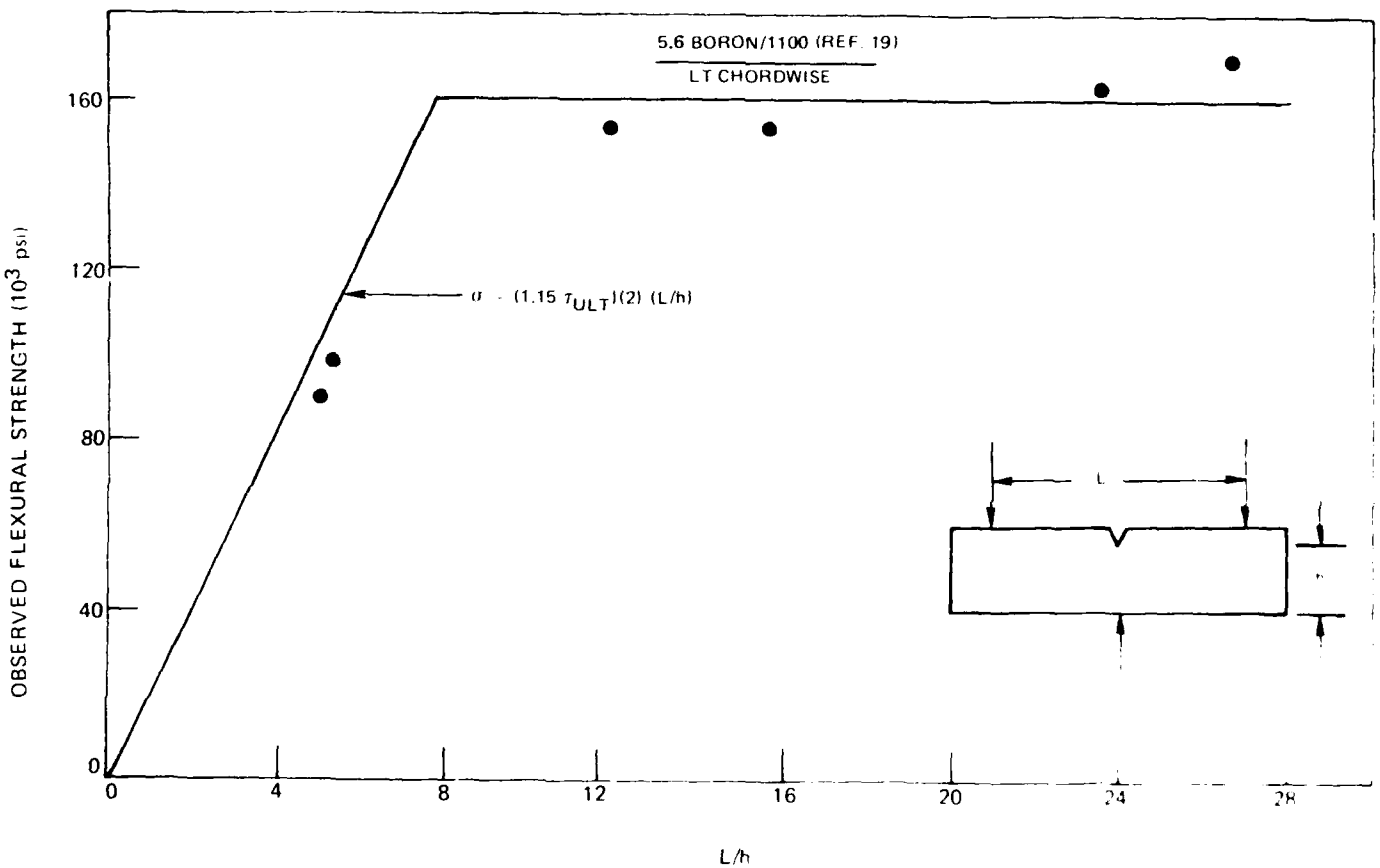

FIG. 15 FLEXURAL INTERACTION DIAGRAM

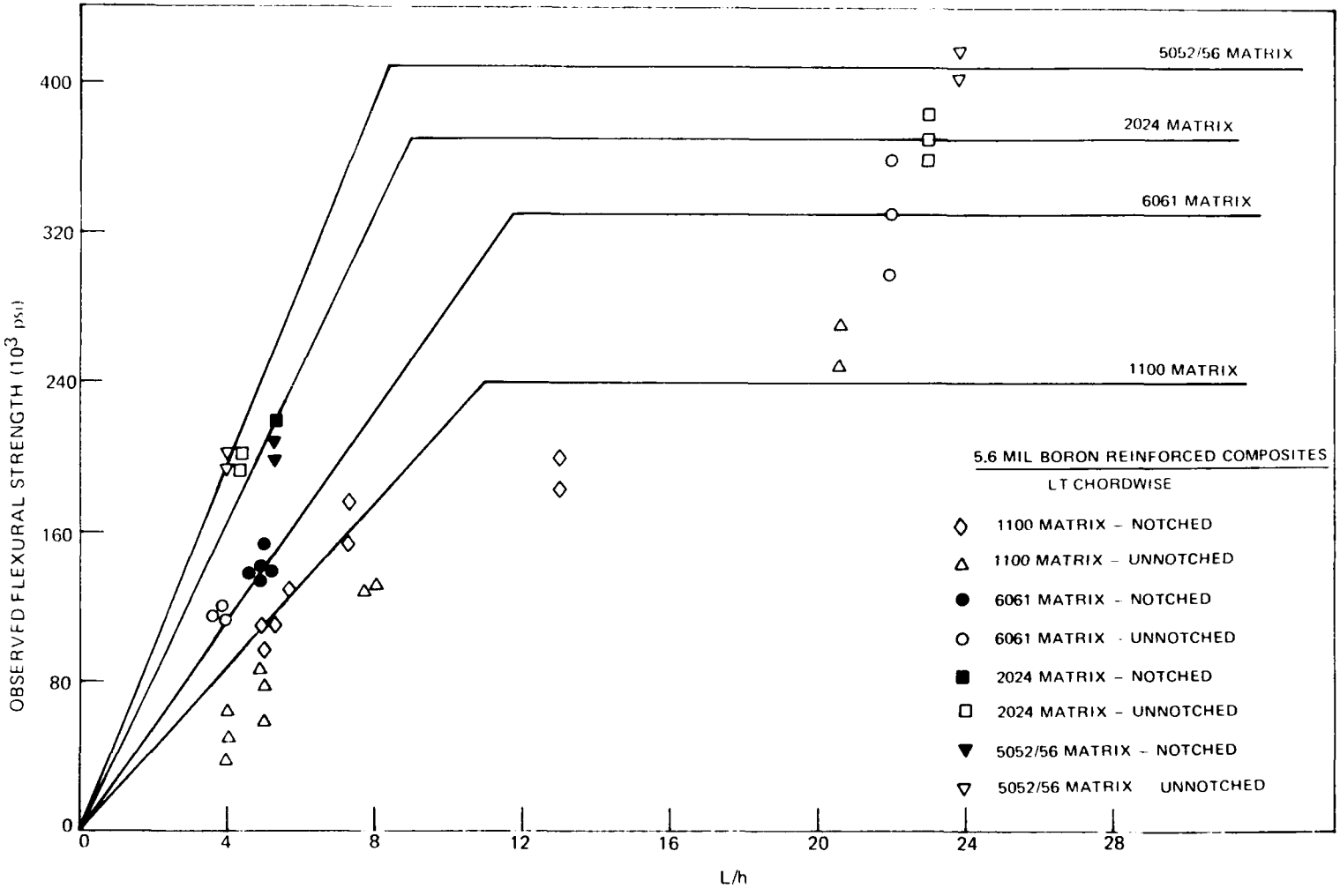

FIG. 16 FLEXURAL INTERACTION DIAGRAM

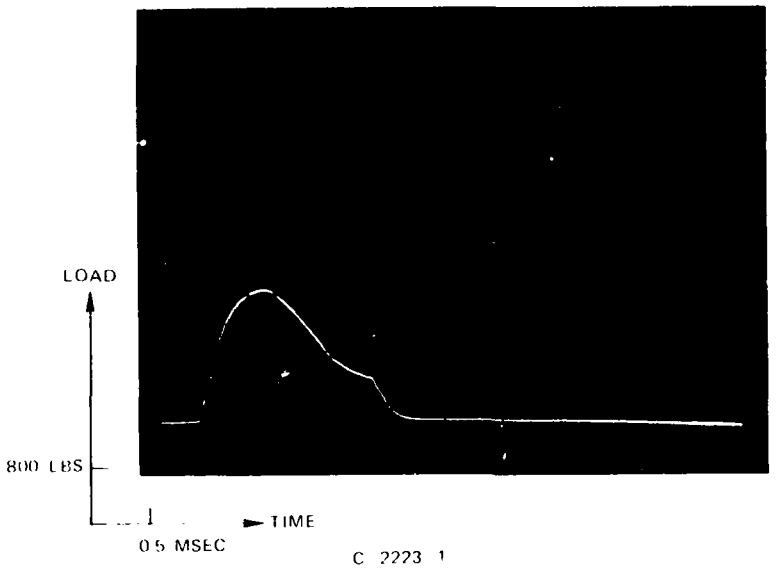

C 2223 1
5.6 B/1100 LT EDGEWISE NOTCHED h 0.318 IN.

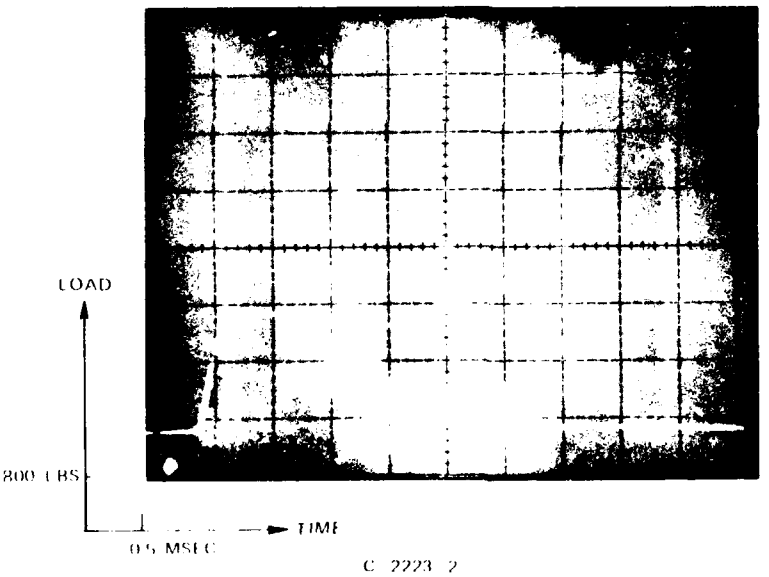

C 2223 2
5.6 B/1100 LT CHORDWISE NOTCHED h 0.318 IN

FIG. 17 INSTRUMENTED IMPACT TRACES

C–2223–1 EDGEWISE NOTCHED

C–2223–2 CHORDWISE NOTCHED

FIG. 18 LT–5.6 B–1100 IMPACT SPECIMENS

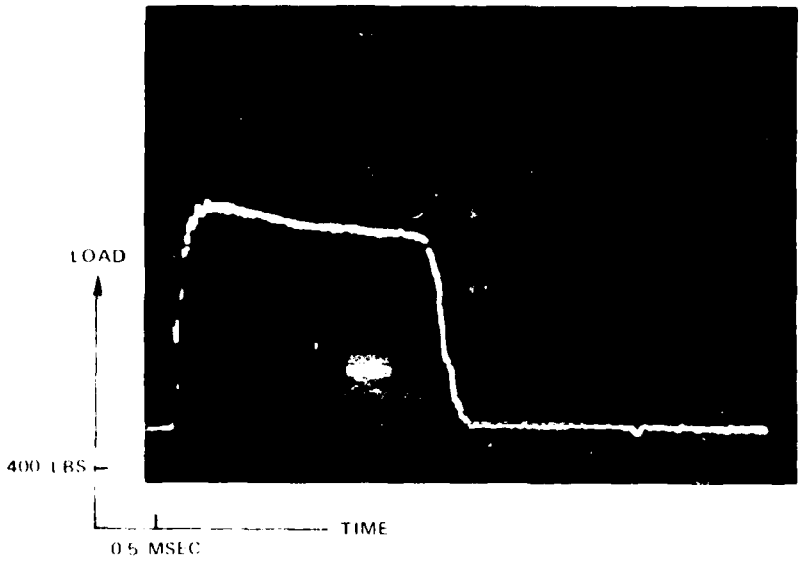

P_{MAX} 1461 LBS

E_{TOTAL} 48 FT LBS

C 2257 2

5.6 B/1100 LT CHORDWISE NOTCHED h 0.318 IN

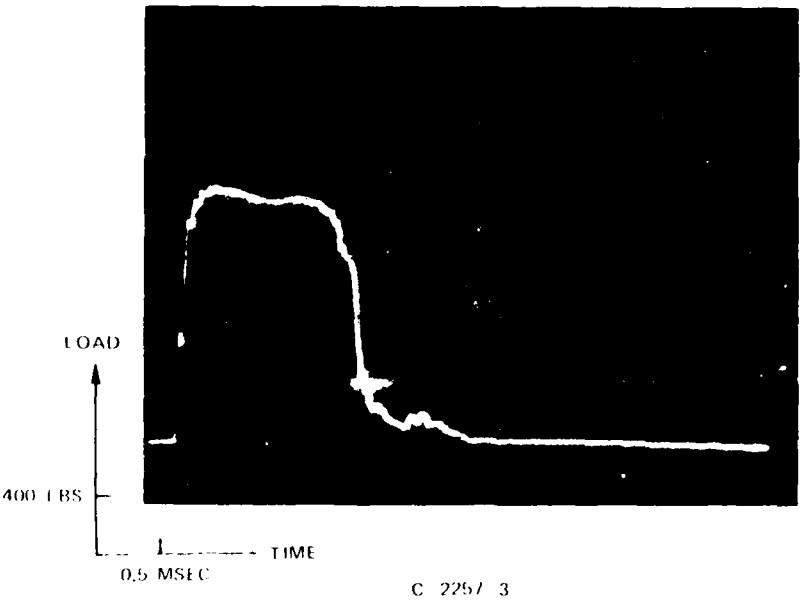

P_{MAX} 1692 LBS

E_{TOTAL} 39 FT LBS

C 2257 3

5.6 B/1100 LT CHORDWISE UNNOTCHED h 0.394 IN

FIG. 19 INSTRUMENTED IMPACT TRACES

C–2257–2 NOTCHED – CHORDWISE

C – 2257–3 UNNOTCHED – CHORDWISE

FIG. 20 LT–5.6 B–1100 IMPACT SPECIMENS

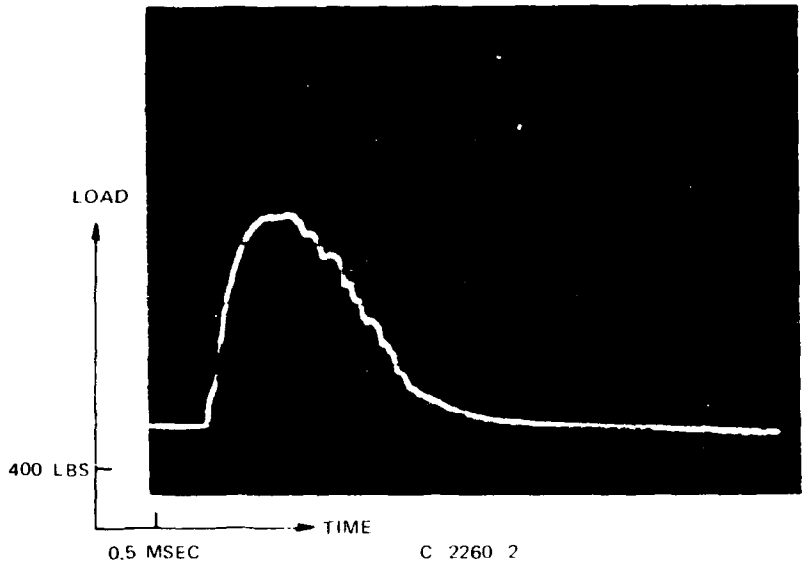

P_{MAX} 1392 LBS
E_{TOTAL} 13.3 FT LBS

C 2260 2
5.6 B/1100 LT CHORDWISE NOTCHED h 0.215 IN.

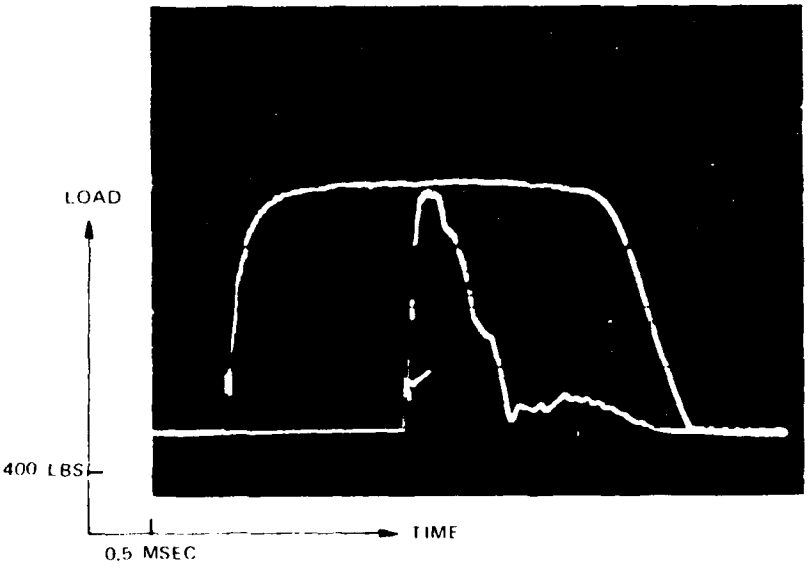

P_{MAX} 1624 LBS
E_{TOTAL} >23 FT LBS

C 2260 3
5.6 B/1100 LT CHORDWISE UNNOTCHED h 0.294 IN.

FIG. 21 INSTRUMENTED IMPACT TRACES

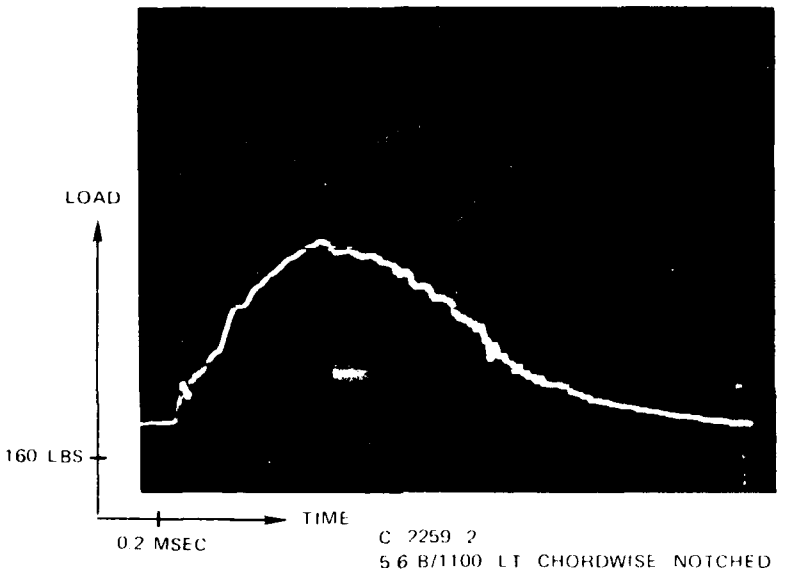

C 2259 2
5 6 B/1100 LT CHORDWISE NOTCHED h 0.121 IN.

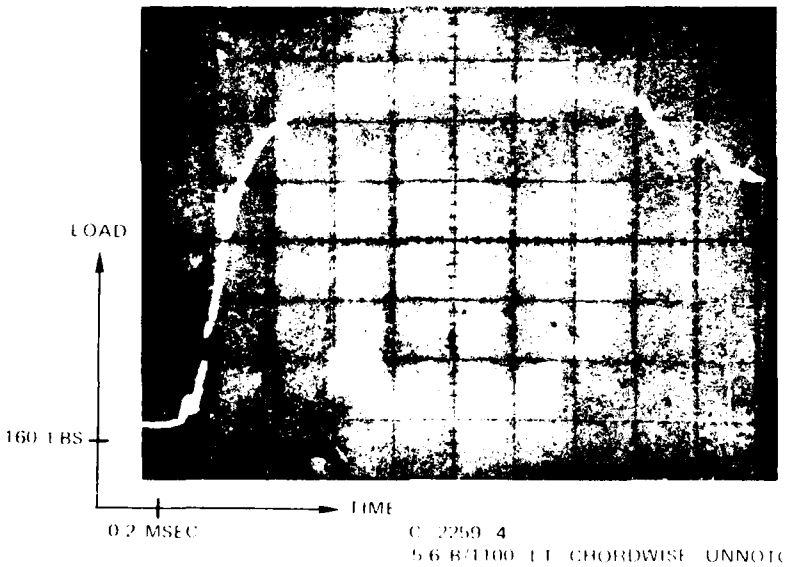

C 2259 4
5 6 B/1100 LT CHORDWISE UNNOTCHED h 0.200 IN

FIG. 22 INSTRUMENTED IMPACT TRACES

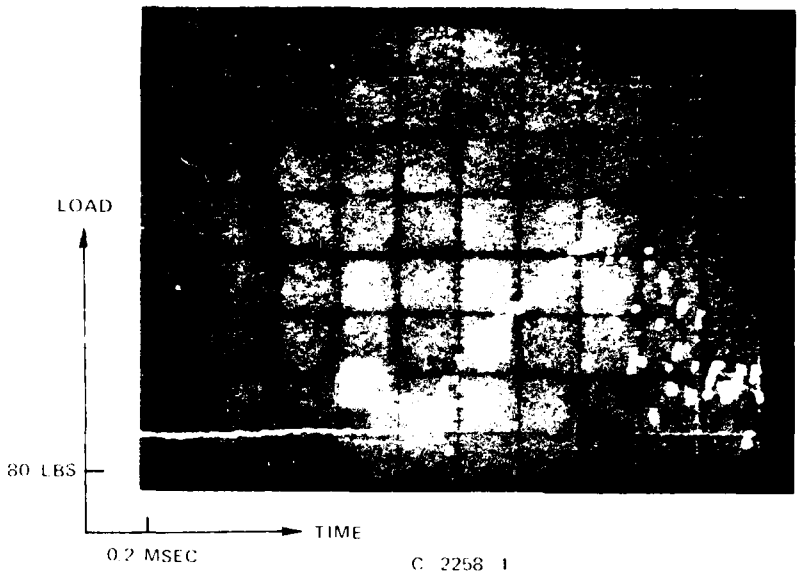

P_{MAX} 264 LBS

E_{TOTAL} 1.65 FT LBS

C 2258 1

5.6 B/1100 LT CHORDWISE UNNOTCHED h 0.076 IN

FIG. 23 INSTRUMENTED IMPACT TRACES

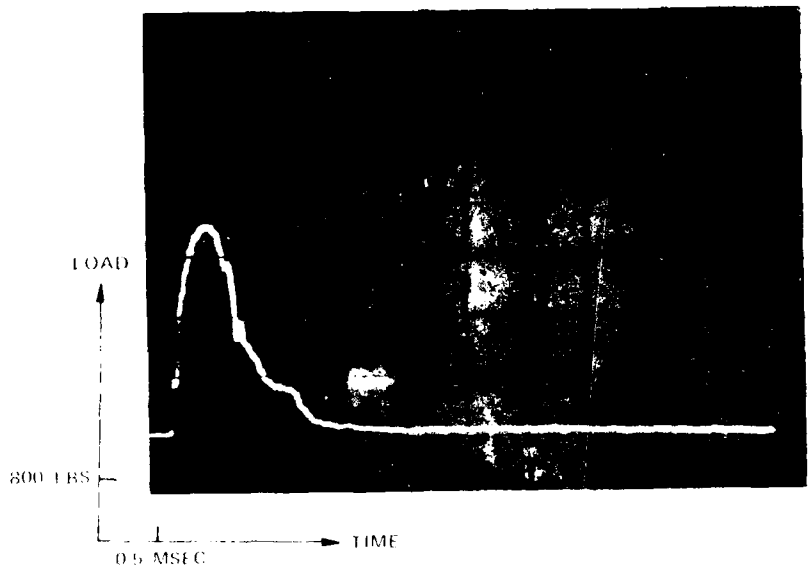

P_{MAX} 2783 LBS
E_{TOTAL} 26 FT LBS

C 2287-1
5.6 B 6061 LT CHORDWISE NOTCHED b = 0.329 IN

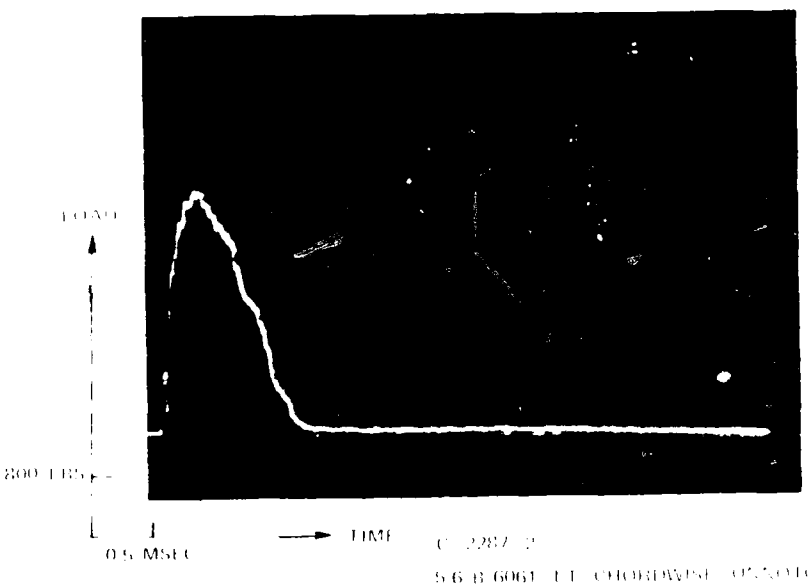

P_{MAX} 3200 LBS
E_{TOTAL} 34 FT LBS

C 2287-2
5.6 B 6061 LT CHORDWISE NOTCHED b = 0.311 IN

FIG. 24 INSTRUMENTED IMPACT TRACES

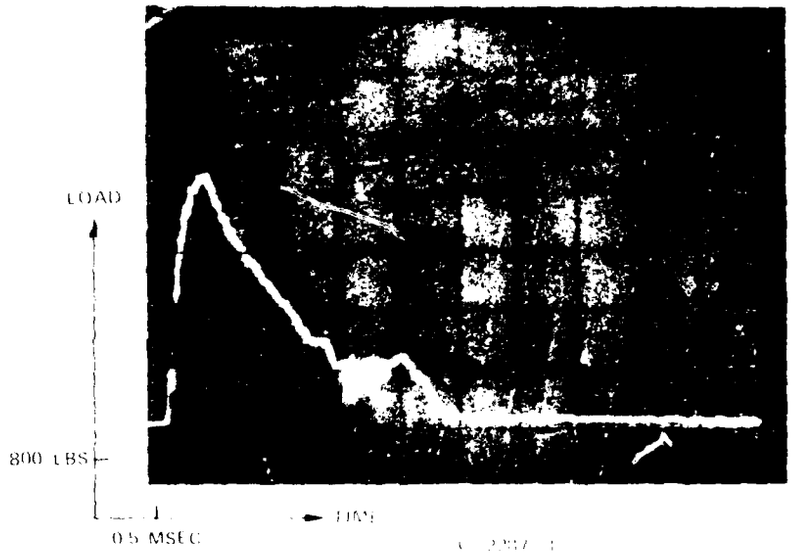

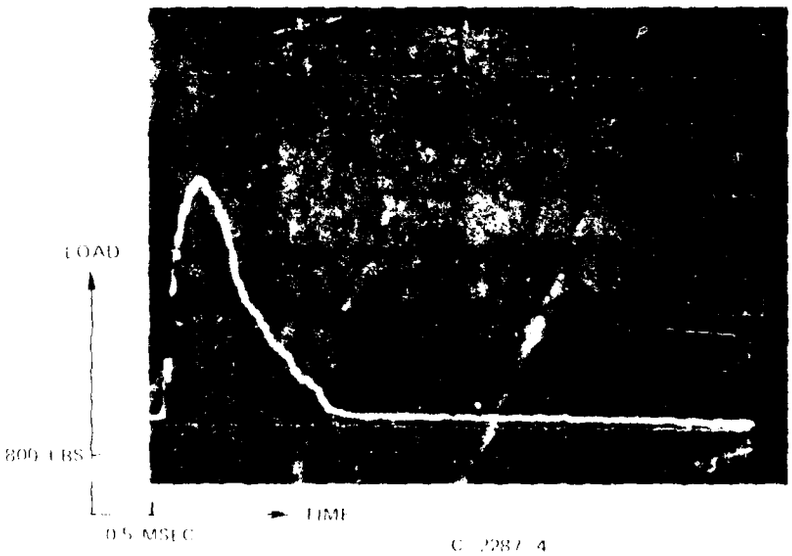

FIG. 25 INSTRUMENTED IMPACT TRACES

C-2287-3 CHORDWISE UNNOTCHED

C-2287-4 CHORDWISE UNNOTCHED

FIG. 26 LT-5.6 B-6061 IMPACT SPECIMENS

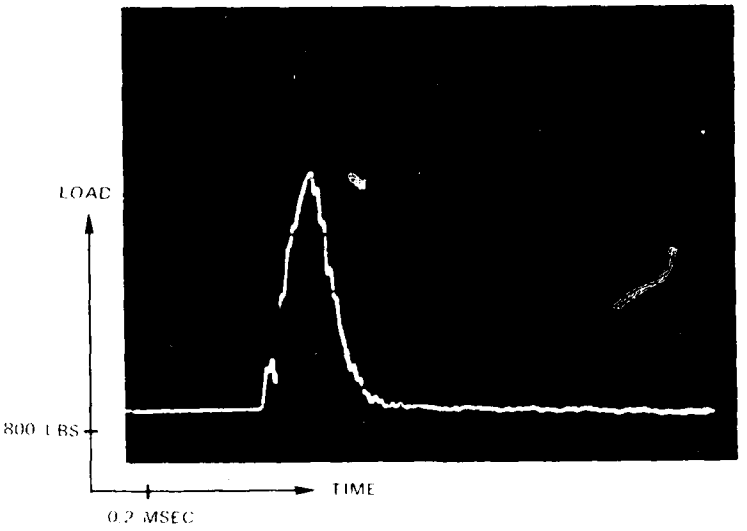

P_{MAX} 3340 LBS

E_{TOTAL} 30 FT LBS

C 2304 3

5.6 B/2024 LT CHORDWISE NOTCHED b 0.300 IN

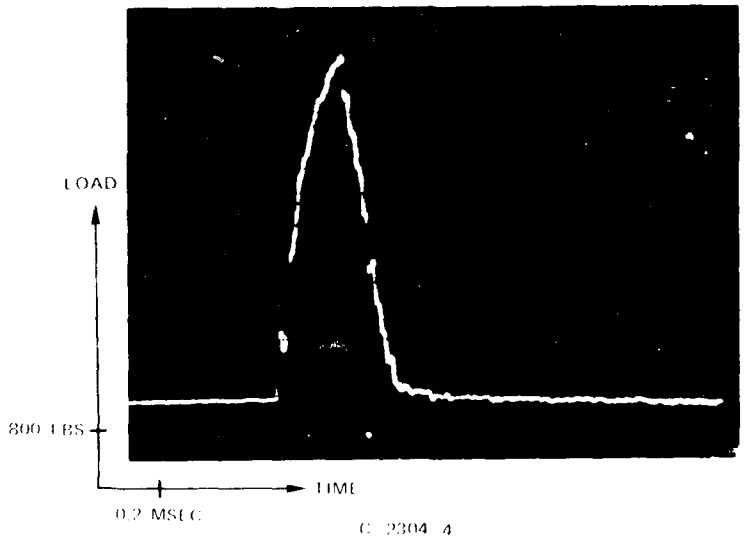

P_{MAX} 4720 LBS

E_{TOTAL} 20 FT LBS

C 2304 4

5.6 B/2024 LT CHORDWISE UNNOTCHED b 0.329 IN

FIG. 27 INSTRUMENTED IMPACT TRACES

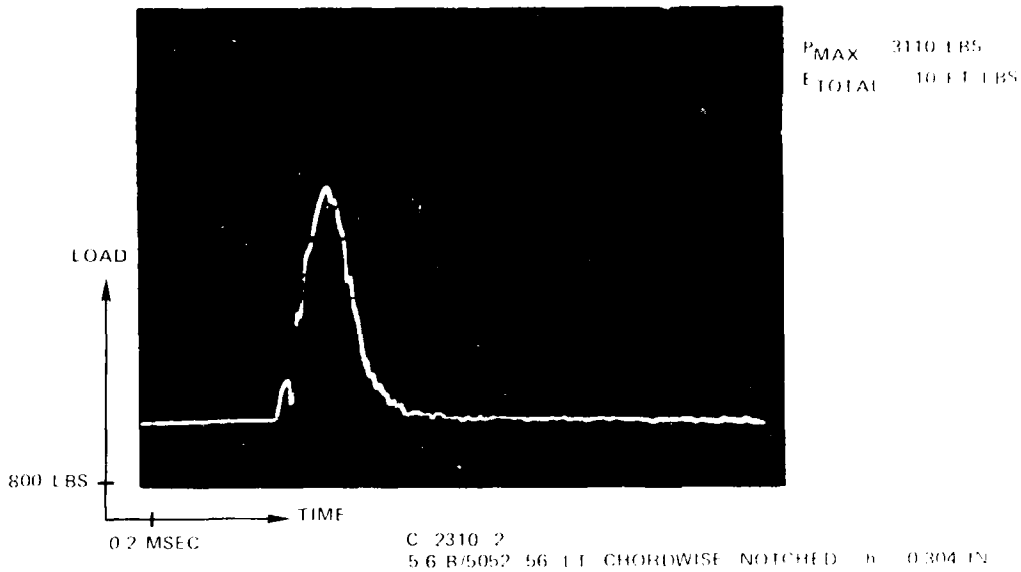

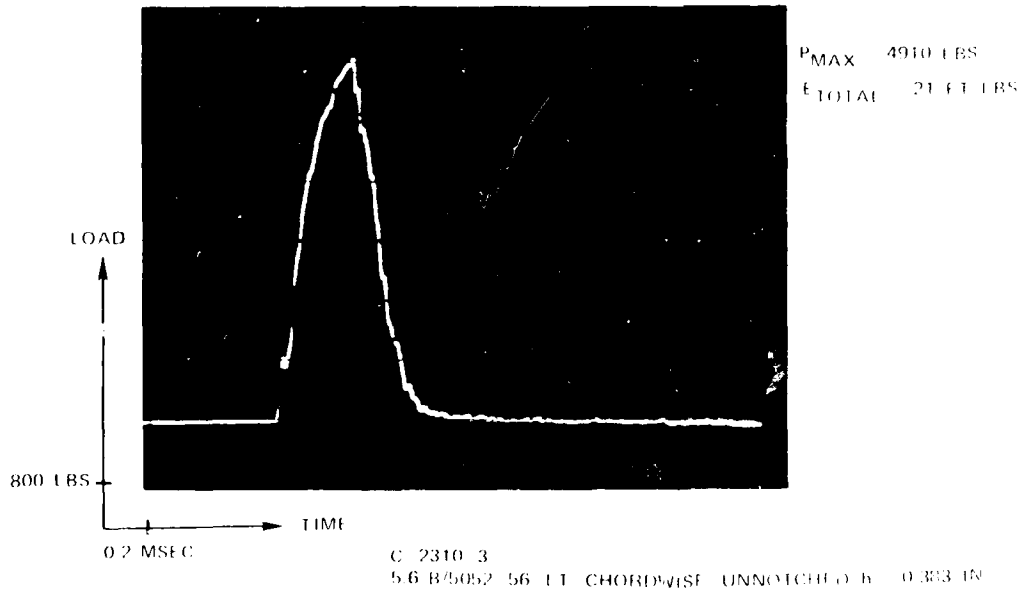

FIG. 28 INSTRUMENTED IMPACT TRACES

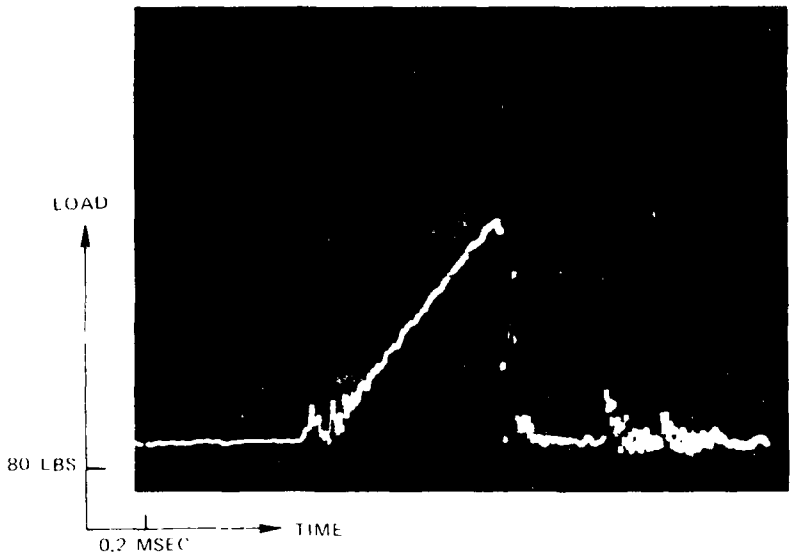

P_{MAX} 278 LBS

E_{TOTAL} 0.94 FT LBS

C 2305 1

5.6 B/2024 LT CHORDWISE UNNOTCHED h 0.068 IN

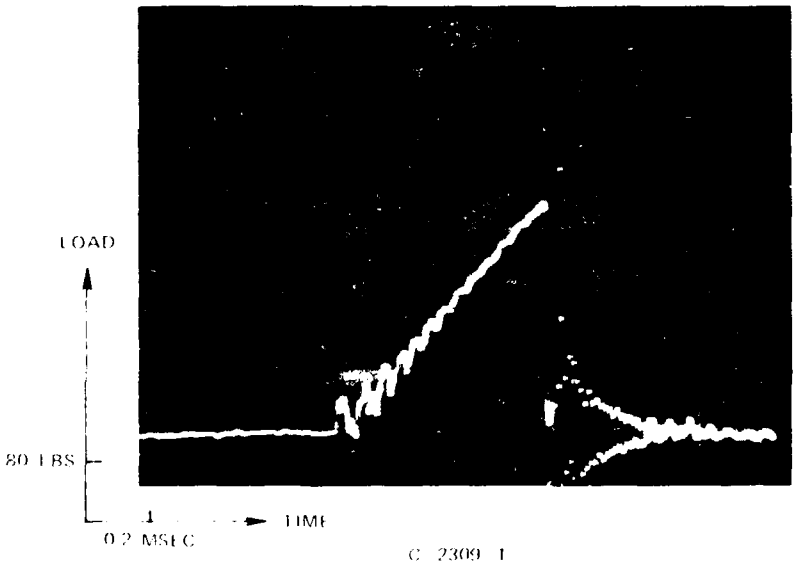

P_{MAX} 306 LBS

E_{TOTAL} 0.97 FT LBS

C 2309 1

5.6 B/5052 56 LT CHORDWISE UNNOTCHED h 0.066 IN

FIG. 29 INSTRUMENTED IMPACT TRACES

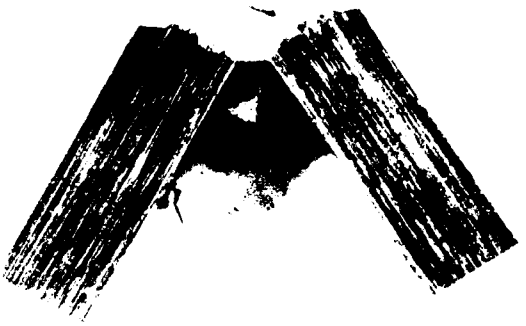

C-2304-2 CHORDWISE NOTCHED

C-2304-4 CHORDWISE UNNOTCHED

FIG. 30. LT-5.6 B-2024 IMPACT SPECIMENS

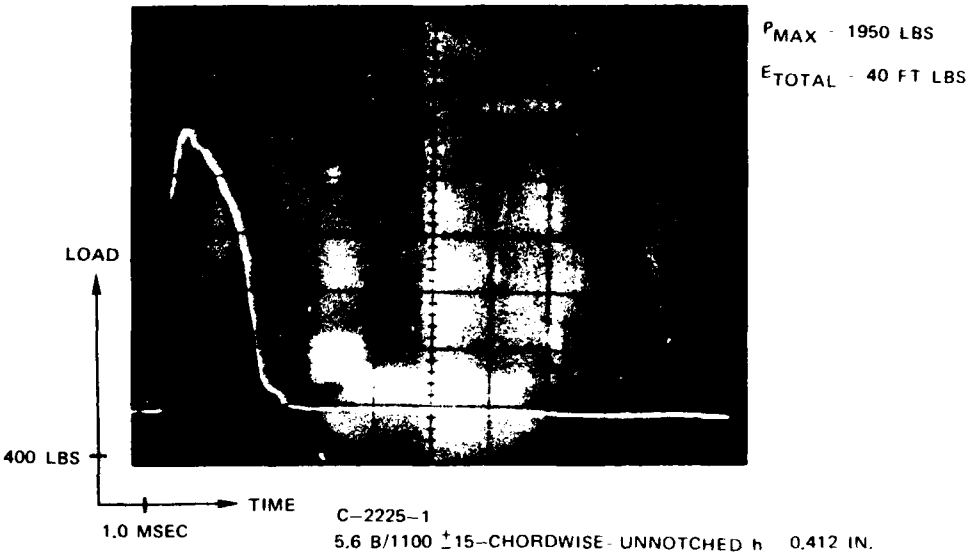

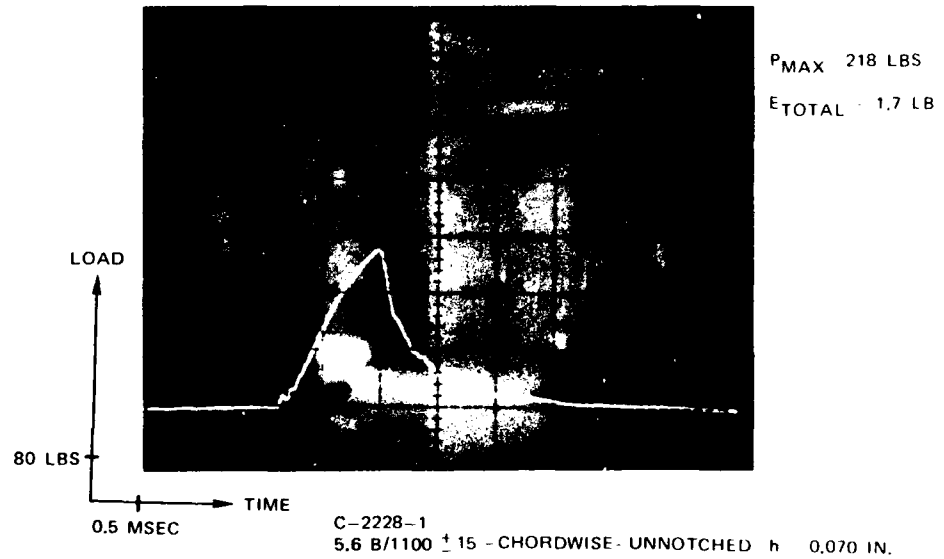

FIG. 31 INSTRUMENTED IMPACT TRACES

C-2225-1

CHORDWISE UNNOTCHED

FIG. 32 $\pm$ 15°-5.6 B-1100 IMPACT SPECIMEN

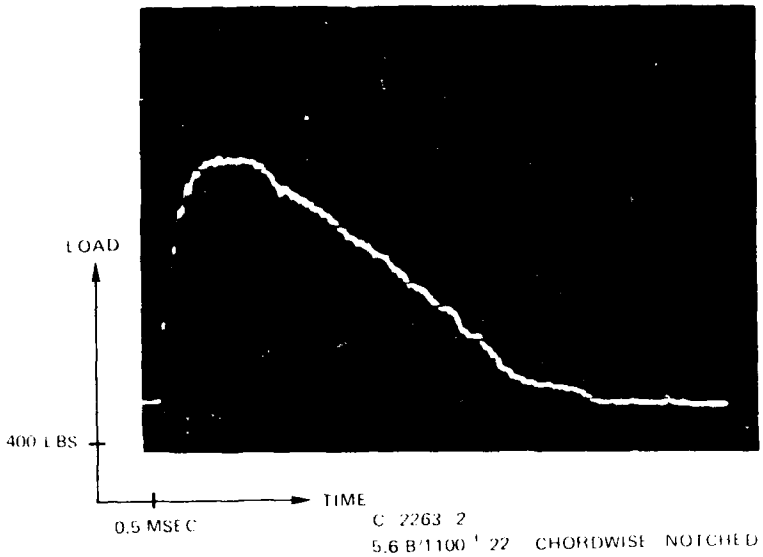

C 2263 2
5.6 B/1100 ' 22 CHORDWISE NOTCHED b 0.315 IN

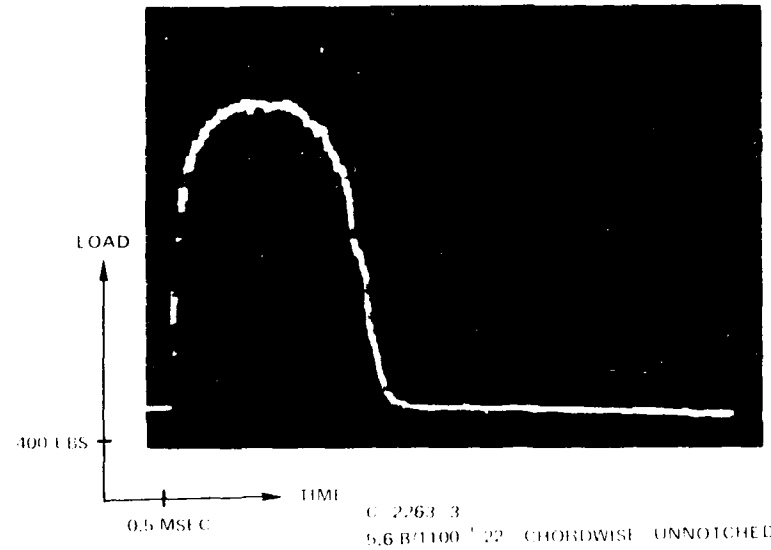

C 2263 3
5.6 B/1100 ' 22 CHORDWISE UNNOTCHED b 0.393 IN.

FIG. 33 INSTRUMENTED IMPACT TRACES

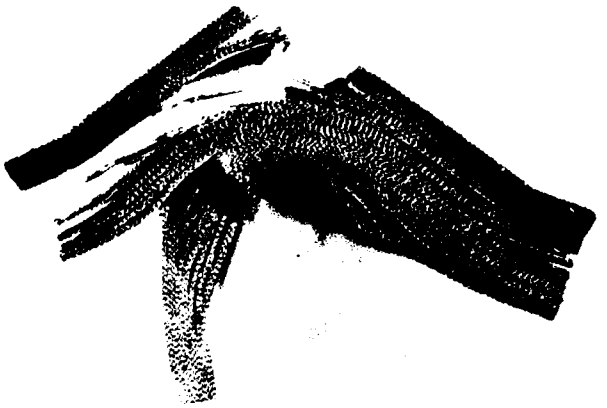

C-2263-2 CHORDWISE UNNOTCHED

C-2263-3 CHORDWISE UNNOTCHED

FIG. 34 $\pm 22^{o}$-5.6 B-1100 IMPACT SPECIMENS

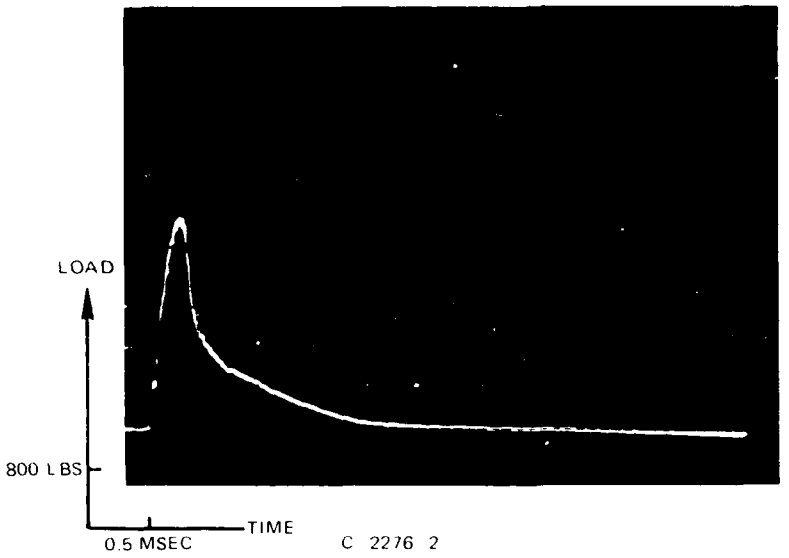

P_{MAX} 2782 LBS

E_{TOTAL} 24 FT LBS

C 2276 2

5.6 B/1100 ' 22 EDGEWISE NOTCHED h 0.313 IN.

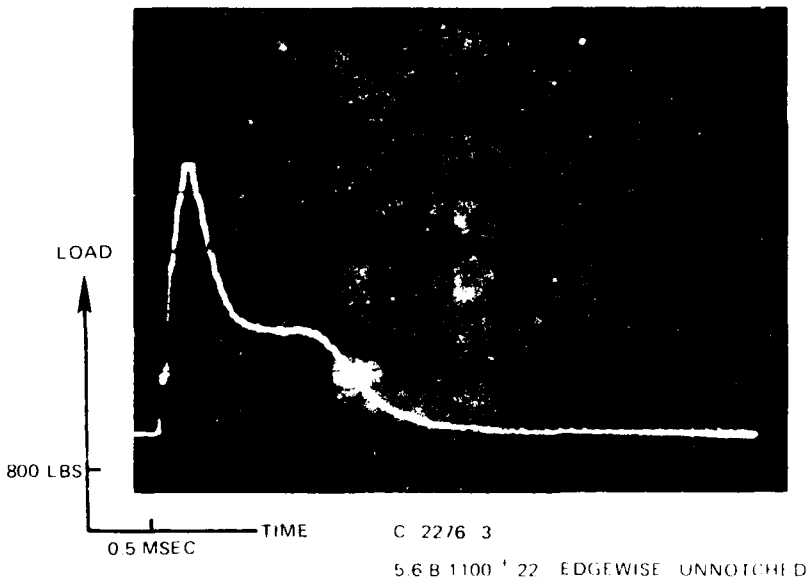

P_{MAX} 3617 LBS

E_{TOTAL} 48 FT LBS

C 2276 3

5.6 B 1100 ' 22 EDGEWISE UNNOTCHED h 0.394 IN

FIG. 35 INSTRUMENTED IMPACT TRACES

C–2276–1 EDGEWISE NOTCHED

C–2276–3 CHORDWISE UNNOTCHED

FIG. 36 ± 22–5.6 B–1100 IMPACT SPECIMENS
(REGION OF TUP – SPECIMEN CONTACT)

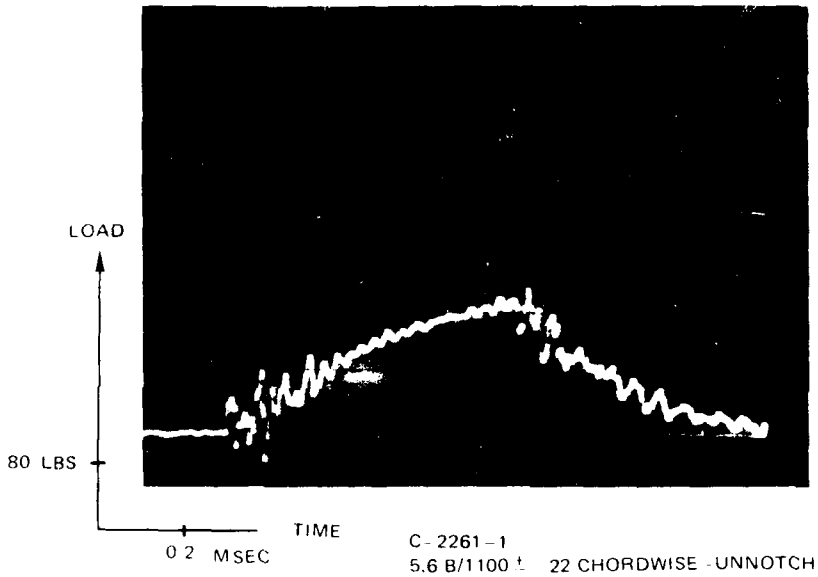

FIG. 37 INSTRUMENTED IMPACT TRACES

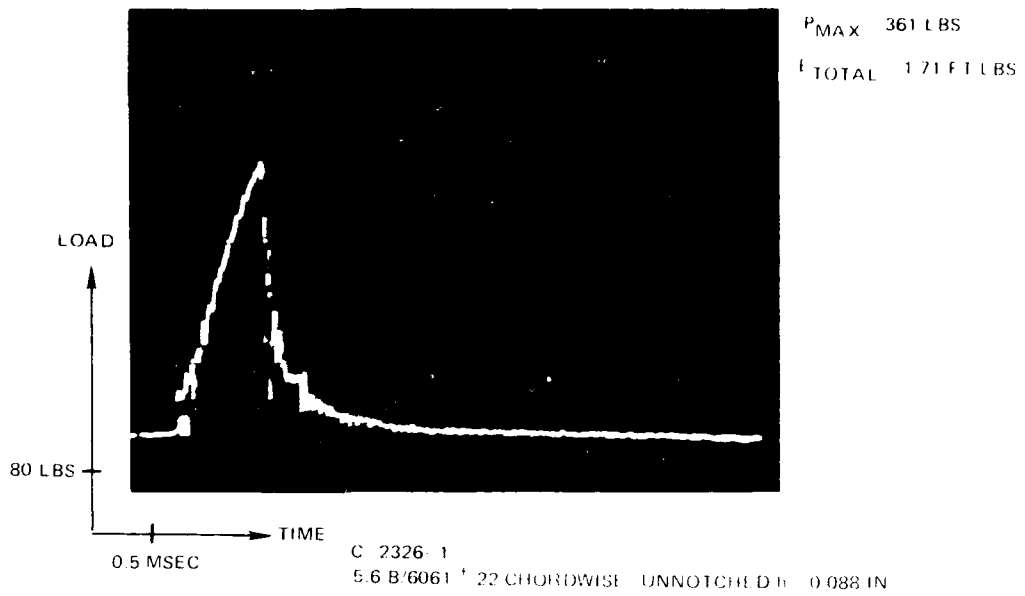

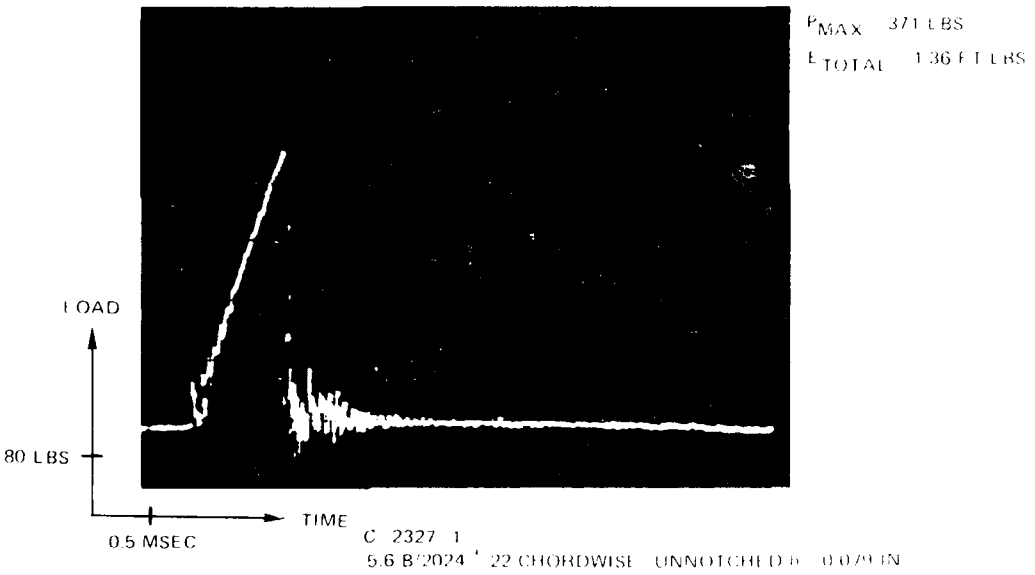

FIG. 38 INSTRUMENTED IMPACT TRACES

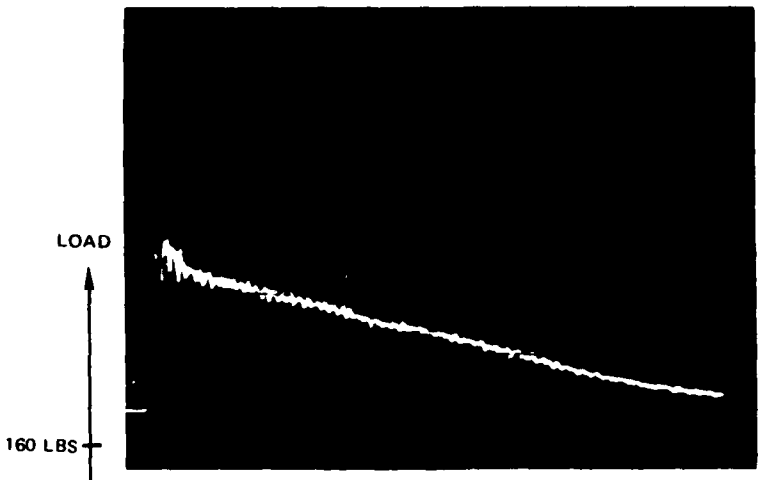

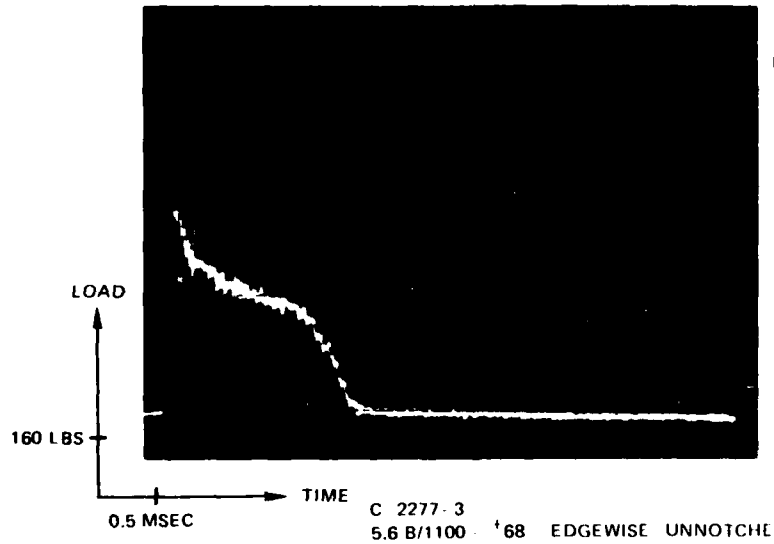

FIG. 39 INSTRUMENTED IMPACT TRACES

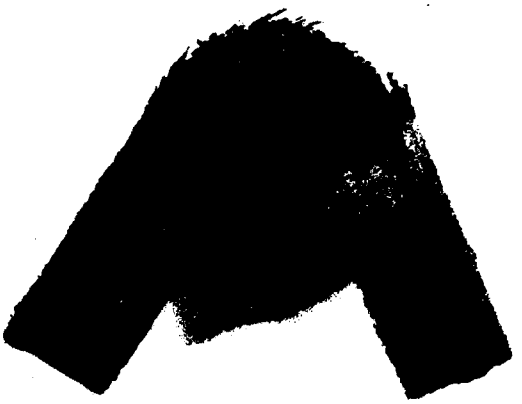

C–2277–1 CHORDWISE UNNOTCHED

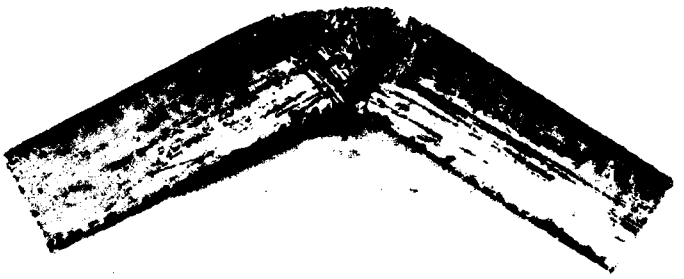

C–2277–3 EDGEWISE UNNOTCHED

FIG. 40 ±68–5.6 B–1100 IMPACT SPECIMENS

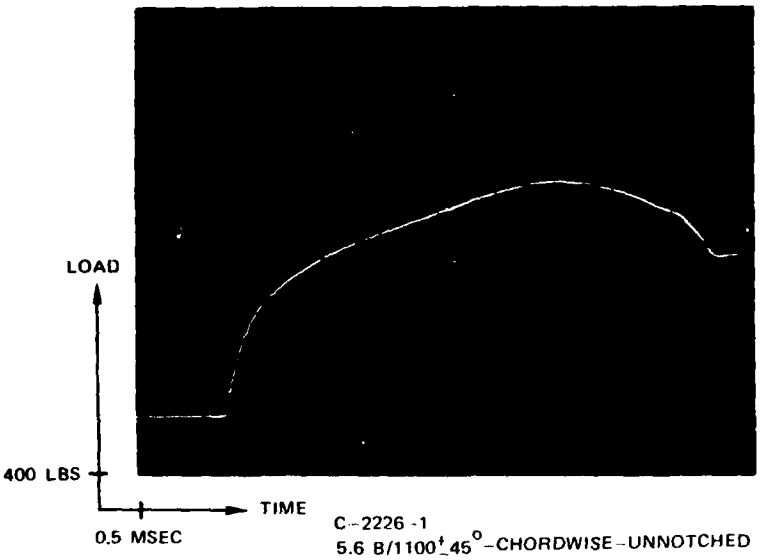

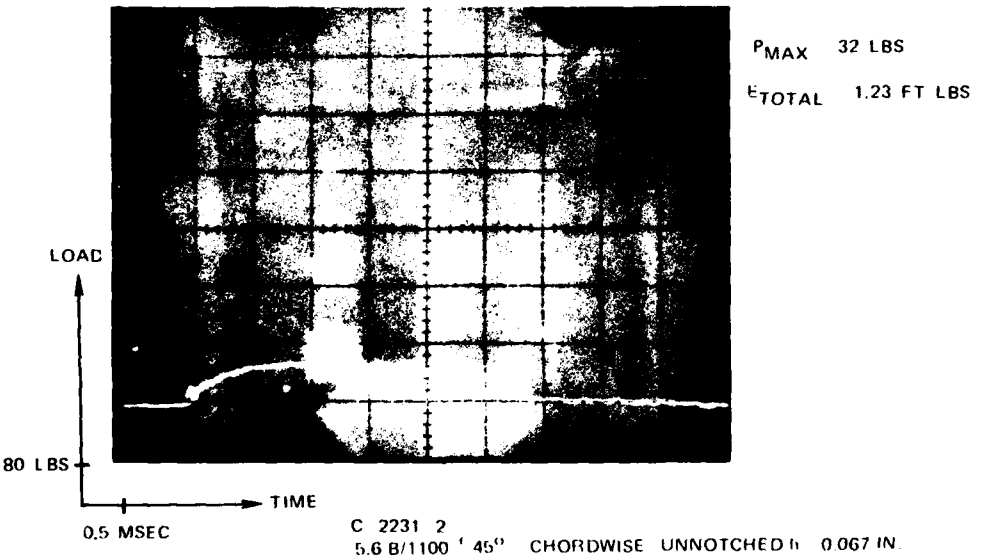

FIG. 41 INSTRUMENTED IMPACT TRACES

C–2226–1 CHORDWISE UNNOTCHED

C–2226–2 EDGEWISE UNNOTCHED

FIG. 42 $\pm 45^{o}$–5.6 B–1100 IMPACT SPECIMENS

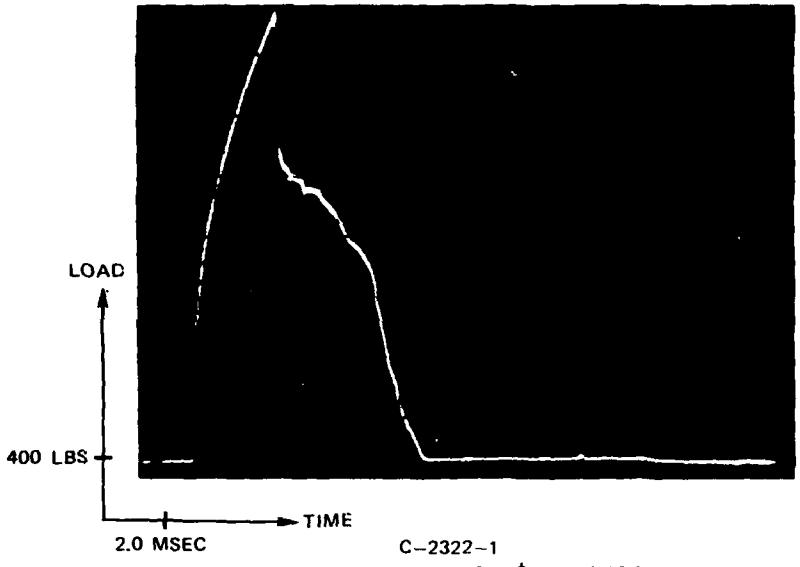

P_{MAX} - 3020 LBS

E_{TOTAL} - 155 FT LBS

C-2322-1

5.6 B/6061 $\pm$ 45 – CHORDWISE-UNNOTCHED h 0.435 IN.

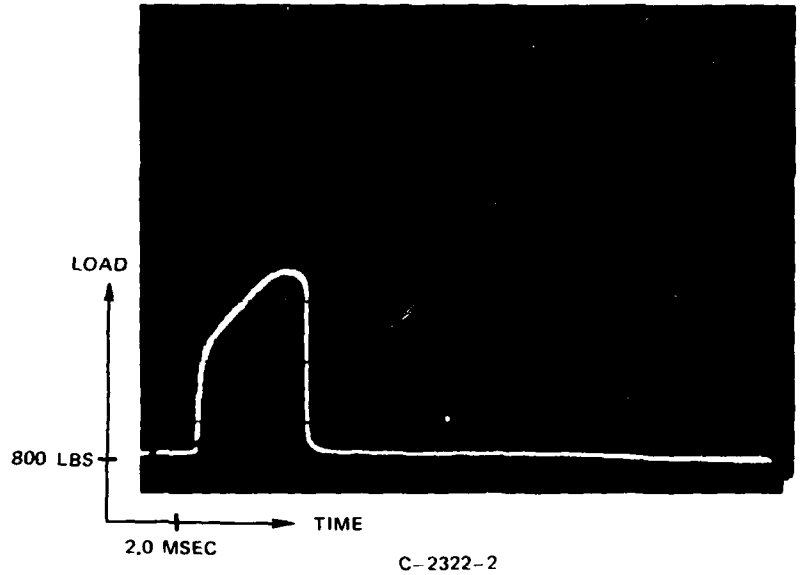

P_{MAX} 2410 LBS

E_{TOTAL} 105 FT LBS

C-2322-2

5.6 B/6061 $\pm$ 45-EDGEWISE-UNNOTCHED h 0.396

FIG. 43 INSTRUMENTED IMPACT TRACES

C-2322-1 CHORDWISE UNNOTCHED

C 2322 2 EDGEWISE UNNOTCHED

FIG. 44 $\pm 45^{o}$-5.6 B-6061 IMPACT SPECIMENS

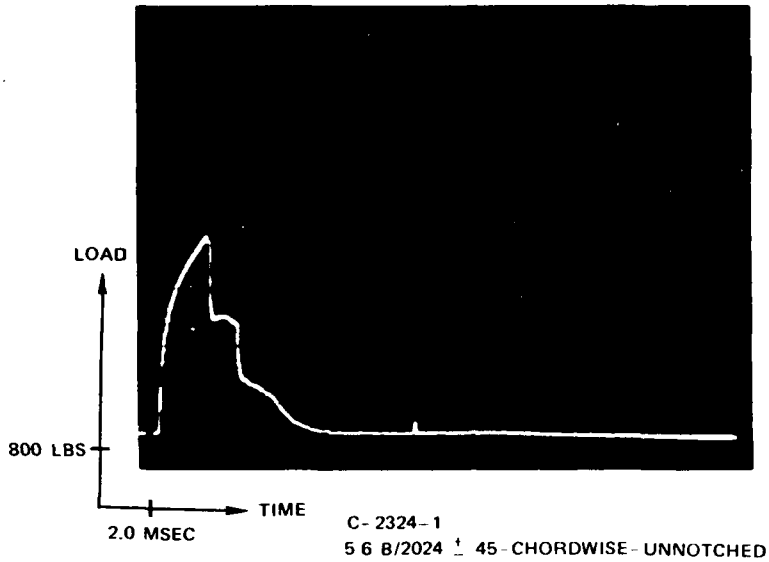

P_{MAX} 2780 LBS

E_{TOTAL} 88 FT LBS

C-2324-1

5 6 B/2024 ± 45-CHORDWISE-UNNOTCHED h 0.380 IN

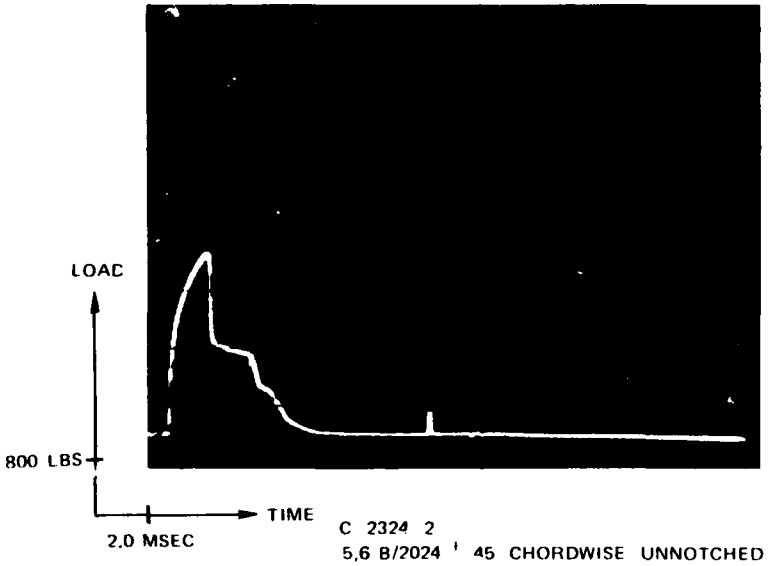

P_{MAX} 2500 LBS

E_{TOTAL} 75 FT LBS

C 2324 2

5,6 B/2024 ± 45 CHORDWISE UNNOTCHED h 0.380 IN.

FIG. 45 INSTRUMENTED IMPACT TRACES

C–2324–1 CHORDWISE UNNOTCHED

FIG. 46 . $\pm 45^{o}$–5.6 B–2024 IMPACT SPECIMENS

P_{max} = 936LBS

E_{TOTAL} = 11.8FT/LBS

c–2369–2

5.6B/1100–$[\pm\ 45_3/0_9]_s$

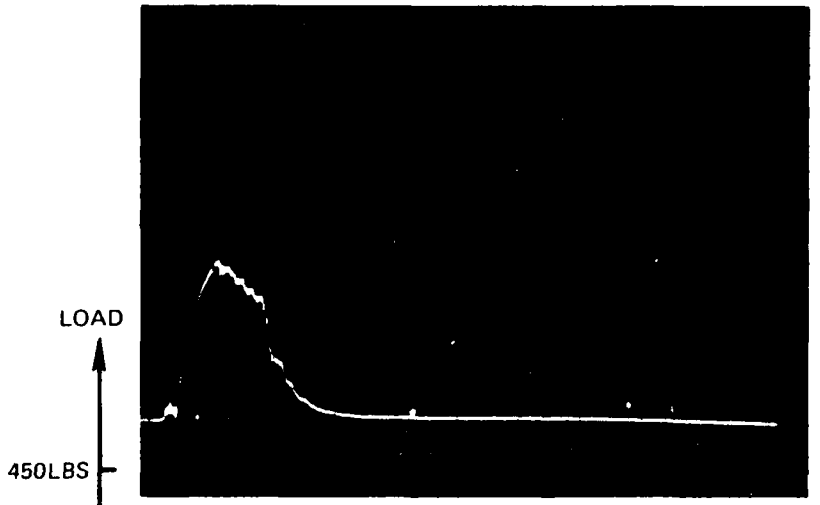

P_{max} = 1020 LBS

E_{TOTAL} = 6.1 FT/LBS

c–2371–T4–2

5.6B/1100–$[(0–45/0/+45)_3 0_3]_s$

FIG. 47. INSTRUMENTED IMPACT TRACES

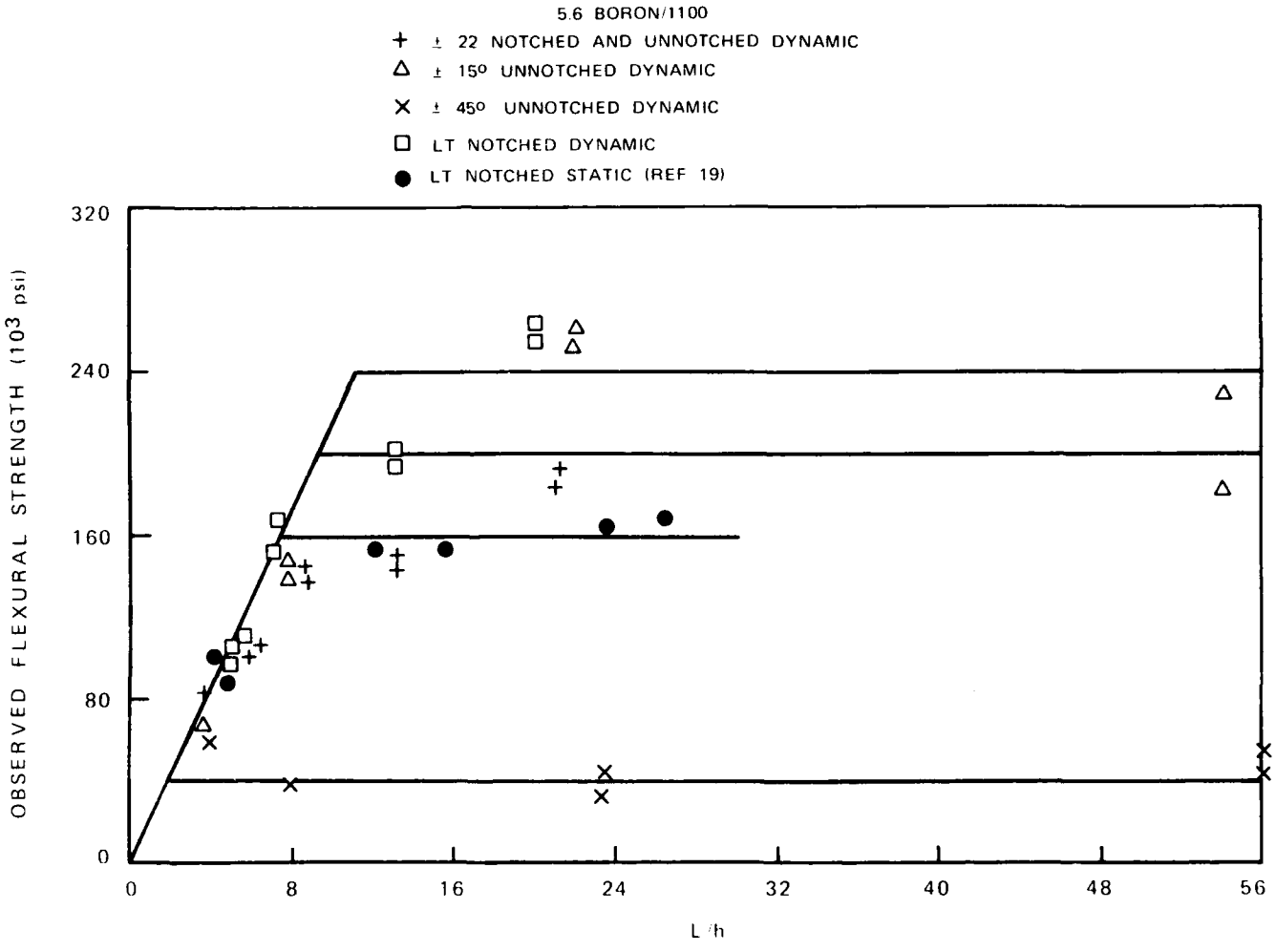

FIG. 48. FLEXURAL INTERACTION DIAGRAM

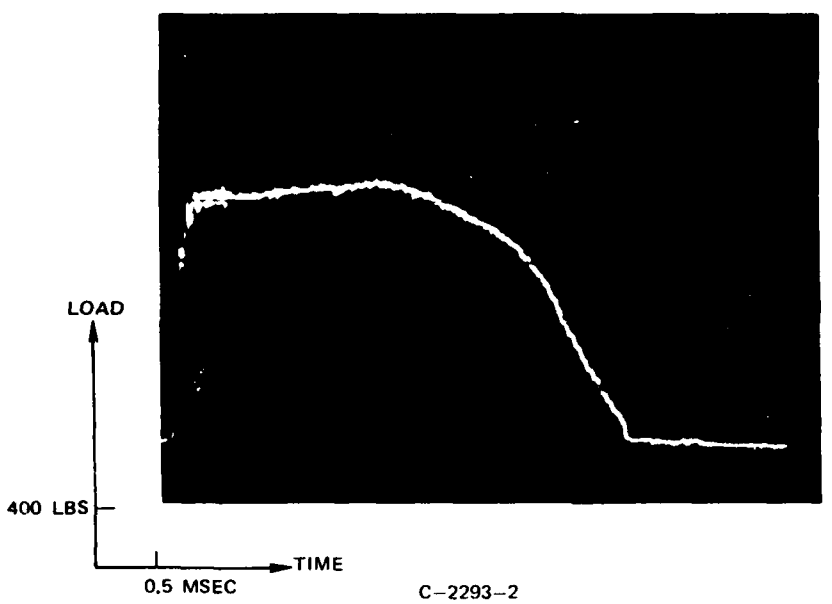

P_{MAX} = 1625–1715 LBS
E_{TOTAL} = 77 FT LBS

C–2293–2
8.0 B/1100–LT–CHORDWISE–NOTCHED h = 0.337 IN.

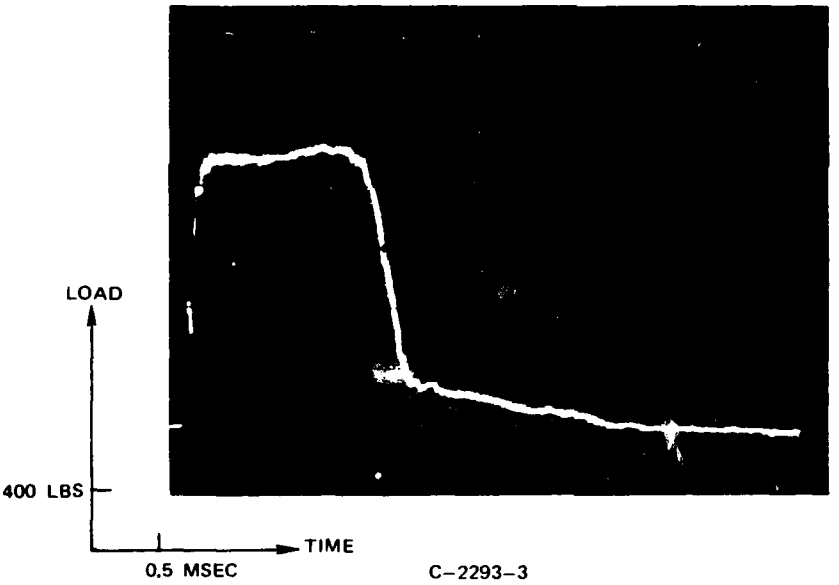

P_{MAX} = 1760–1810 LBS
E_{TOTAL} = 49 FT LBS

C–2293–3
8.0 B/1100–LT–CHORDWISE–UNNOTCHED h 0.416 IN

FIG. 49 INSTRUMENTED IMPACT TRACES

C-2293-2 CHORDWISE NOTCHED

C-2293-3 CHORDWISE UNNOTCHED

FIG. 50 LT-8.0 B-1100 IMPACT SPECIMENS

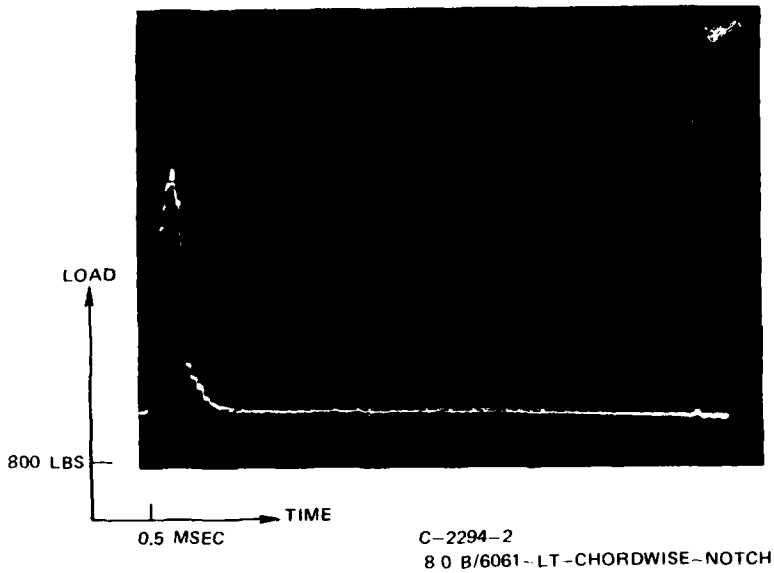

P_{MAX} 3430 LBS
E_{TOTAL} 13.5 FT LBS

C-2294-2
8.0 B/6061-LT-CHORDWISE-NOTCHED h = 0.339 IN.

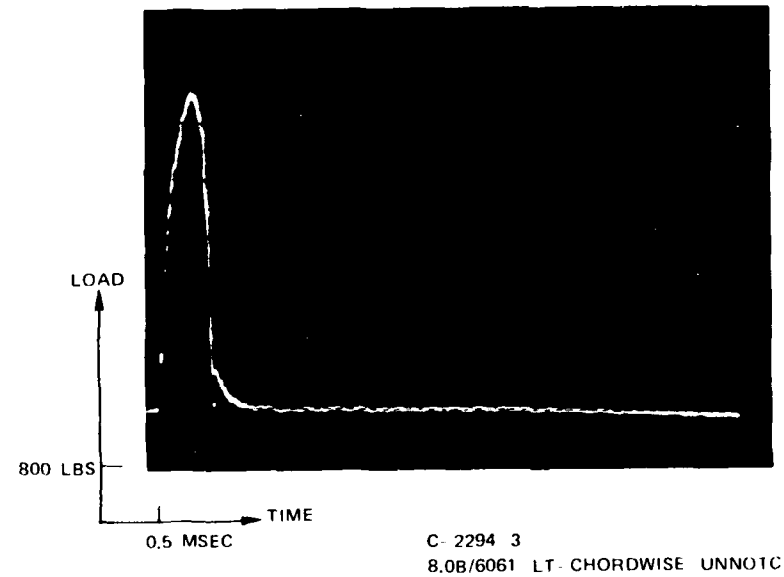

P_{MAX} 4460 LBS
E_{TOTAL} = 25 FT LBS

C-2294-3
8.0B/6061 LT-CHORDWISE UNNOTCHED h 0.418 IN.

FIG. 51 INSTRUMENTED IMPACT TRACES

C–2294–3 CHORDWISE NOTCHED

C–2294–2 CHORDWISE UNNOTCHED

FIG. 52 LT–8.0 B–6061 IMPACT SPECIMENS

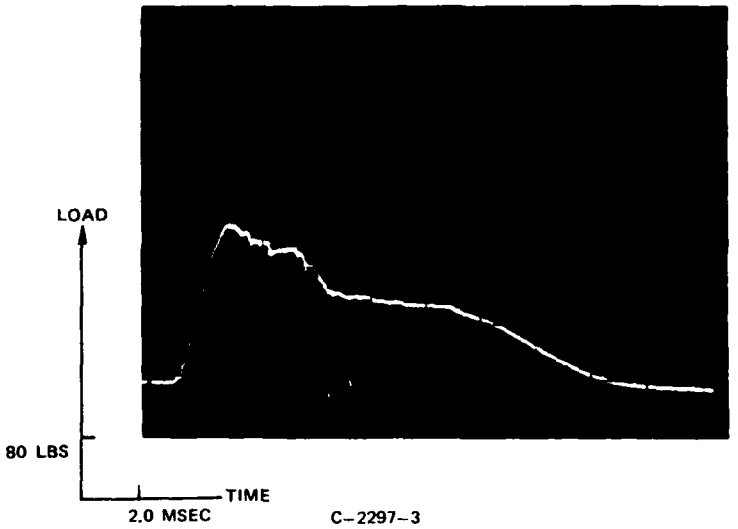

P_{MAX} = 232 LBS
E_{TOTAL} = 3.4 FT LBS

C-2297-3
8.0 B/1100-LT-CHORDWISE-UNNOTCHED h = 0.073 IN.

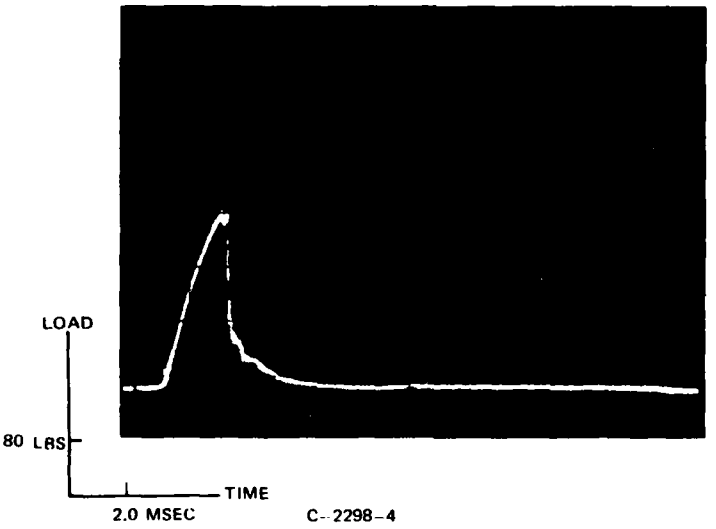

P_{MAX} = 260 LBS
E_{TOTAL} = 1.1 FT LBS

C-2298-4
8.0 B/6061-LT-CHORDWISE-UNNOTCHED h 0.073 IN.

FIG. 53 INSTRUMENTED IMPACT TRACES

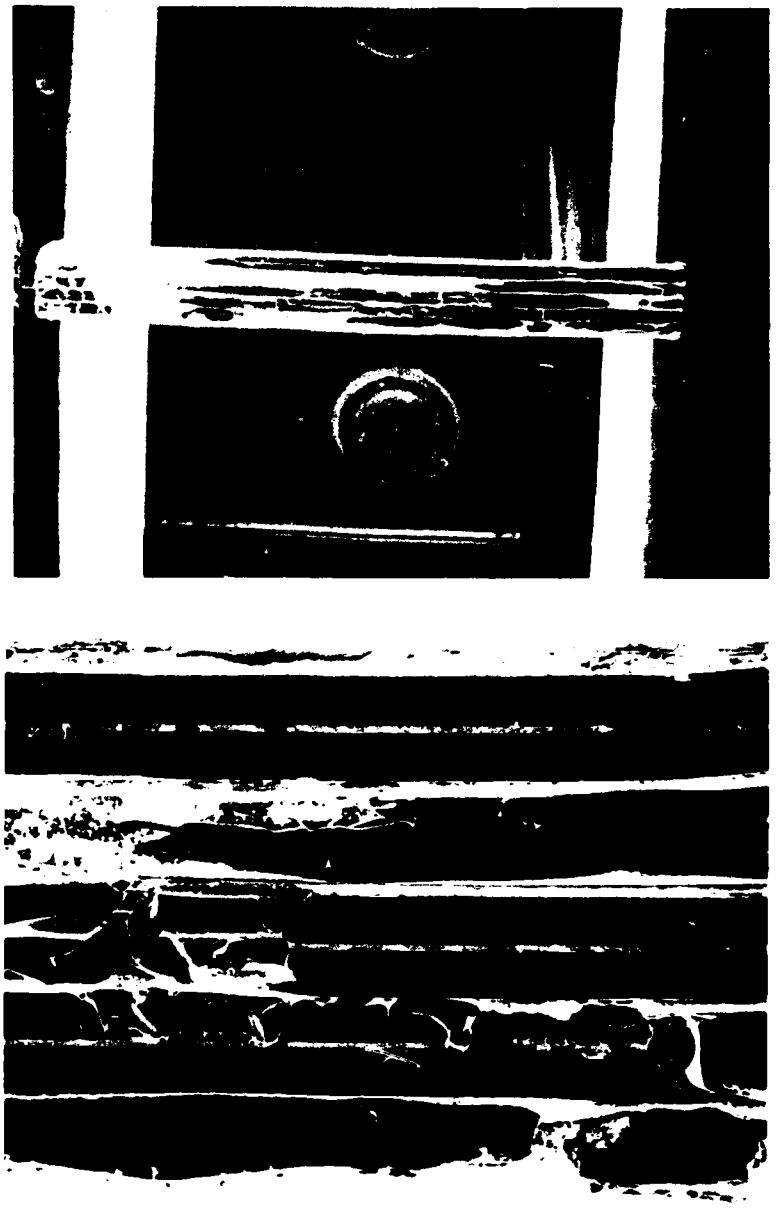

FIG. 54 FIBER SPLITTING IN TRANSVERSE TENSION

SPEC 2300–1 AVCO 8B–6061

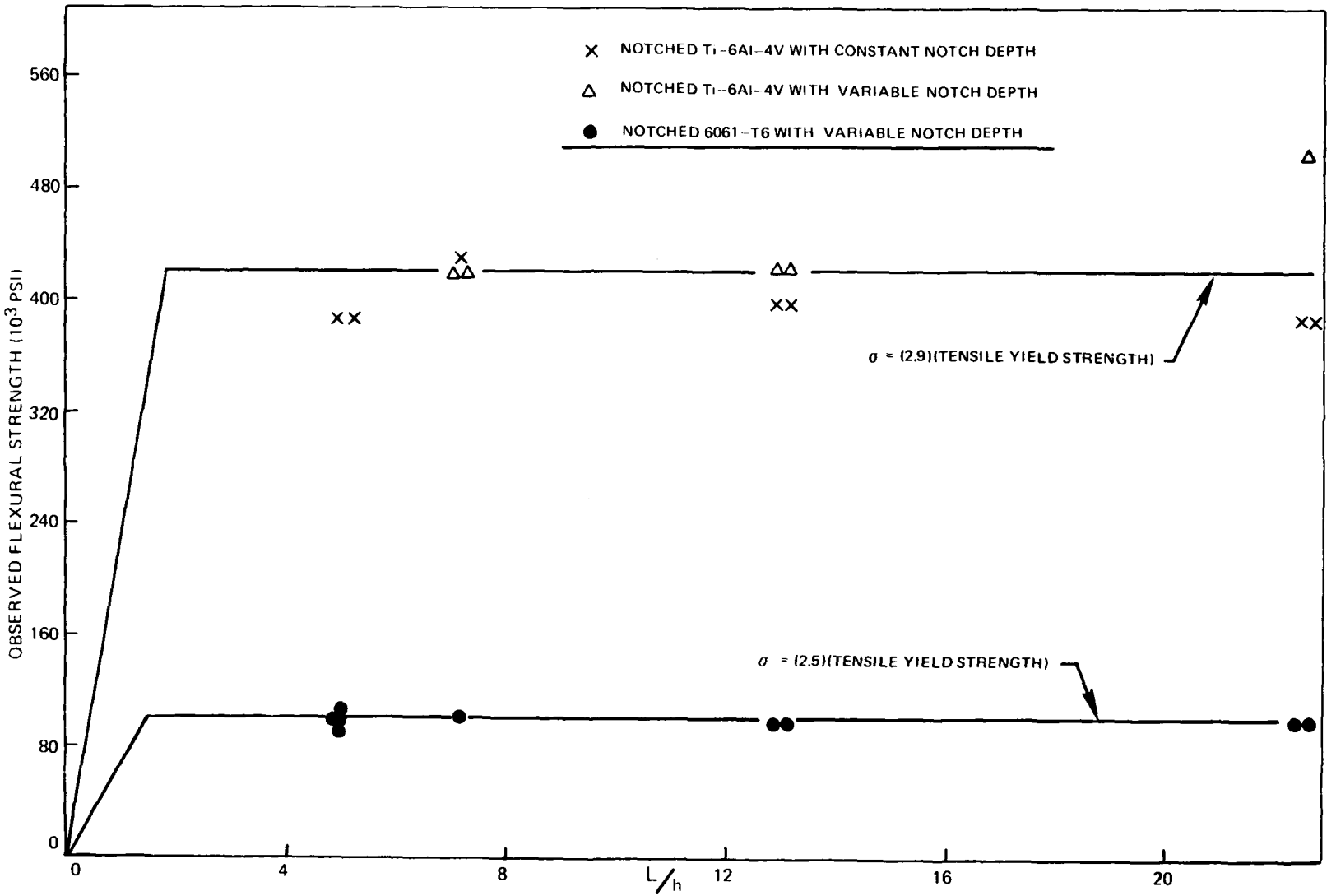

FIG. 55 FLEXURAL INTERACTION DIAGRAM

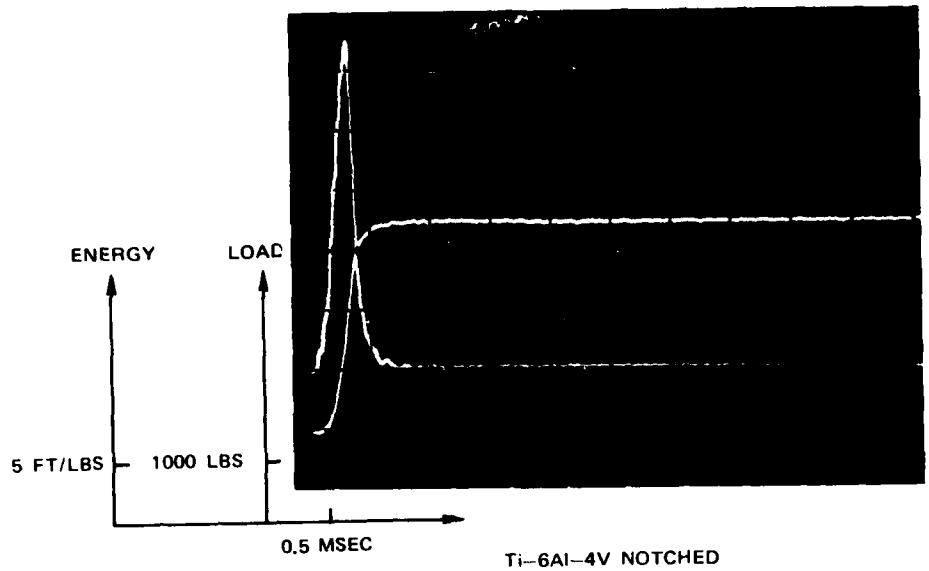

P_{MAX} = 5300 LBS
E_{TOTAL} = 16.5 FT LBS
$E_{INST.}$ = 8 FT LBS

Ti–6Al–4V NOTCHED

h = 0.315 IN.

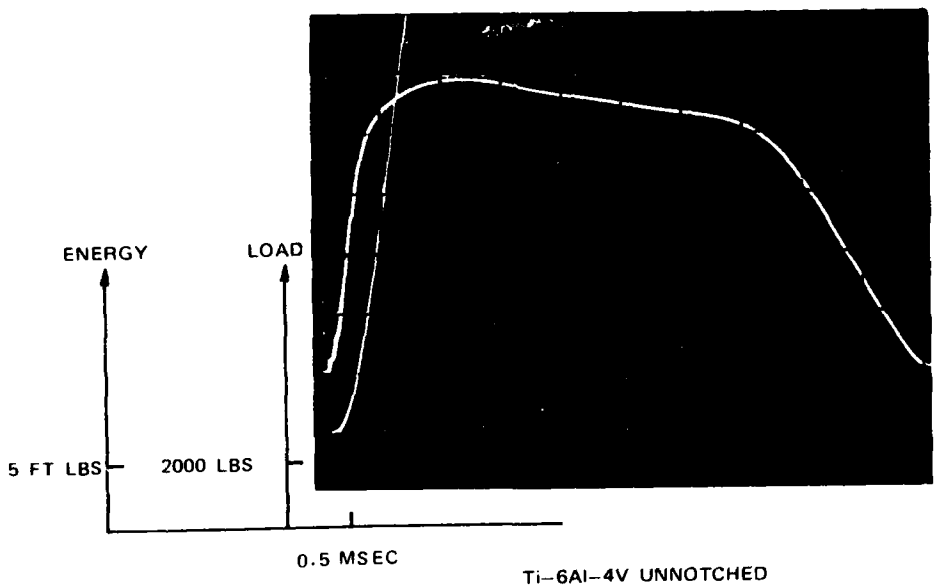

P_{MAX} = 12,000 LBS FT
E_{TOTAL} > 260 FT LBS

Ti–6Al–4V UNNOTCHED

h = 0.394 IN.

FIG. 56 INSTRUMENTED IMPACT TRACES

FIG. 57 NOTCHED AND UNNOTCHED Ti–6Al–4V IMPACT SPECIMENS

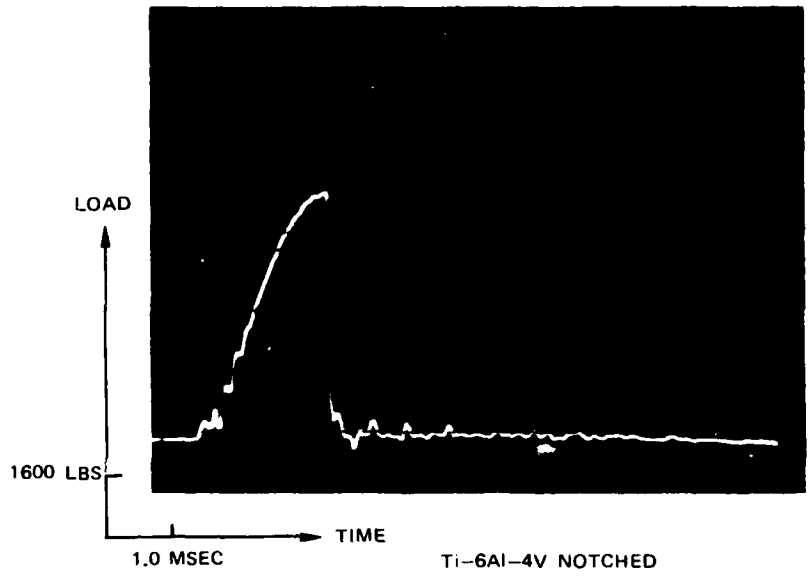

P_{MAX} = 6500 LBS

E_{TOTAL} = 13.2 FT LBS

Ti-6Al-4V NOTCHED

h = 0.315 IN.

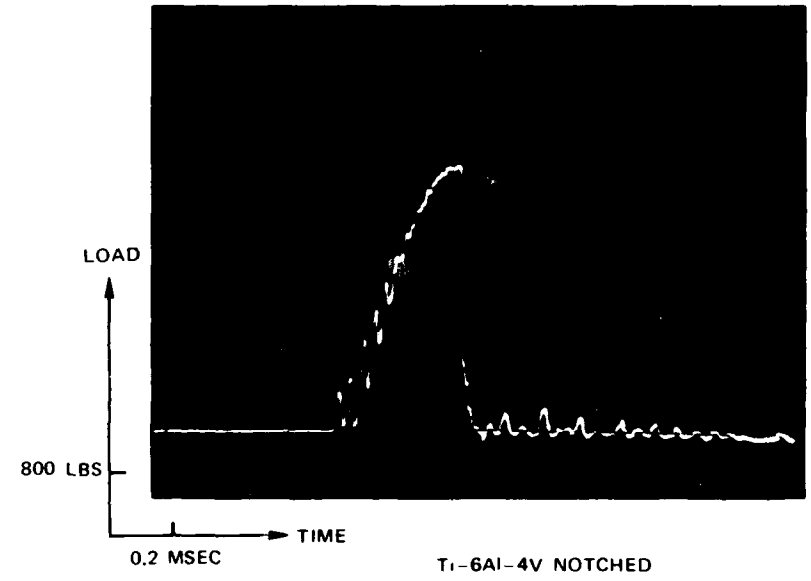

P_{MAX} = 3520 LBS

E_{TOTAL} = 7.5 FT LBS

Ti-6Al-4V NOTCHED

h = 0.221 IN.

FIG. 58 INSTRUMENTED IMPACT TRACES

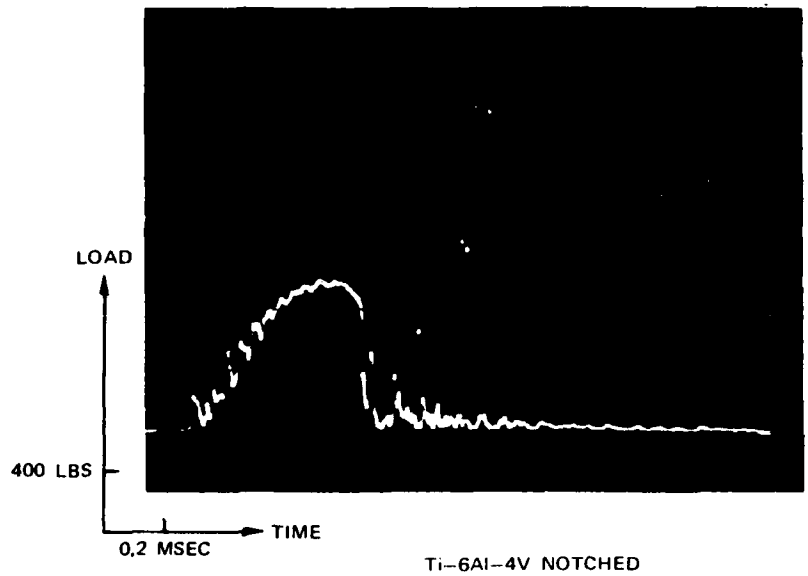

P_{MAX} = 972 LBS
E_{TOTAL} = 3.8 FT LBS

Ti–6Al–4V NOTCHED h = 0.121 IN.

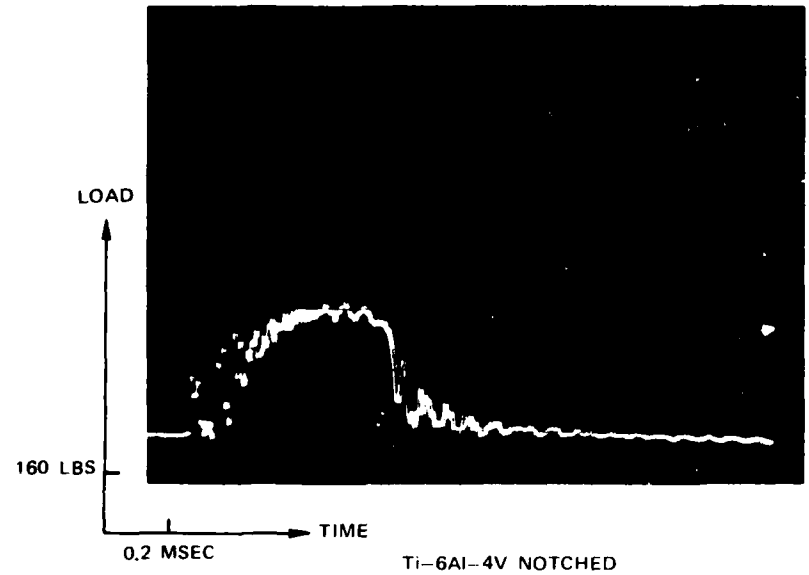

P_{MAX} = 325 LBS
E_{TOTAL} = 1.8 FT LBS

Ti–6Al–4V NOTCHED h = 0.071 IN

FIG. 59 INSTRUMENTED IMPACT TRACES

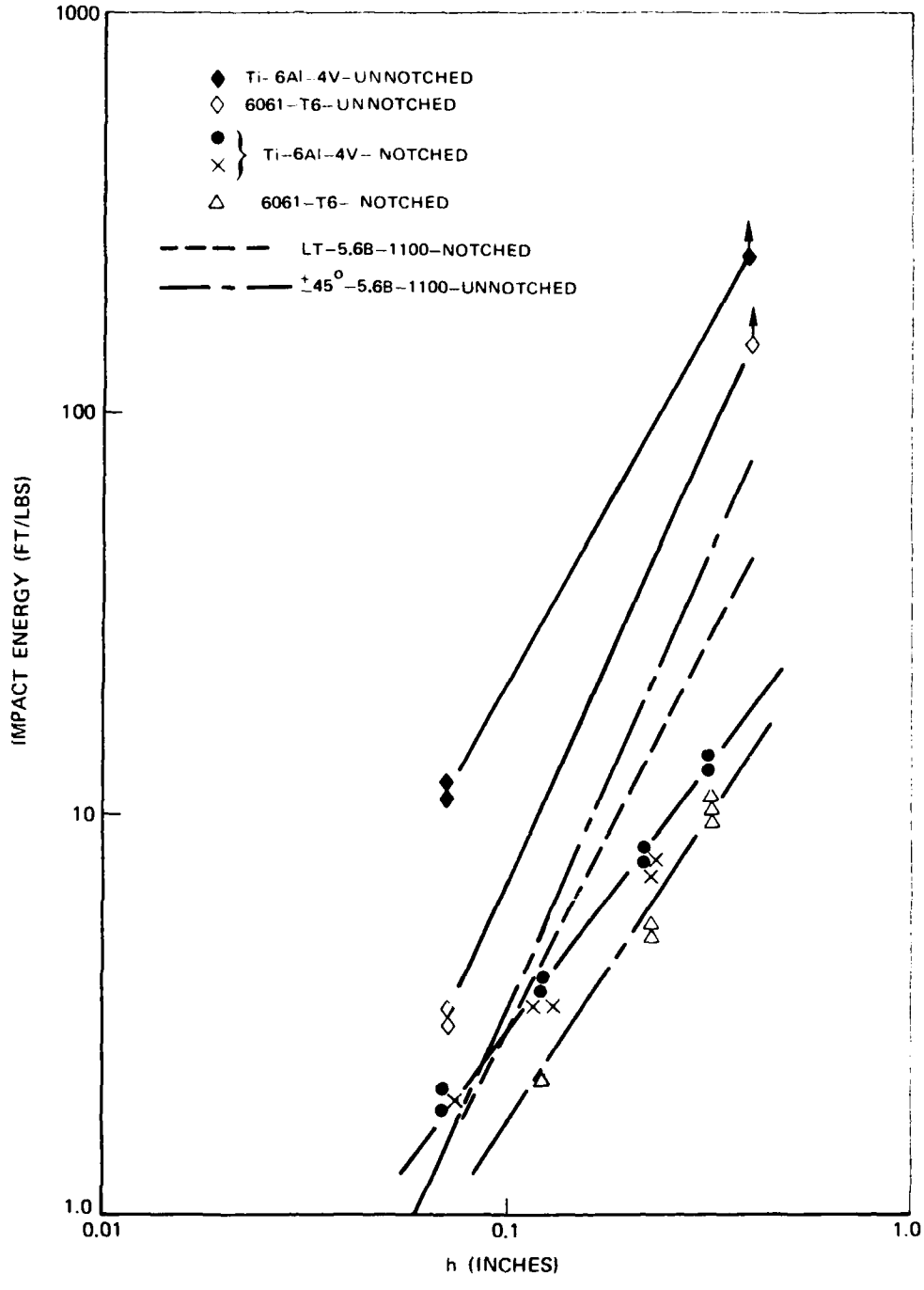

FIG. 60 ENERGY DISSIPATED AS A FUNCTION OF SPECIMEN GEOMETRY

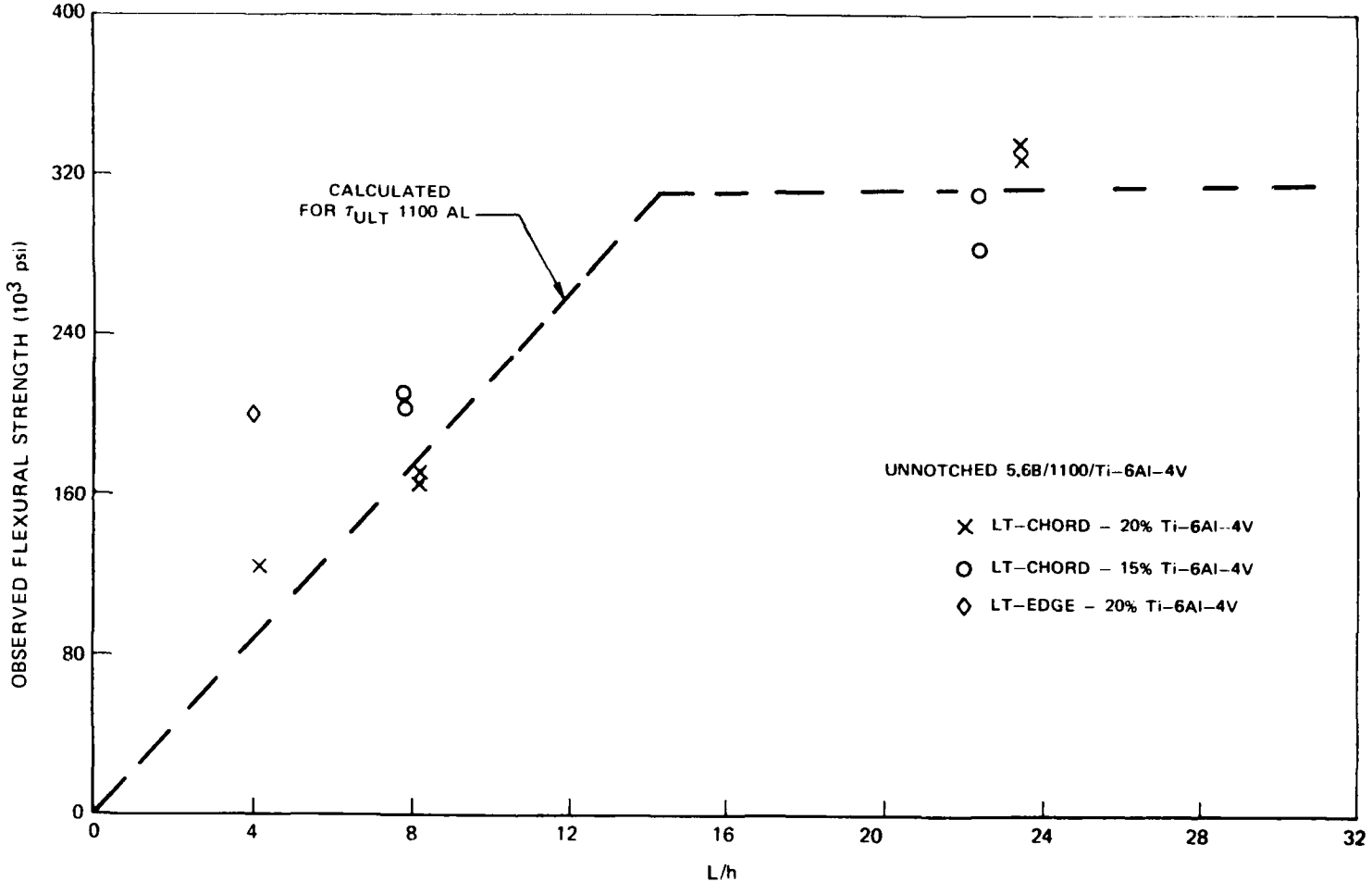

FIG. 61 FLEXURAL INTERACTION DIAGRAM

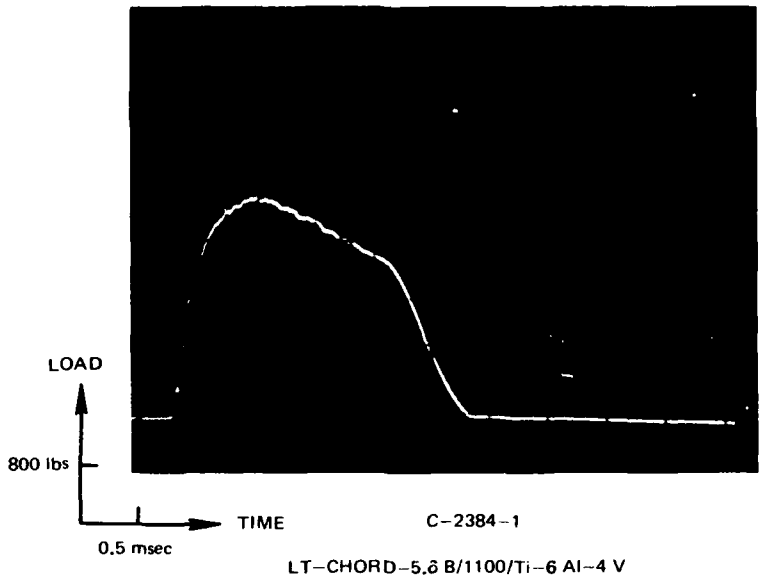

P_{MAX} = 3060 lbs

E_{TOTAL} >23 ft lbs

SPECIMEN
UNBROKEN

C-2384-1

LT-CHORD-5.6 B/1100/Ti-6 Al-4 V

UNNOTCHED h = 0.381 IN

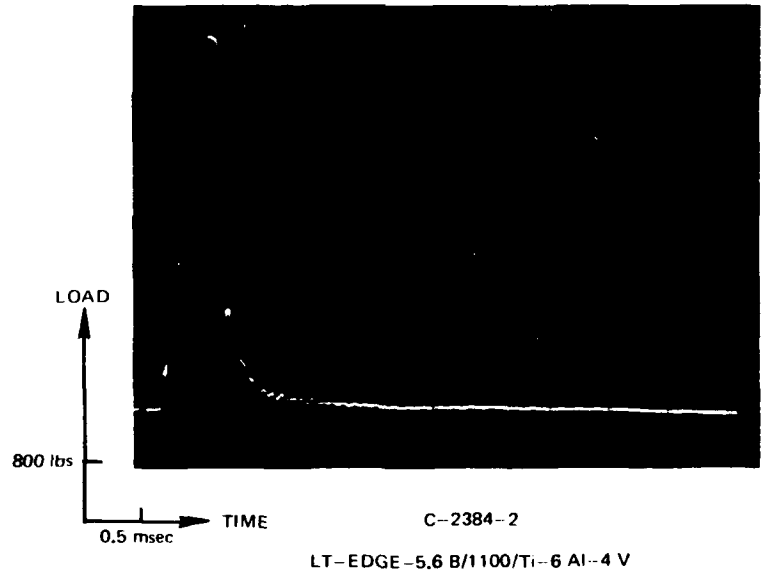

P_{MAX} = 5150 lbs

E_{TOTAL} = 16.6 ft lbs

C-2384-2

LT-EDGE-5.6 B/1100/Ti-6 Al-4 V

UNNOTCHED h = 0.396 IN

FIG. 62 INSTRUMENTED IMPACT TRACES

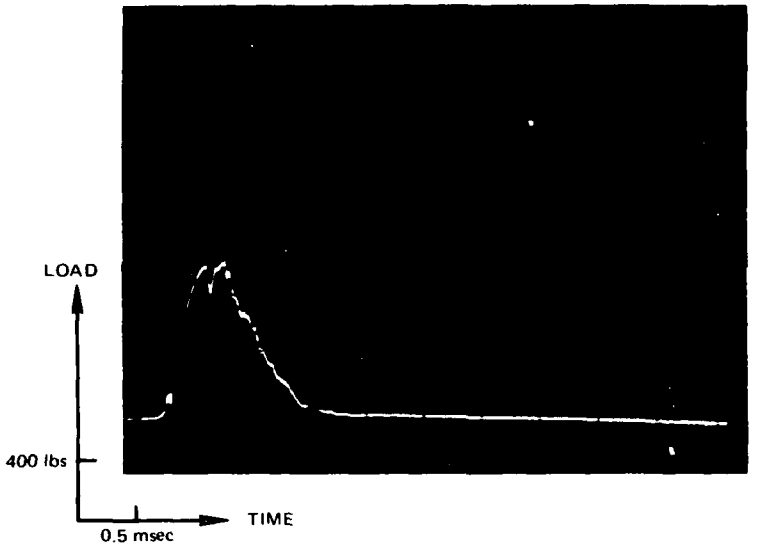

P_{MAX} 1040 lbs

E_{TOTAL} 6.6 ft

C 2385 1

LT CHORD 5.6 B/1100/Ti 6 Al 4 V

UNNOTCHED h 0.192 IN

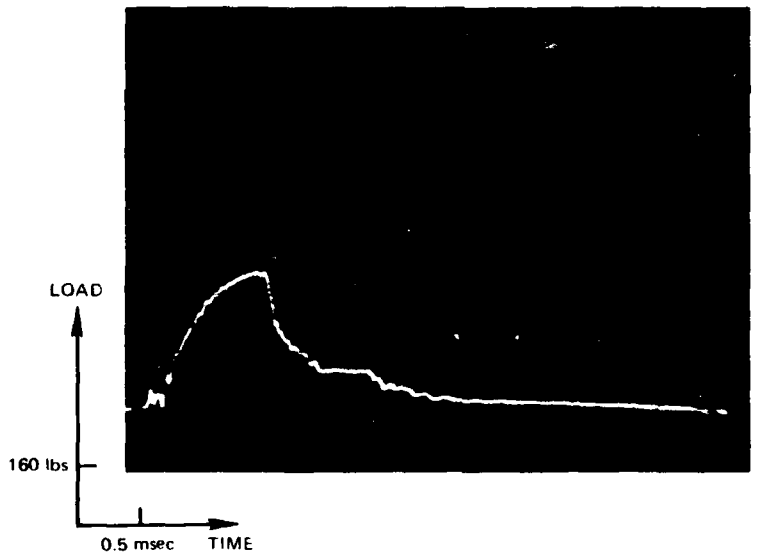

P_{MAX} 370 lbs

E_{TOTAL} 3.9 ft lbs

C 2385 3

TT 5.6 B/1100/Ti 6 Al 4 V

UNNOTCHED h 0.196 IN

FIG. 63 INSTRUMENTED IMPACT TRACES

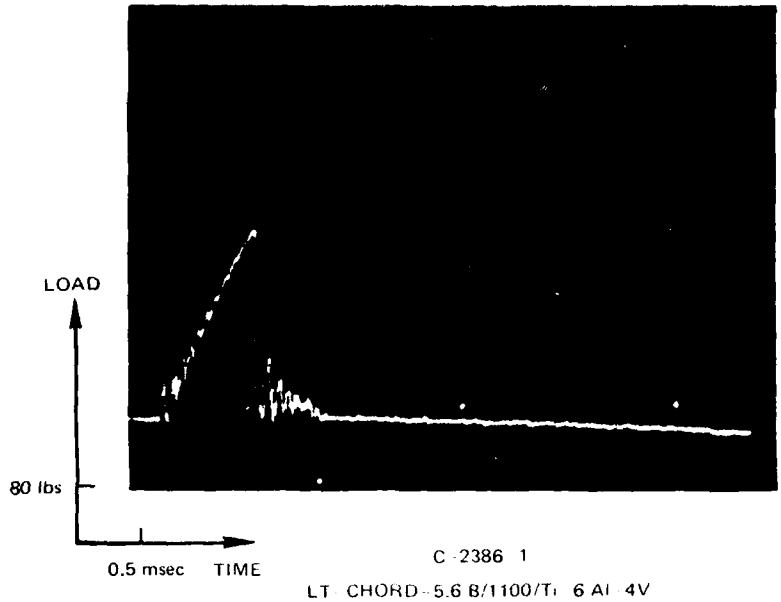

P_{MAX} = 255 lbs

E_{TOTAL} 1.1 ft lbs

C-2386-1

LT CHORD-5.6 B/1100/Ti 6 Al 4V

UNNOTCHED h = 0.067 IN

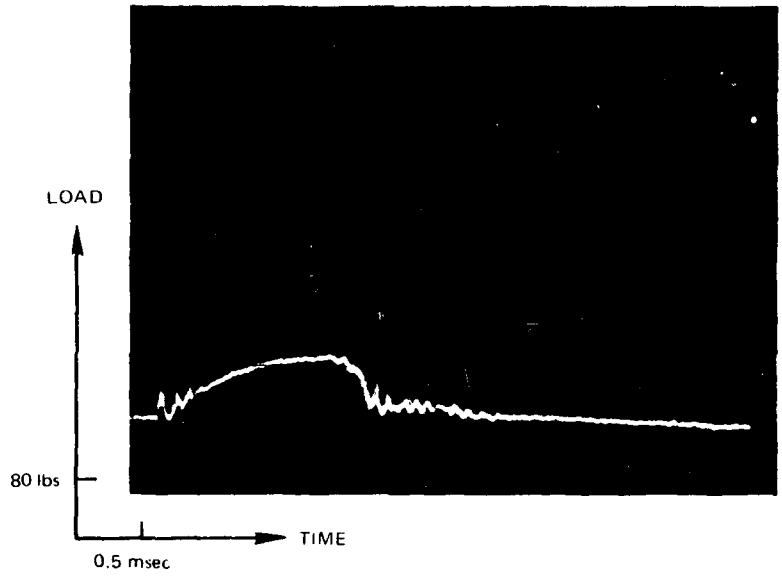

P_{MAX} = 84 lbs

E_{TOTAL} = 1.0 ft lbs

C 2386-4

TT 5.6 B/1100/Ti 6 Al 4 V

UNNOTCHED h = 0.067 IN

FIG. 64 INSTRUMENTED IMPACT TRACES

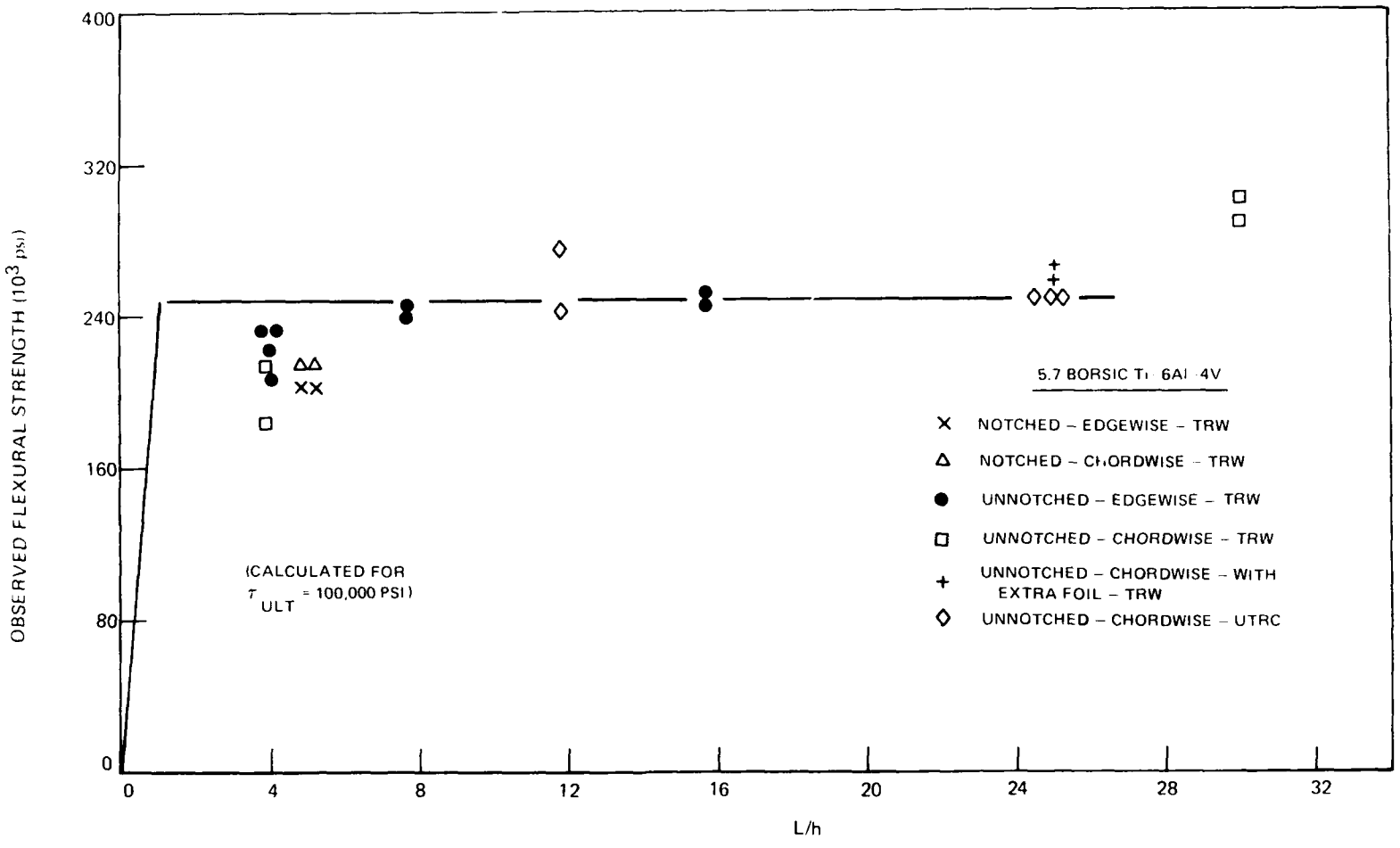

FIG. 65 FLEXURAL INTERACTION DIAGRAM

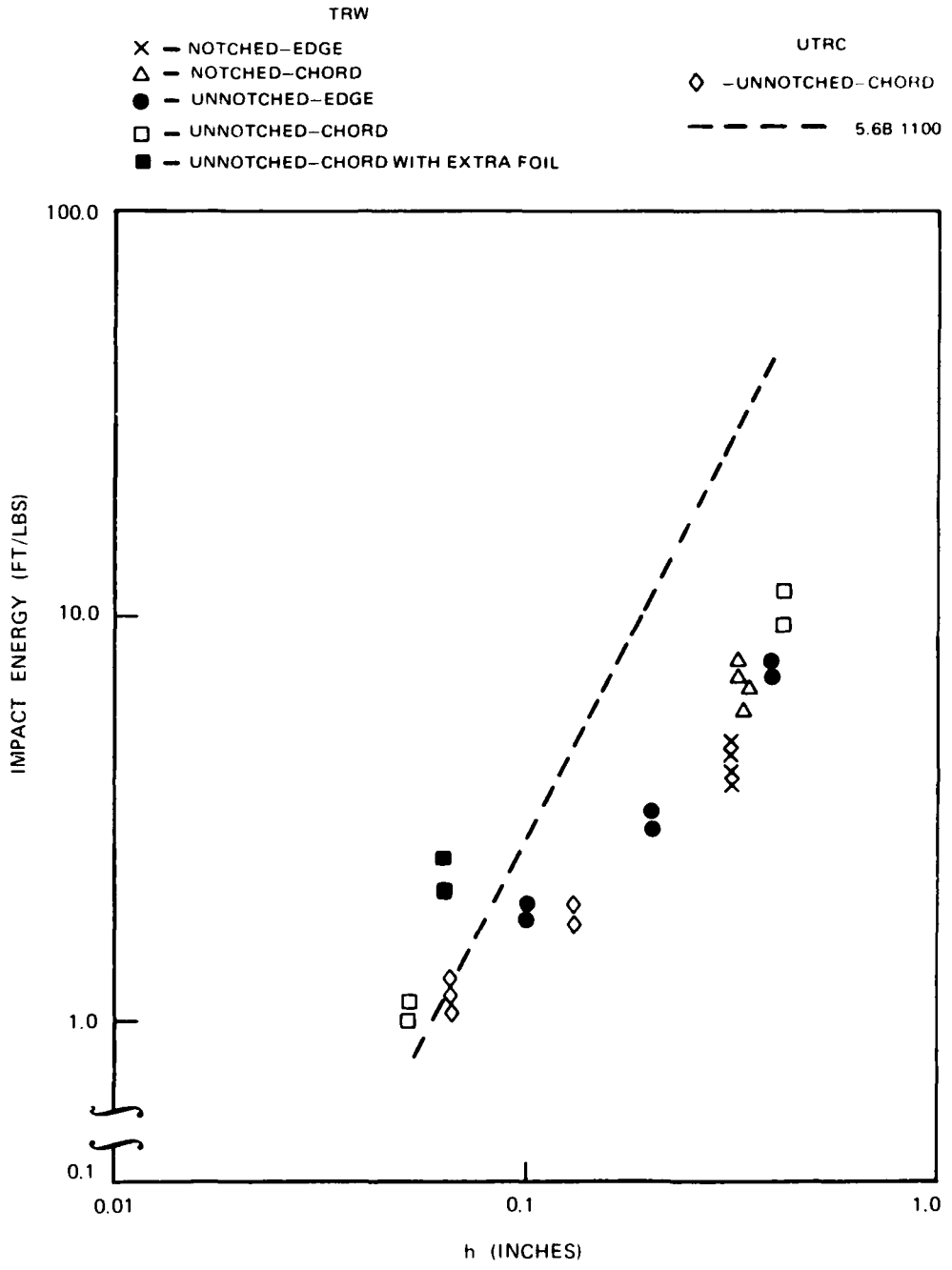

FIG. 66 ENERGY DISSIPATED AS A FUNCTION OF SPECIMEN GEOMETRY FOR 5.7 BORSIC REINFORCED Ti–6Al–4V IN LT ORIENTATION

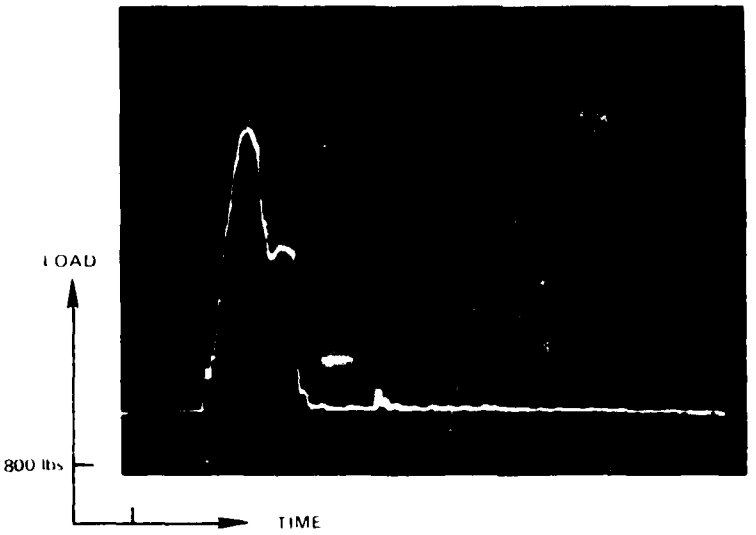

P_{MAX} 4,000 lbs

E_{TOTAL} 7.1 ft lbs

SN 139 2

LT CHORD 5.7 BORSIC/Ti 6 Al 4V

NOTCHED h 0.333 IN

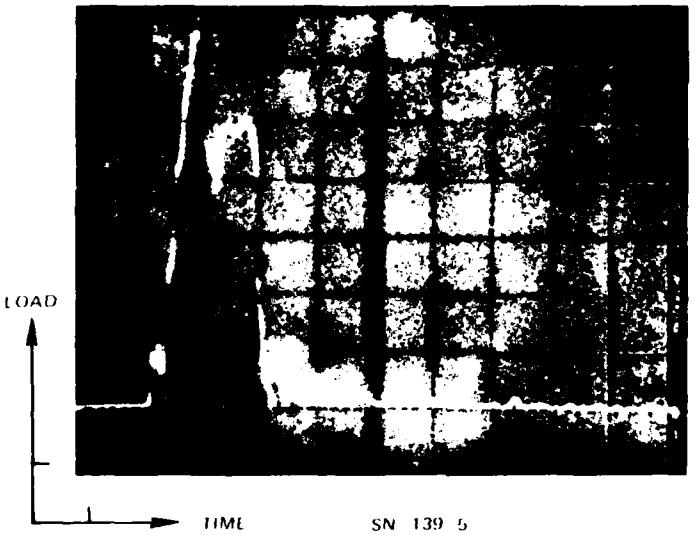

P_{MAX} 5180 lbs

E_{TOTAL} 11.4 ft lbs

SN 139 5

LT CHORD 5.7 BORSIC/Ti 6 Al 4V

UNNOTCHED h 0.412 IN

FIG. 67 INSTRUMENTED IMPACT TRACES

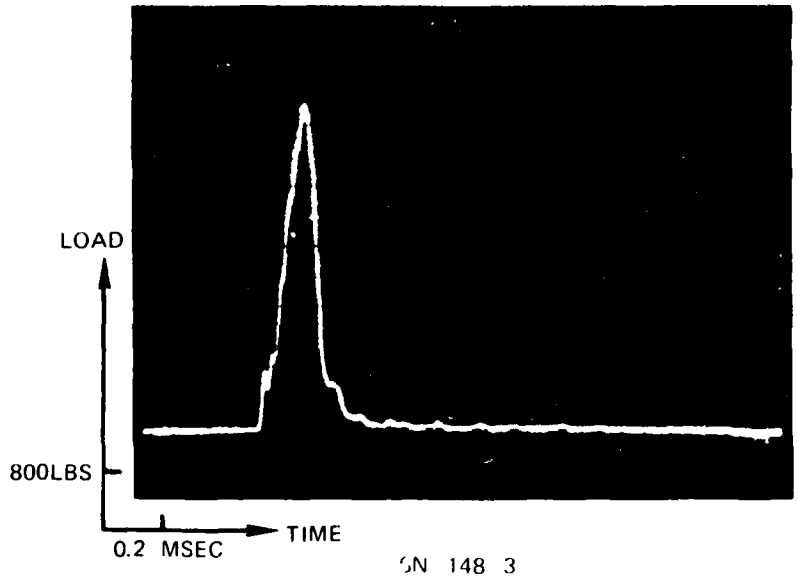

P_{max} 3840
E_{TOTAL} 4.7FT/LBS

SN 148 3
LT EDGE-5.7BORSIC/Ti-6Al-4V
NOTCHED h 0.321

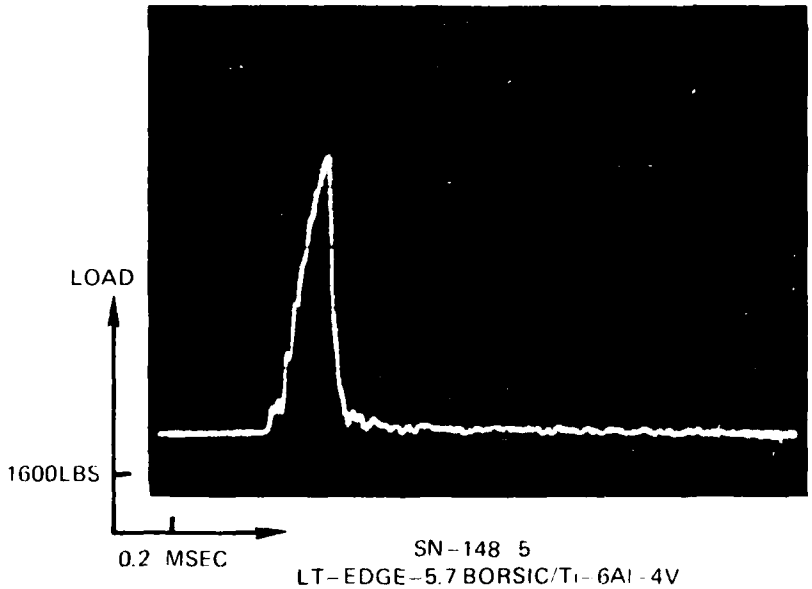

P_{max} 6.542
E_{TOTAL} 7.9FT LBS

SN-148 5
LT-EDGE-5.7 BORSIC/Ti-6Al-4V
UNNOTCHED h 0.396

FIG. 68 INSTRUMENTED IMPACT TRACES

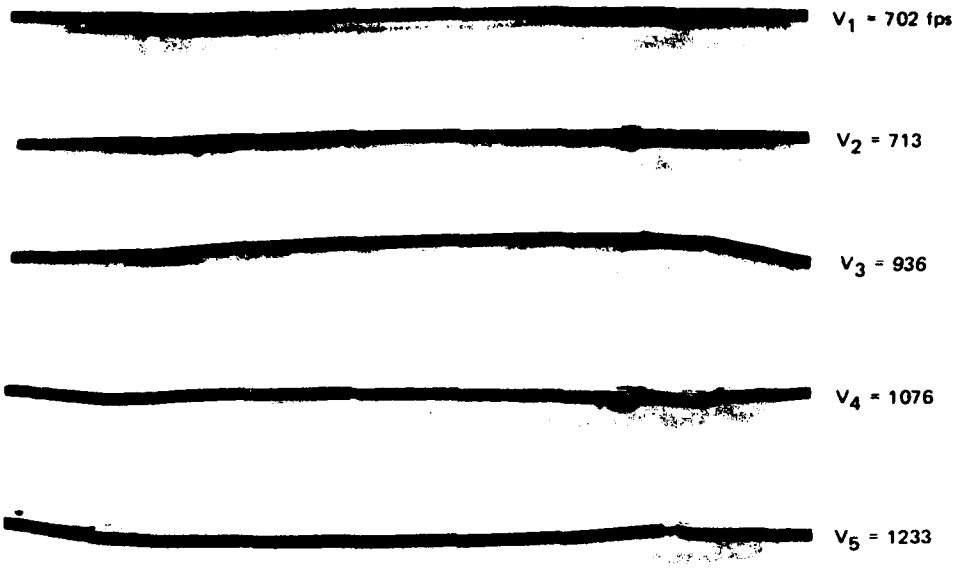

C–2479

$[\pm 22]_5$ 5.6B/6061 t = 0.069IN.

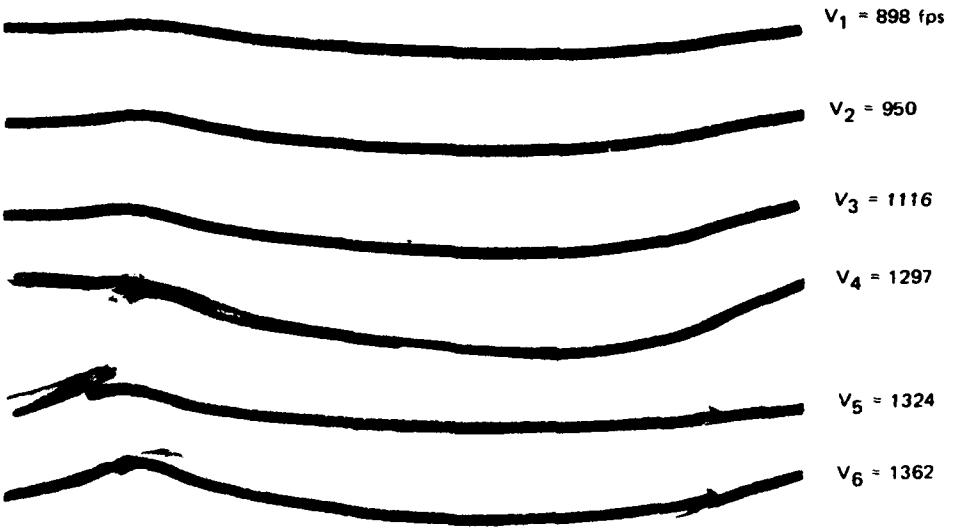

C–2480

$[\pm 22]_5$ 5.6B/1100 t - 0.066IN.

FIG. 69 CANTILEVERED BALLISTIC TEST SPECIMENS (CLAMPED AT RIGHT END)

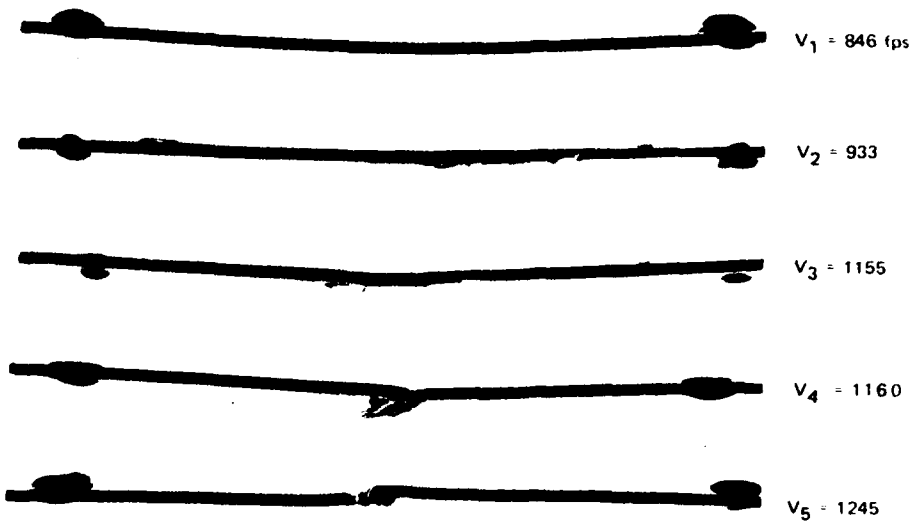

C–2479

$[\pm 22]_5$ 5.6B/6061 t = 0.069IN.

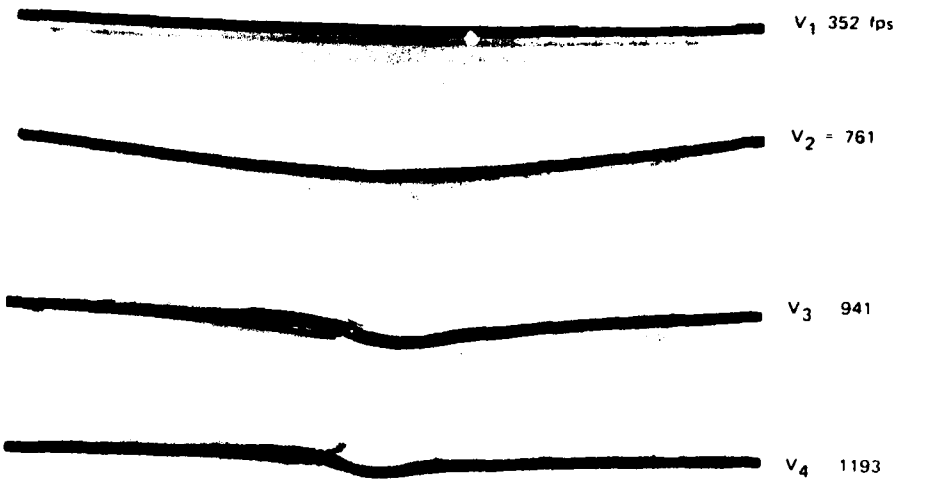

C–2480

$[\pm 22]_5$ 5.6B/1100 t = 0.066IN.

FIG. 70 SIMPLY SUPPORTED BALLISTIC TEST SPECIMENS

SIMPLY SUPPORTED BALLISTIC TEST SPECIMENS

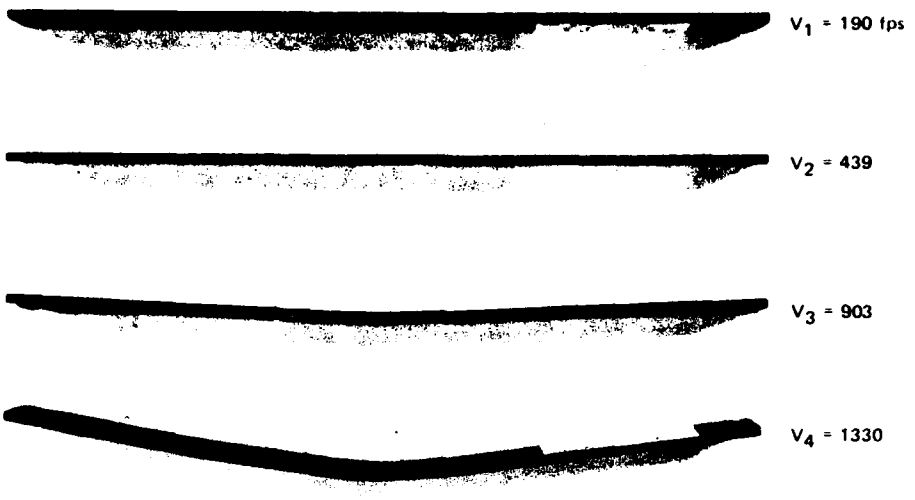

SN–129–2

0^o–5.7 BORSIC/Ti–6Al–4V t ≈ 0.052IN.

CANTILEVERED BALLISTIC TEST SPECIMENS (CLAMPED AT RIGHT END)

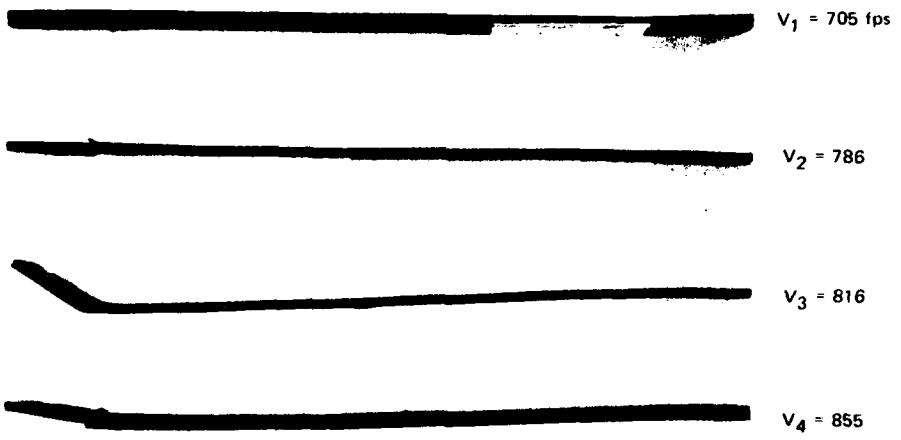

SN–129–1

0^o–5 7 BORSIC/Ti–6Al–4V t = 0.052IN.

FIG. 71 BALLISTIC IMPACT OF BORSIC TITANIUM

C–2475–76

0^{o}–5.6B/1100 WITH 0.009 Ti–6Al–4V
ON EACH FACE t –0.066IN.

FIG. 72 CANTILEVERED BALLISTIC TEST SPECIMENS

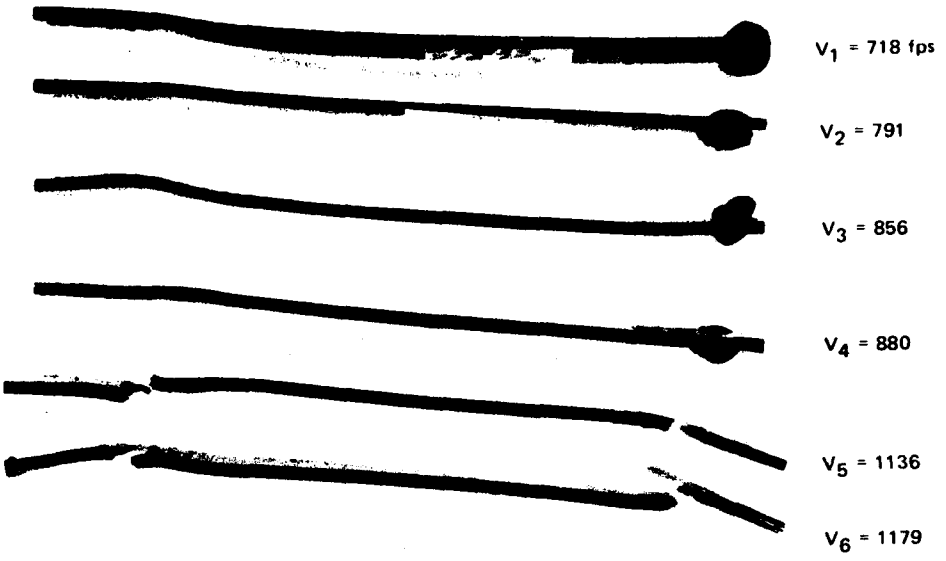

C–2579

$[+45/O_2]_2$ –8.0B/1100 t = 0.075IN.

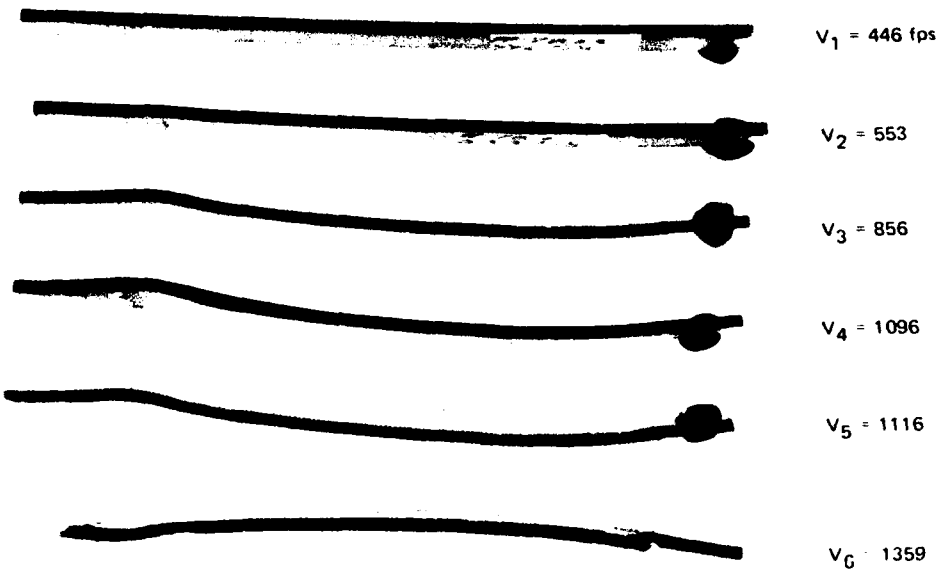

C–2578

$[\pm 22]_4$ –8.0B/1100 t = 0.075IN.

FIG. 73 CANTILEVERED BALLISTIC TEST SPECIMENS (CLAMPED AT RIGHT END)

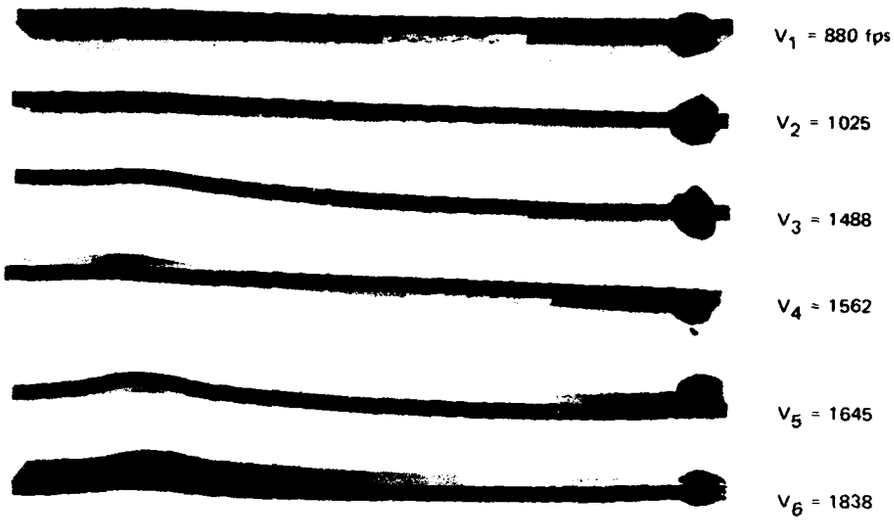

C–2580

0^{o}–8.0B/1100 t = 0.085IN.

WITH THREE LAYERS OF 0.005IN. THICK Ti–6AL–4V ON EACH FACE.

FIG. 74 CANTILEVERED BALLISTIC TEST SPECIMENS (CLAMPED AT RIGHT END)

REFERENCES

1. K. G. Kreider, L. Dardi, K. M. Prewo, AFML-TR-71-204.
2. K. M. Prewo, Jl. Comp. Matls., Vol. 6, p 442, 1972.
3. K. M. Prewo, Proc. Third Intl. Conf. on the Strength of Metals and Alloys, Cambridge, England Vol. 1, paper no. 57. 1973.
4. C. Ellis and B. Harris, Jl. Comp. Matls., Vol. 7, p 76, 1973.
5. T. Guess and W. Hoover, Jl. Comp. Matls., Vol. 7, p 2, 1973.
6. W. R. Hoover and R. E. Allred, Sandia Labs. Rept. SAND-74-0193, 1974.
7. W. R. Hoover, Sandia Labs. Rept., SAND-74-0323, 1975.
8. R. A. Wullaert, in "ASTM-STP 466," 1970 pp 148-164.
9. W. R. Hoover, Sandia Labs. Rept. SLA-73-0972, 1973.
10. D. R. Ireland, Effects Technology Reprint, TR-73-25R.
11. D. R. Ireland, Effects Technology, Santa Barbara, Calif.
12. W. R. Hoover, Sandia Labs., Albuquerque, New Mexico.
13. J. V. Mullin and A. C. Knoell, Matls. Res. and Stds., Vol. 10, #12, p 16.
14. A. W. Christiansen, et al, Fib. Sci. & Tech., Vol. 7, 1974, p 1.
15. C. A. Berg, et al, ASTM-STP-497, 1972 pp 206-218.
16. S. A. Sattar and D. H. Kellogg, ASTM-STP-460, 1969, p 62.
17. K. T. Kedivard, Fib. Sci. & Tech., Vol. 5, 1972, p 85.
18. C. Chamis, private communication.
19. K. M. Prewo, Third International Conference on the Strength of Metals and Alloys, Cambridge, England 1973.